STRENGTH AND STIFFNESS OF WEAK-AXIS MOMENT END-PLATE CONNECTIONS

Kyle Richard Dominisse

Thesis submitted to the Faculty of the Virginia Polytechnic Institute and State University in partial fulfillment of the requirements for the degree of

Master of Science

in

Civil Engineering

APPROVED:

Thomas M. Murray, Chairman

W. Samuel Easterling

Raymond H. Plaut

December 10, 2004

Blacksburg, VA

Keywords: Steel, End-Plate, Finite Element, Yield Line, Column, Web, Moment, Weak-Axis

STRENGTH AND STIFFNESS OF WEAK-AXIS MOMENT END-PLATE CONNECTIONS

by

Kyle Richard Dominisse

(ABSTRACT)

Three full-scale experimental tests were conducted to investigate the strength and stiffness of weak-axis moment end-plate connections. Each test consisted of two girders connected to a column web with four-bolt extended moment end-plates. Two tests were conducted with bare steel. One test included a composite concrete slab that confined the top extension of the end-plate.

Finite element models of the tests were created with the commercial software SAP2000. A simplified modeling procedure was developed to overcome the contact problems between the end-plates and column web, and between the bolts and holes in the end-plates and web. The simplified modeling procedure accurately predicted the experimental elastic stiffness, in the form of column web rotations, of the connections.

Yield line theory was used to investigate the plastic strength of the column web. Several yield line patterns were examined. Analytical plastic moment strengths were very conservative when compared to the observed behavior of the column web.

The experimental stiffness of the test with the concrete slab confining the top extension of the end-plate was compared to the stiffness of a similar test without a slab. The slab increased the elastic stiffness of the connection; however, after the concrete began cracking and crushing around the connection, the stiffness was greatly decreased.

ACKNOWLEDGEMENTS

I want to extend my gratitude to Dr. Thomas Murray for serving as my committee chair. His teaching, guidance, and encouragement throughout the course of this research and my graduate career will always be appreciated. I would also like to thank Dr. W. Samuel Easterling and Dr. Raymond Plaut for serving on my committee. Dr. Finley A. Charney was also very helpful with his knowledge of computer modeling.

Appreciation is extended to Brett Farmer and Dennis Huffman for their help in the construction of test setups and assembling of test specimens. Thanks to my colleagues, Steve Blumenbaum, David Martin, Tim Banta, Onur Avci, and Benjamin Mohr, for their time and efforts helping assemble test specimens and sharing their knowledge of the data acquisition systems. These friends made the time spent in the structures lab an unforgettable experience.

Special thanks go out to family for their continual support throughout my education. Their love and encouragement account for a large part of everything that I have accomplished in my life.

TABLE OF CONTENTS

LIST OF FIGURES

LIST OF TABLES

CHAPTER 1

INTRODUCTION

1.1 Background

A moment end-plate connection is designed as a fully restrained (FR) moment connection. The connection is composed of a steel plate, with punched or drilled holes, that is welded to the end of a beam section. The welding is performed during fabrication and the end-plate is field bolted to the supporting member during erection.

Moment end-plates can be separated into two general classes, flush end-plates and extended end-plates. A flush end-plate does not extend beyond the beam flanges with all bolts located between the beam flanges. An extended end-plate is one which extends far enough beyond the beam tension flange to allow the location of bolts. The scope of this research is restricted to symmetrical 4-bolt extended end-plate configurations, as illustrated in Figure 1.1.

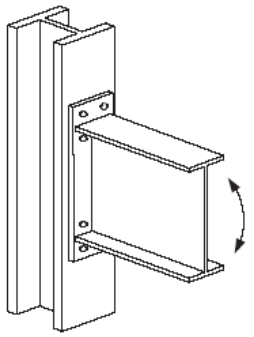

FIGURE 1.1: FOUR BOLT EXTENDED END-PLATE

Design of moment end-plate connections is controlled by the limit states of end-plate yield and bolt rupture. Extensive research exists for these types of connections;

however, very little research exists for the limit states of the column side of the connection. This is especially true for the case that the end-plate is connected to a more flexible element, such as the web of a column. The following sections will investigate the stiffness and strength of 4-bolt extended end-plates connected to the web of a column.

1.2 Literature Review

There is extensive research available on the analysis and design of moment end-plate connections; however, a minimal amount of this research investigates the limit states associated with the column side of the connection. This is especially true for moment end-plate connections that frame into the web of a column. The research that has been conducted on column web connections is limited to bracket connections, stiffened seat connections, and beams welded directly to the column web.

Abolitz and Warner (1965) performed a theoretical investigation of plate bending under bracket connections welded to a column web. They used a linear pressure distribution to distribute the compression and tension between the bracket and web. Yield line analysis and the method of work were used to develop an upper bound solution that estimates the capacity of the column web. Patterns were established for two cases: the flanges offer full restraint of the web, and the flanges offer no restraint of the web. They concluded that the solution held equally well in cases where bending is applied to plates by connections other than brackets: for example, a fixed-ended connection of a beam that develops negative moment.

Blodgett (1966) used yield line theory to develop a design model for welding rolled sections to built-up box columns. The box column flange was treated as a beam simply supported at its two outer edges, which gives it the same maximum bending moment as a rolled column flange treated as a beam supported at its center. The welded beam flange was treated as a single plate applying a uniform tensile load to the box column flange.

Stockwell (1974) developed a design model for beams welded to a column web. He used yield line theory to develop a series of curves relating beam moment to column web thickness for a series of beam sizes and for W14 columns with yield strengths of 36 and 50 ksi. The curves are based on plastic yielding of the column web and the assumption that ultimate strength is determined by yielding in a bending mode along an assumed yield line pattern.

Kapp (1974) used yield line theory to develop a design procedure for light bracing web connections in direct tension. The connections discussed were: a welded plate, a bolted Tee connection, and a bolted Tee connection reinforced with a plate on the opposite side of the column web. Kapp recommended that the web of a member subjected to a tension force should always be checked to insure that it develops the full connection tension.

Hoptay and Ainso (1981) conducted eight tests on bracket connections connected to the web of a wide flange section. They then compared the experimental results to the solution proposed by Abolitz and Warner (1965). Hoptay and Ainso concluded that the flanges of the column did not offer any restraint for the web and the results of the test program verified the soundness of the approach developed by Abolitz and

Warner. It was also concluded that membrane action was responsible for the load capacity beyond that predicted by the theoretical solution.

Hopper et al. (1985) conducted five tests on bracket to web connections with web slenderness ratios less than 15. They reported that a new maximum load mechanism develops in sections with very low web slenderness ratios. This mechanism is characterized by plastic hinges forming in the flanges of the section as a result of the low web slenderness ratio and low section modulus about the weak axis of the column. They concluded that the yield line pattern predicted by Abolitz and Warner did not fully develop for sections with web slenderness ratios less than 15.

Ellifritt and Sputo (1999) studied and developed design guidelines for stiffened seated connections welded to column webs. Nearly fifty full-scale tests were performed on stiffened seats welded to various column webs to determine if the tables in Volume II of the AISC Manual for calculating the capacity of stiffened seats attached to a column flange were applicable for the case of web attachment. They determined that the tables were appropriate for the web-attached seat, with a few exceptions noted at the bottom of the tables. They also presented a yield line procedure that must be checked if a "beam" section is used as the column.

1.3 Scope of Research

The objective of this research is to investigate the behavior of four-bolt extended weak-axis moment end-plate connections. Three full-scale weak-axis moment end-plate connections were subjected to moments to observe the stiffness and strength of the connection.

The observed elastic stiffness of each connection is compared to analytical results using finite element models. A simplified modeling procedure is developed to overcome the problems associated with the contact between the bolts, end-plates, and column web. The effects of a concrete slab on the stiffness of the connection are also investigated.

The plastic strength of the column web is investigated using yield line theory and compared to the experimental results. The observed strength of each connection is compared to the predicted strength using the design procedure provided in AISC Design Guide 16, "Flush and Extended Multiple-Row Moment End-Plate Connections" (Murray and Shoemaker, 2002).

The experimental tests and results are discussed in Chapters 2 and 3. Finite element modeling procedures, including a simplified modeling method and results, are presented in Chapter 4. A yield line analysis and the predicted plastic moment strengths of the column web are presented in Chapter 5. The experimental and analytical results are analyzed in Chapter 6, and Chapter 7 includes conclusions and future research needs.

CHAPTER 2

EXPERIMENTAL TESTS

2.1 Overview

Tests of three 4-bolt extended weak-axis moment end-plate connections were conducted to determine their strength and stiffness. Each test consisted of two W24x55 or W27x84 A572 Grade 50 girder sections connected to the weak axis of a W14x99 A992 column section.

Two tests were conducted in a horizontal test setup and included the bare steel only. Descriptions of the test specimens, test setup, and testing procedure are in the following sections. Each test is described in further detail by Dominisse and Murray (2003).

One test was conducted in a vertical test setup that included a composite slab attached to the girders. Seven load sequences were conducted on the girder-to-column web connection. The scope of this research is restricted to the first and fifth load sequences, which represent the stiffness of the connection, and the last load sequence in which the connection was loaded until failure. Descriptions of the test specimens, test setup, and testing procedure are in the following sections. This test, including all seven load sequences, is described in further detail by Dominisse and Murray (2004).

2.2 Bare Steel Tests

2.2.1 Test Specimens

Test specimen details are shown in Figure 2.1. The test girders were W24x55 or W27x84 and had a length of 135-¼ in. The W24x55 girders had ¾ in. end-plates and the W27x84 girders had 1 in. end-plates welded to each end. The end-plates had identical hole patterns on each end; however, the hole patterns varied between the two tests. A clevis was bolted to the end of the girder not being tested, thereby allowing load to be applied to the connection. The moment applied to the connection was equal to the applied load multiplied by the distance between the connection faying surface and the point where the concentrated load was applied to the clevis. As-measured connection drawings are in Appendix A.

The columns, W14x99 sections, measured 266-½ in. long and had 1 in. thick plates welded on each end to allow attachment to the test reaction frame. The columns had distinct sets of hole patterns on the web to match each hole pattern on each test beam end-plate.

The test specimen girders were ASTM A572 Grade 50 steel, the columns were ASTM A992 steel, and all plate material was ASTM A36 steel. All bolts were A325-X. Tensile coupon tests were conducted by lab personnel, using material identical to that used for the girders and columns. The measured yield stresses for the W24x55 girders, W27x84 girders, and columns were 63.0 ksi, 55.1 ksi, and 58.0 ksi, respectively. Coupon tests were not conducted for the end-plates. Mill certification reports show the yield stresses to be 46.0 ksi for the ¾ in. plates and 48.15 ksi (average of two tests) for the 1 in. plates. Because mill testing generally results in

slightly higher yield stresses than standard ASTM testing, the reported stresses were reduced 8%. The reduced values 42.3 ksi and 44.3 ksi were used in the following strength analyses. Four ¾-in. diameter bolts were tested for tensile strength, resulting in an average strength of 112.4 ksi. Three 1-in. diameter bolts were tested for tensile strength, resulting in an average strength of 117.3 ksi.

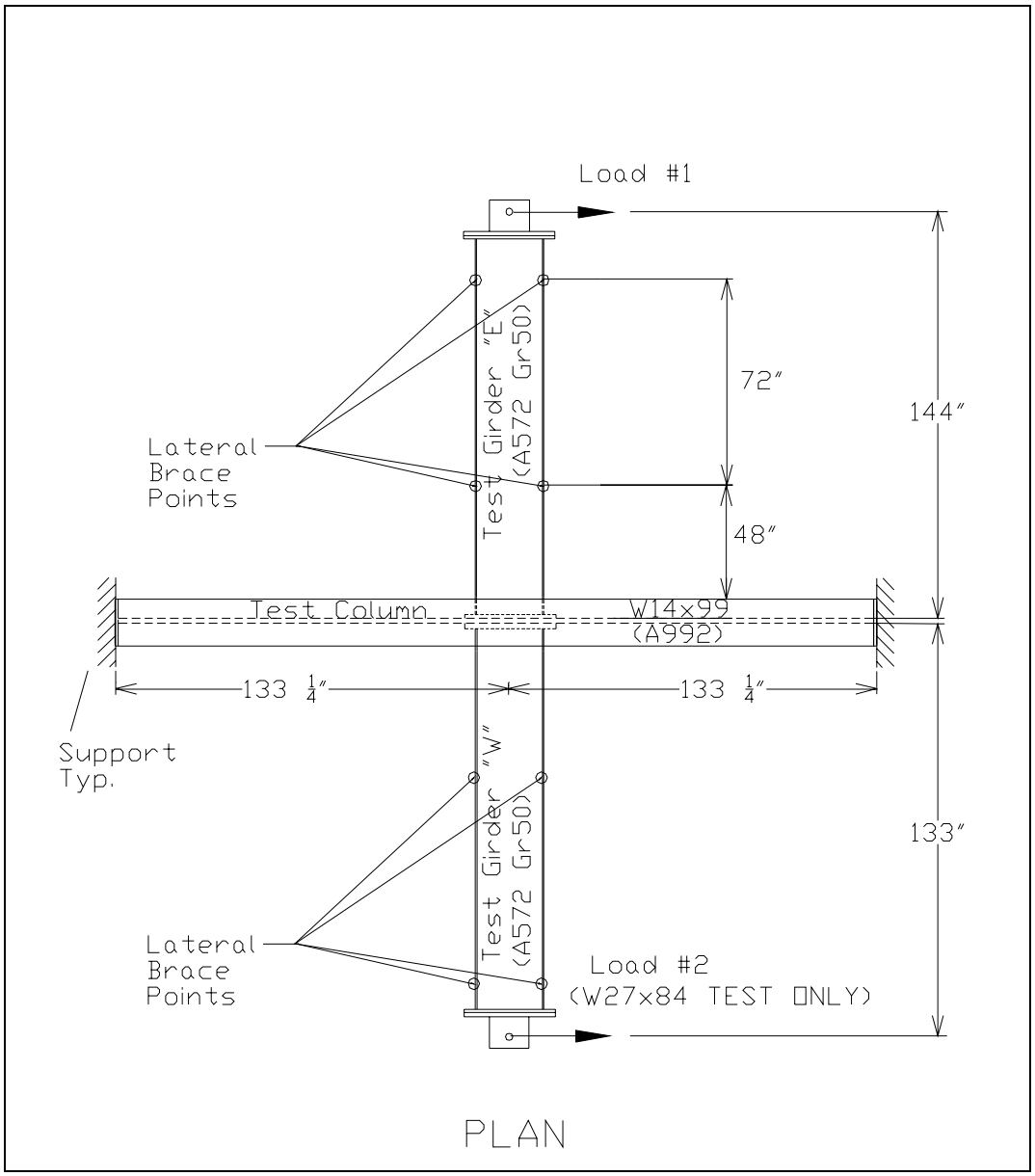

FIGURE 2.1: TEST SPECIMEN DETAIL, W24x55 AND W27x84

2.2.2 Test Setup

Testing was conducted in the horizontal position during loading. Figure 2.2 is a plan view of the specimen and reaction framing arrangement used for the W24x55 and W27x84 tests.

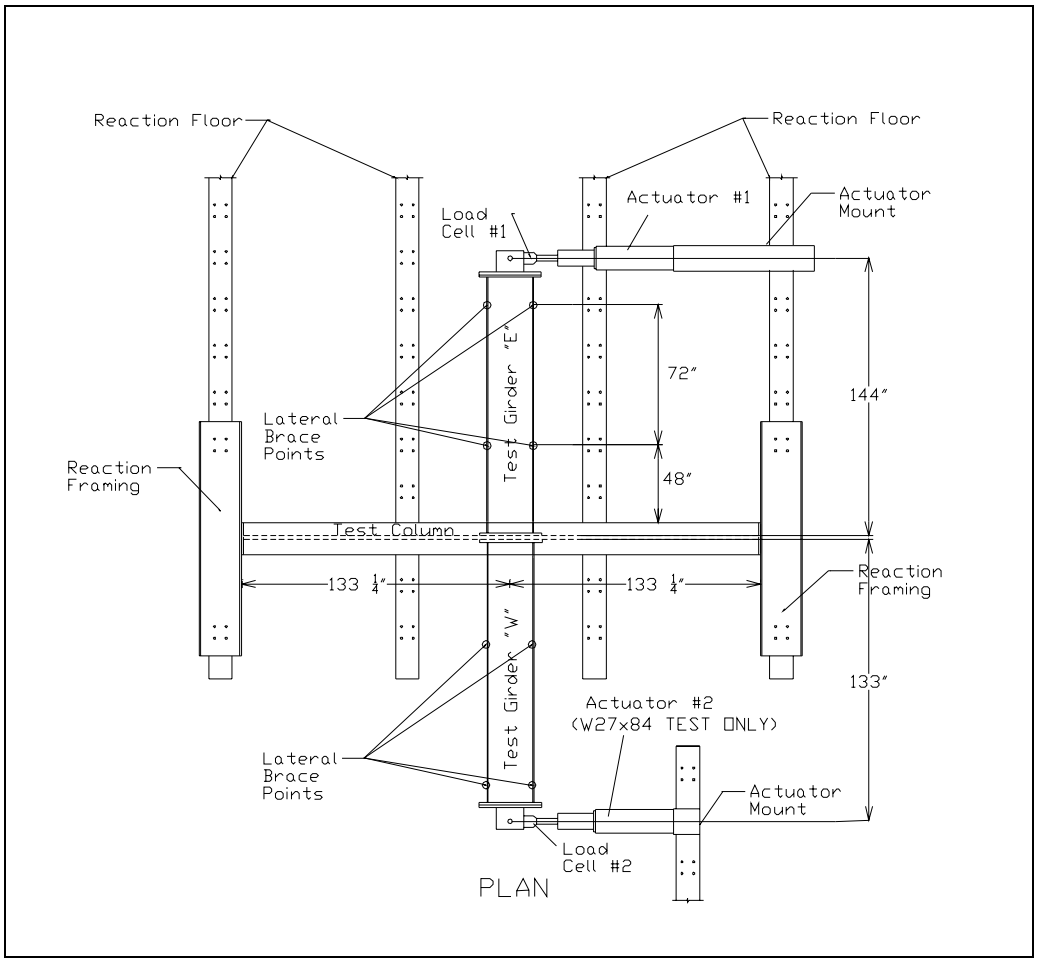

FIGURE 2.2: TEST SETUP, W24x55 AND W27x84

The ends of the test column were bolted to support beams, which in turn were bolted to the reaction floor. In each test, girders were connected to each side of the column web with eight A325-X torque-control bolts. For the W24x55 test, ¾ in.

diameter bolts were used, and for the W27x84 test, 1 in. diameter bolts were used. All bolts were tightened using a tone wrench. In the following sections of the report, the girder that was loaded until failure will be referred to as the East (E) girder, and the other girder will be referred to as the West (W) girder. To reduce gravity forces on the end-plate connections, a roller was used to support the free end of each girder. Lateral braces were provided at locations 4 ft and 10 ft from each connection faying surface to prevent lateral torsional buckling of each girder. A load cell was used to measure the load applied by a hydraulic ram.

2.2.3 Instrumentation

The instrumentation layout for the W24x55 and W27x84 tests is shown in Figure 2.3. A PC-based data acquisition system was used to collect the data from all of the instruments.

The girder tip displacements were measured using string-type potentiometers (ΔGTR, ΔGTL). Plunger-type potentiometers, one placed at each column end (ΔCT and ΔCB), were used to measure rigid-body rotation. The rigid body rotation is equal to the difference between the measured displacements at ΔCT and ΔCB, divided by the distance between those two instruments. Lateral translation of the test setup in the direction of the applied load was measured using a plunger-type potentiometer (ΔT), located at the girder end-plate. The net girder deflection at the girder tip is equal to the measured displacement at ΔGTR, minus the deflection due to rigid body rotation (determined using ΔCT and ΔCB), minus the lateral translation of the test setup. Plunger-type potentiometers (ΔDT and ΔDB) were also used to measure the net end-

plate and column web rotation at the girder flanges. Column web rotation is equal to the difference between the measured deflections (ΔDT and ΔDB), divided by the distance between the potentiometers. The net column web rotation is equal to the column web rotation minus the rigid body rotation.

For the W24x55 test, a single hydraulic ram was used to apply the load to the "E" girder. For the W27x84 test, two hydraulic rams were used to apply a load to each of the girders. The load from each hydraulic ram was measured using a compression-tension load cell, which was calibrated on a SATEC Universal Testing Machine prior to testing.

For each test, two bolts were instrumented with strain gages: one bolt outside the beam flange and one bolt inside the beam flange, diagonally opposite. The instrumented bolts were calibrated prior to testing. The bolts were connected to the data acquisition system prior to tightening. Bolt forces were monitored during tightening and testing.

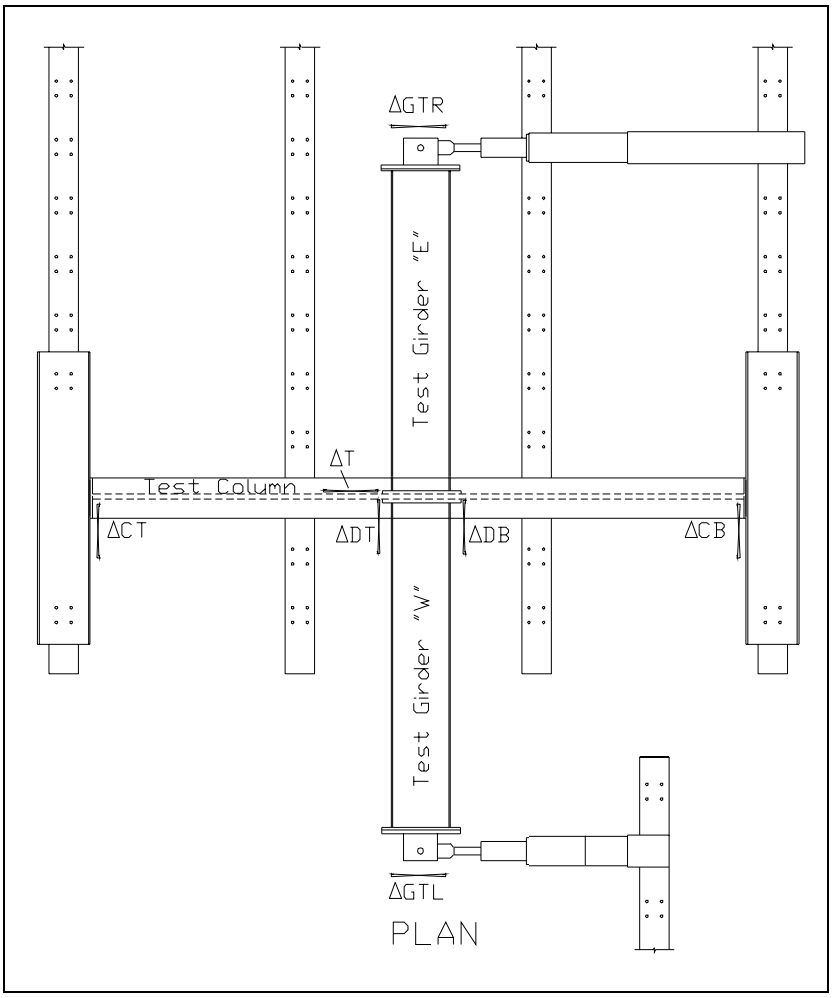

FIGURE 2.3: INSTRUMENTATION, W24x55 AND W27x84

2.2.4 Testing Procedure

The test girders were attached to the column, but the bolts were not tightened. All of the instruments were attached to the data acquisition system, and then the bolts were tightened and a check was made for proper calibration of all potentiometers. Then, a preload cycle of approximately one quarter of the expected failure load was applied and all PC output checked for accuracy. Any necessary adjustments were made before actual testing began.

Real-time plots of load versus deflection were generated as a visual reference. A theoretical load line also was added to ensure the test specimen behaved as predicted. Bolt forces and potentiometer displacements were monitored in real-time as load was applied.

The loading sequence used for the W24x55 test is a modification of Section S6.3 of the 1997 AISC Seismic Provisions for Structural Steel Buildings (AISC, 1997). Table 2.1 shows the modified loading sequence that was used. The value of the deformation quantity at first significant yield of each test specimen (δ_y) was determined analytically. For each cycle, the girder was loaded in the positive direction until the corresponding deflection was reached. Then, the positive load was removed and the girder was loaded in the negative direction with one-half of the positive load. Each Load Step consisted of three positive/negative cycles.

TABLE 2.1: MODIFIED LOADING SEQUENCE, TEST W24x55

Load Step	Number of Cycles	Required Deformation	Positive Load	Negative Load
I	3	0.50 δ_y	0.50 P_y	0.25 P_y
II	3	0.75 δ_y	0.75 P_y	0.375 P_y
III	3	1.00 δ_y	1.00 P_y	0.50 P_y
IV	3	1.50 δ_y	1.50 P_y	0.75 P_y
V	3	2.00 δ_y	2.00 P_y	1.00 P_y
VI	3	2.50 δ_y	2.50 P_y	1.25 P_y

The loading sequence used for the W27x84 test differed from the W24x55 test because two hydraulic rams were used. A second hydraulic ram and load cell was attached to the end of the girder that was not being tested to failure (West). This ram

was used to apply one-half the moment that was applied to the girder being tested to failure (East), up to a maximum load of 130 ft-kips. When this load was reached, a constant moment of 130 ft-kips was maintained on this girder. The other ram was used to load the East girder until failure. No load sequence was used. The load applied by each ram was increased at a uniform rate and neither girder was subjected to negative loading.

2.3 W27x84 with Concrete Slab Test

2.3.1 Test Specimen

Test specimen details are shown in Figure 2.4. The test girders were W27x84 and measured 164 in. long. Each girder had 1 in. end-plates welded to one end, and ½ in. full depth stiffeners at the reaction points. Six filler beams were supplied to support the slab. Each was attached to the girder web or column flanges with a shear tab and three ¾ in. A325 bolts. The four filler beams attached to the girder webs measured 41-¼ in. long, and the two attached to the column flanges measured 34-½ in. long.

The W14x99 test column measured 146-½ in. long and had a 1 in. thick plate welded on the bottom end to allow attachment to a pinned support. The column also had a 1 in. thick plate welded to the top and a ½ in. thick full depth stiffener at the point of load application to reduce web deformation. Load application was through a clevis attached to the web of the column at a location 72 in. above the center of the connection. The column had a hole pattern on the web to match the hole pattern on the test girder end-plates. As-measured connection drawings are in Appendix A.

The slab was constructed using lightweight concrete over 2 in.- 18 GA composite deck. The deck was puddle welded to the girders prior to the concrete placement. The slab was 6 ft. wide by 21 ft. long by 5-¼ in. deep. It was made partially composite in the direction perpendicular to the girders using ¾ in. x 3 - ½ in. welded shear studs, welded to the top flanges of the filler beams at approximately 12 in. on center. No shear studs were welded to the top of the W27x84 girders. The slab was reinforced with 6X6/W1.4XW1.4 welded wire fabric.

The test specimen girders and filler beams were ASTM A572 Grade 50 steel, the column was ASTM A992 steel, and all plate material was ASTM A36 steel. All bolts were 1 in. diameter A325-X. Tensile coupon tests were conducted by lab personnel, using material identical to that used for the girders, column, and end-plates. The measured yield stresses for the girders, column, and end-plates were 56.5 ksi, 54.7 ksi, and 41.1 ksi, respectively. Eight 4 in. diameter cylinders were cast at the time of the concrete placement. Two cylinders were tested to find the 7-days compressive strength of the slab and two were tested on the day of the first load sequence (21-days). The average 7-days compressive strength and 21-days compressive strength were 4.6 ksi and 6.7 ksi, respectively.

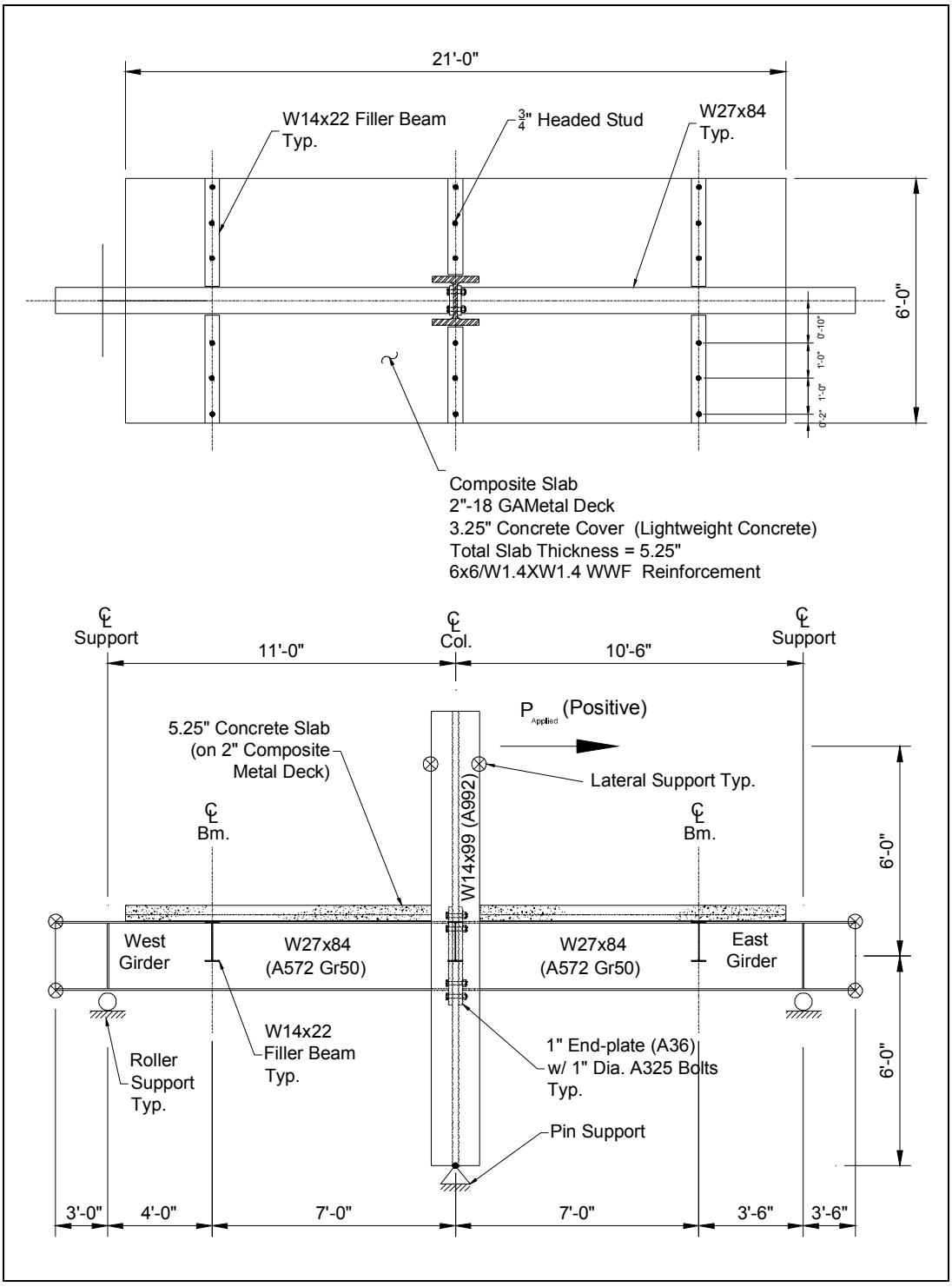

FIGURE 2.4: TEST SPECIMEN DETAIL, W27x84-SLAB

2.3.2 Test Setup

The connection was tested with the column standing vertical and the beams, girders, and slab spanning horizontally. Figure 2.5 is an elevation view of the test setup. The bottom end of the test column was bolted to a hinge, which in turn was bolted to the reaction floor. The column was laterally braced at a location 58 in. above the center of the connection. A clevis was attached to the web of the column at a location 72 in. above the center of the connection in order to apply a load to the connection. A load cell was used to measure the load that was applied by a hydraulic ram.

The girders were connected to each side of the column web with eight 1 in. diameter A325-X bolts. All bolts were tightened to a minimum bolt pretension of 51 kips using an impact wrench. The reaction location of the West girder was 132 in. from its connection faying surface and that of the East girder, was 126 in. from its connection faying surface. Each girder was laterally braced at a distance 142 in. from the respective connection faying surface. The vertical reactions at the two girder ends were measured using a load cell attached to a clevis connection on the girder and a hydraulic ram, which was attached to a pinned support. The hydraulic rams were "locked off" for the first five load sequences and were used to apply load during the two final load sequences.

In the following sections of the report, the girders will be referred to as the "East" and "West" girders, as labeled in Figure 2.5.

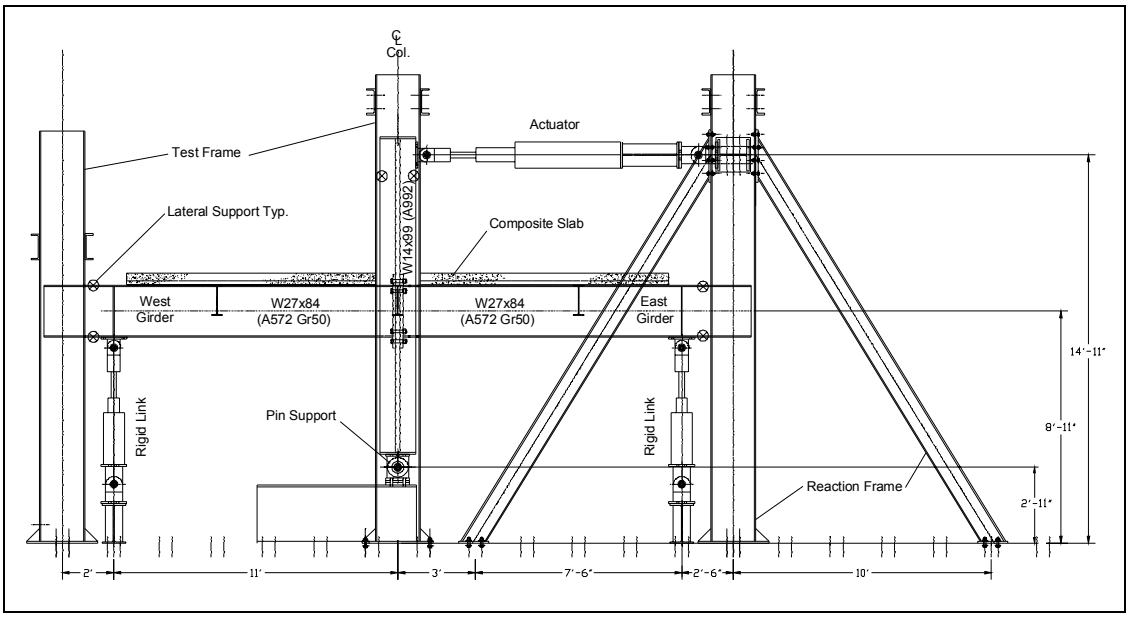

FIGURE 2.5: TEST SETUP, W27x84-SLAB

2.3.3 Instrumentation

Data was collected during the test using a PC-based data acquisition system and a number of instruments. The basic instrumentation layout for the test is shown in Figure 2.6.

The horizontal top column tip and west girder tip displacements were measured using string-type potentiometers (ΔHTC, ΔHWG). Lateral translation of the entire test setup in the direction of the applied load was measured using a plunger-type potentiometer (ΔHBC), located at the bottom plate of the column. The net horizontal top column tip displacement is equal to the measured displacement at ΔHTC, minus the lateral translation measured at ΔHBC. The net horizontal west girder tip displacement is equal to the measured displacement at ΔHWG, minus the lateral translation measured at ΔHBC. String-type potentiometers were used to measure the vertical east and west girder tip displacements (ΔVWG, ΔVEG). Plunger-type

potentiometers, one placed on each girder at the edge of the slab, were used to measure the slip between the slab and girders (ESlip, WSlip).

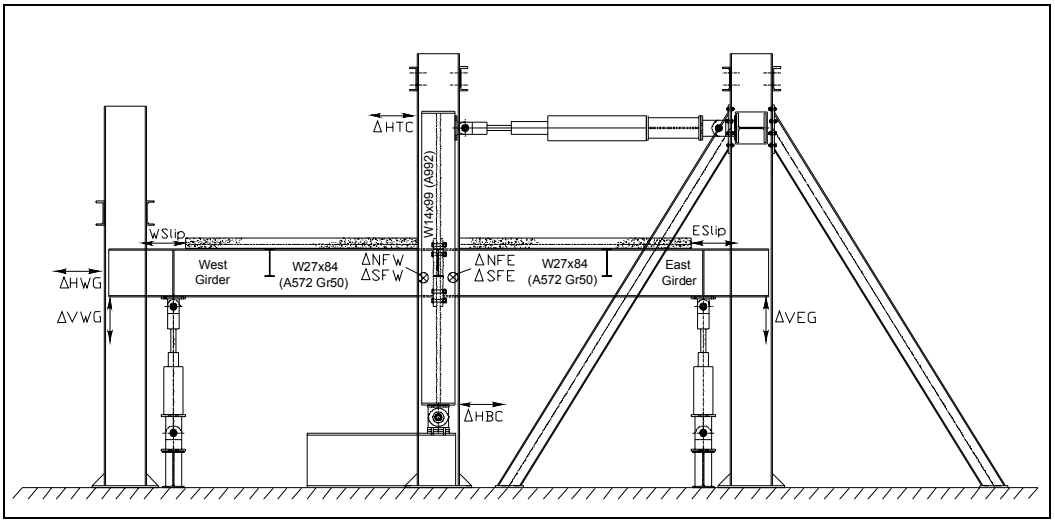

FIGURE 2.6: INSTRUMENTATION, W27x84-SLAB

Plunger-type potentiometers were used to measure the north and south column flange out of plane displacements at the center of the connection, located as shown in Figure 2.7. Two potentiometers were located on the east and west edges of the north column flange (ΔNFE, ΔNFW) and two were located on the east and west edges of the south column flange (ΔSFE, ΔSFW). The north column flange rotation is equal to the difference between the measured deflections at ΔNFE and ΔNFW, divided by the distance between the potentiometers. The south column flange rotation is equal to the difference between the measured deflections at ΔSFE and ΔSFW, divided by the distance between the potentiometers.

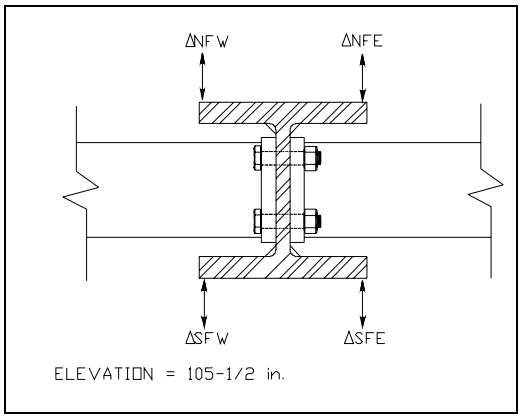

FIGURE 2.7: COLUMN FLANGE ROTATION, W27x84-SLAB

Two methods were used to measure the column web rotation. For Load Sequences 1 and 2, two plunger-type potentiometers, located as shown in Figure 2.8, were used. Each was attached to a steel bracket, which was clamped to the west side of the column between the two column flanges. One was located just below the girder end-plate (ΔBW) and the other was located just above the concrete slab (ΔTW). The web rotation is then the difference between the column web displacements (ΔBW and ΔTW), divided by the vertical distance between the potentiometers. This method of measurement was changed prior to the third loading sequence because the column flange rotation was loosening the clamps that attached the potentiometer brackets to the column flanges.

For the remaining load sequences, four string-type potentiometers were used to measure the column web rotation, as shown in Figure 2.8. Two were located just below the girder end-plate and measured the column web displacement (ΔBW) and the column flange displacement (ΔBF) in the direction of the applied load. The other two measured the column web displacement (ΔTW) and the column flange

displacement (ΔTF) just above the concrete slab. The net top and bottom web displacements are calculated by taking the difference between the web and flange displacements. The column web rotation is then determined by taking the difference between the net top and net bottom web displacements, and dividing by the vertical distance between the potentiometers.

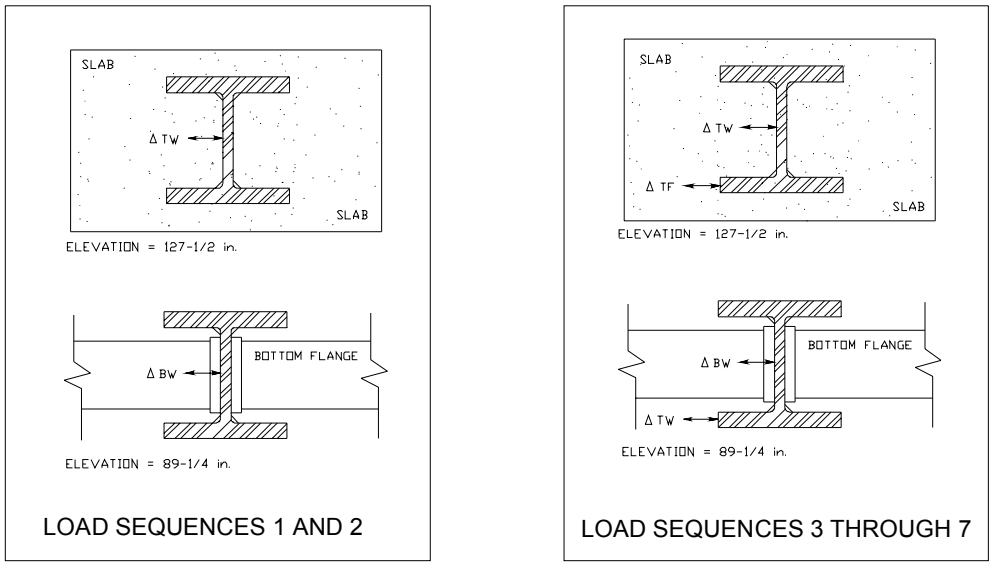

FIGURE 2.8: COLUMN WEB ROTATION, W27x84-SLAB

The load from the hydraulic ram, applied at the column tip, and the reactions at the girder tips were measured using compression-tension load cells. The load cells were calibrated on a SATEC Universal Testing Machine prior to testing.

Four bolts were instrumented with strain gages inserted in holes drilled through the bolt heads into the unthreaded portion of the bolt shank. One instrumented bolt was located outside each girder flange and one was located inside each girder flange, diagonally opposite. The instrumented bolts were calibrated prior to testing. The

bolts were connected to the data acquisition system prior to tightening. Bolt forces were monitored during tightening and testing.

2.3.4 Testing Procedure

The test girders were attached to the column and the connection bolts tightened to the required pretension. After the bolt pretension forces were recorded, they were disconnected from the data acquisition system and the deck and slab was constructed.

Once the slab cured, all of the instruments were connected to the data acquisition system, and a check was made for proper calibration of all potentiometers. A preload cycle of approximately one tenth of the expected failure load was then applied and all PC output checked for accuracy. Any necessary adjustments were made before actual testing began.

Real-time plots of load versus column tip deflection, load versus girder tip reactions, and load versus column web rotation were generated as a visual reference. A computed elastic deflection line was added to the load versus column tip deflection plot to compare to the actual behavior of the specimen. Bolt forces, girder tip reactions, column web rotations, and potentiometer displacements were monitored in real-time as load was applied.

CHAPTER 3

EXPERIMENTAL RESULTS

3.1 General

The performances of the connections in the three tests are discussed in the following sections. The specimens were evaluated based on the elastic stiffness of the connection and the overall strength of the connection. The connection area of each of the tests was whitewashed so areas of yielding could be easily recognized when the whitewash flaked off the specimen. Photographs showing the condition at the end of the tests, and the experimental Moment vs. Column Web Rotation plots, are included in each section. As-measured connection drawings are provided in Appendix A.

3.2 Bare Steel Test W24x55

In this test, the East girder was loaded until the connection failed, while the West girder was allowed to move freely on a roller. The loading sequence that was used for the test is shown in Table 3.1 as well as the measured girder deflections for each load cycle and the permanent set for each load step.

The specimen began to exhibit inelastic behavior during Load Step 2 at a load of approximately 200 ft-kips. During all three cycles of Load Steps 3 and 4 a significant amount of column distortion was seen, as illustrated in Figure 3.1. This distortion seemed to be elastic because the column appeared to return to its original shape when the load was removed. Prior to the completion of Load Cycle 5.2, at a moment of 350

ft-kips, all four bolts ruptured on the tension side. The failed connection can be seen in Figure 3.2.

Figure 3.3 is a plot of the Moment vs. Column Web Rotation. Appendix E contains plots of Moment vs. Chord Rotation and Bolt Tension vs. Moment for Test W24x55. This test is described in further detail in a separate Virginia Tech research report (Dominisse and Murray, 2003).

TABLE 3.1: TEST W24x55 LOADING SEQUENCE

TEST W24x55 LOADING SEQUENCE

Step	Cycle	Positive Moment (ft-kips)	Displacement (in.)	Negative Moment (ft-kips)	Displacement (in.)
I	1	161.4	2.025	-78.5	-0.886
	2	161.4	2.028	-80.2	-0.903
	3	160.7	2.020	-79.2	-0.884
	Permanent Set = 0.101				
II	1	232.2	3.242	-123.8	-1.307
	2	233.9	3.256	-124.4	-1.294
	3	234.6	3.272	-124.4	-1.295
	Permanent Set = 0.242				
III	1	280.9	4.418	-147.0	-1.372
	2	279.2	4.422	-148.0	-1.373
	3	279.2	4.418	-149.6	-1.377
	Permanent Set = 0.502				
IV	1	331.2	6.608	-167.4	-1.178
	2	330.2	6.616	-165.1	-1.120
	3	328.2	6.611	-164.0	-1.101
	Permanent Set = 1.195				
V	1	349.7	8.095	NA	NA
	2	NA	NA	NA	NA
	3	NA	NA	NA	NA
	Permanent Set = NA				

FIGURE 3.1: COLUMN DISTORTION, TEST W24x55

FIGURE 3.2: BOLT RUPTURE AT END OF TEST W24x55

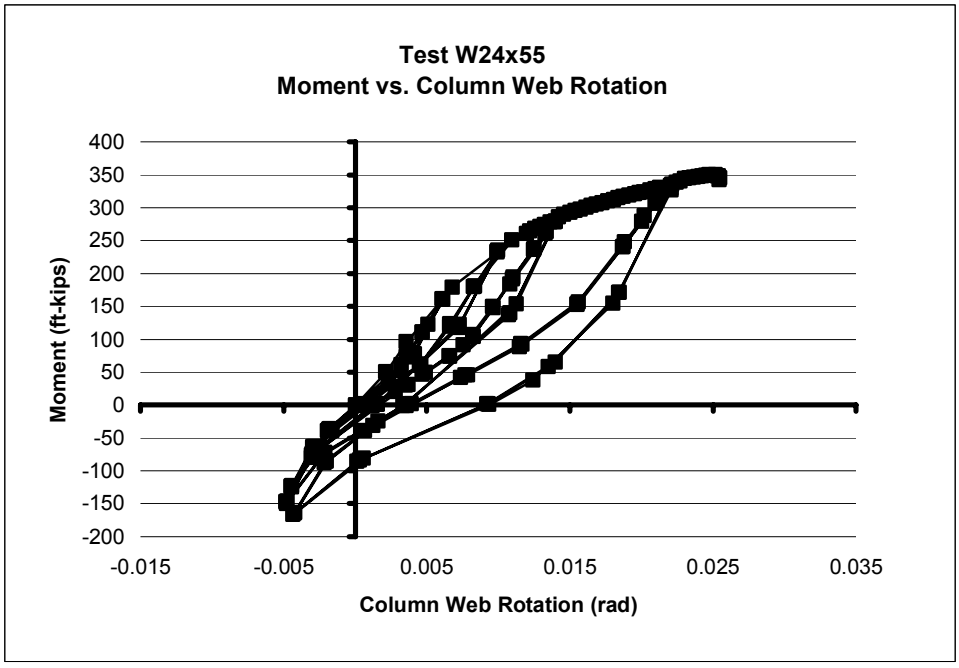

FIGURE 3.3: MOMENT VS. COLUMN WEB ROTATION, TEST W24x55

3.3 Bare Steel Test W27x84

In this test, a loading sequence was not used. The East girder was loaded with a positive moment until the connection failed. The West girder was subjected to the same moment as the East girder until 130 ft-kips was reached. Above that load level on the East girder, the moment on the West girder was held constant at 130 ft-kips. The East girder was then loaded until failure while the load of 130 ft-kips was maintained on the West girder.

During the test, a significant amount of column distortion could be seen. This distortion seemed to be elastic because the column appeared to return to its original shape when the load was removed. A significant amount of end-plate separation and column web distortion was also observed on the tension side of the East girder

(Figure 3.4). At a moment of 751 ft-kips, all four bolts ruptured on the tension side. The failed connection can be seen in Figure 3.5.

Figure 3.6 is a plot of the Moment vs. Column Web Rotation. Appendix F contains plots of Moment vs. Chord Rotation and Bolt Tension vs. Moment for Test W27x84. This test is described in further detail in a separate Virginia Tech research report (Dominisse and Murray, 2003).

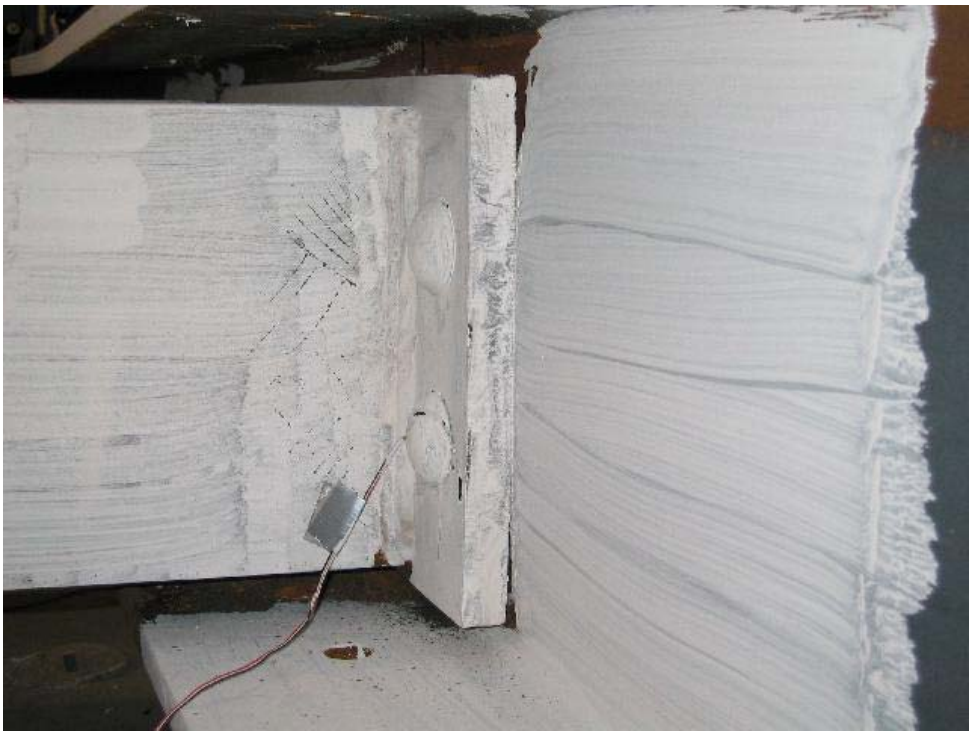

FIGURE 3.4: END-PLATE SEPARATION AND COLUMN WEB DISTORTION, TEST W27x84

FIGURE 3.5: BOLT RUPTURE AT END OF TEST W27x84

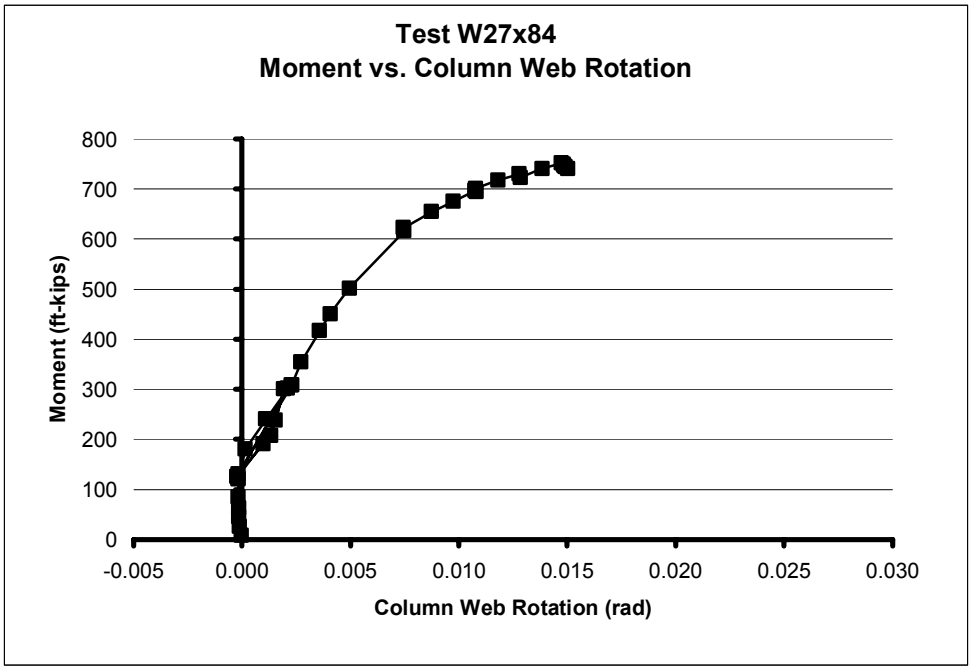

FIGURE 3.6: MOMENT VS. COLUMN WEB ROTATION, TEST W27x84

3.4 Test W27x84 with Concrete Slab

The performance of the connection in load sequences #1, #5 and #7 from Test W27x84-Slab is discussed in the following sections. Experimental Moment vs. Column Web Rotation and Moment vs. Column Flange Rotation plots are included in each section. Appendix G contains plots of Moment vs. Column Tip Deflection, Moment vs. Slab Slip, Moment vs. Girder Tip Reaction, and Bolt Tension vs. Moment for Load Sequences #1 and #5. For Load Sequence #7, plots of Bolt Tension vs. Moment are not included because the instrumented bolts were replaced with non-instrumented bolts prior to testing. Test W27x84-Slab, including all seven load sequences, is described in further detail in a separate Virginia Tech research report (Dominisse and Murray, 2004).

3.4.1 Load Sequence #1

During Load Sequence #1, load was applied using the actuator attached to the top of the column. The connection was loaded in both the positive (east) and negative (west) directions. Each Load Step included three cycles in which the applied negative load was one-half of the applied positive load. The loading sequence that was used, as well as the corresponding moment and measured column tip deflections for each load cycle, are shown in Table 3.2.

Figure 3.7 is a plot of the Moment vs. Column Web Rotation. Only load cycles 1.1 through 2.1 are shown. After the completion of load cycle 2.1, column flange rotations loosened the clamps that held the instrumentation brackets used for measuring column web deflections. This caused the plot to gradually shift leftward

and made the web rotation data obtained after load cycle 2.1 difficult to analyze. Figure 3.8 is a plot of the Moment vs. Column Flange Rotation.

TABLE 3.2: LOAD SEQUENCE #1, TEST W27x84-SLAB

Load Applied to Top Column Tip (East - Positive)					
Step	Cycle	Moment (ft-kips)	Displacement (in.)	Moment (ft-kips)	Displacement (in.)
I	1	49.0	0.258	-24.8	-0.224
	2	50.2	0.265	-25.0	-0.224
	3	49.8	0.271	-24.7	-0.219
II	1	100.0	0.576	-50.2	-0.362
	2	101.0	0.596	-50.2	-0.359
	3	100.0	0.599	-49.8	-0.361
III	1	150.0	1.006	-74.3	-0.462
	2	149.5	1.014	-74.5	-0.462
	3	150.8	1.034	-75.0	-0.466
IV	1	199.8	1.452	-100.5	-0.633
	2	199.2	1.473	-101.8	-0.655
	3	199.8	1.501	-102.5	-0.671
V	1	250.3	1.995	-125.7	-0.861
	2	250.2	2.019	-124.2	-0.855
	3	250.2	2.056	-125.2	-0.862

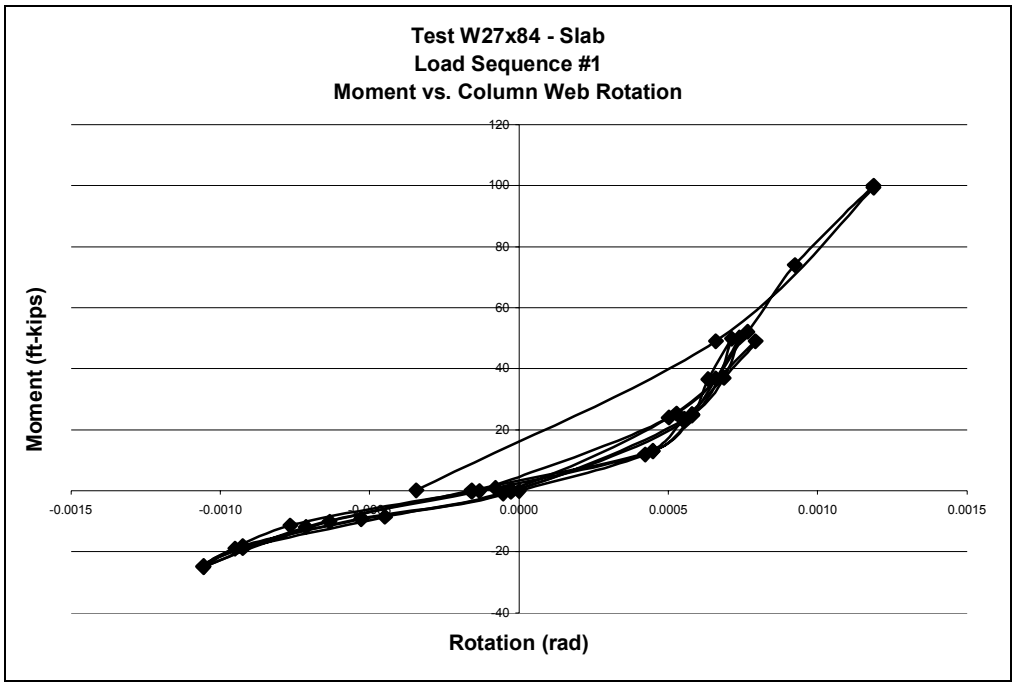

FIGURE 3.7: MOMENT VS. COLUMN WEB ROTATION, TEST W27x84-SLAB, LOAD SEQUENCE #1

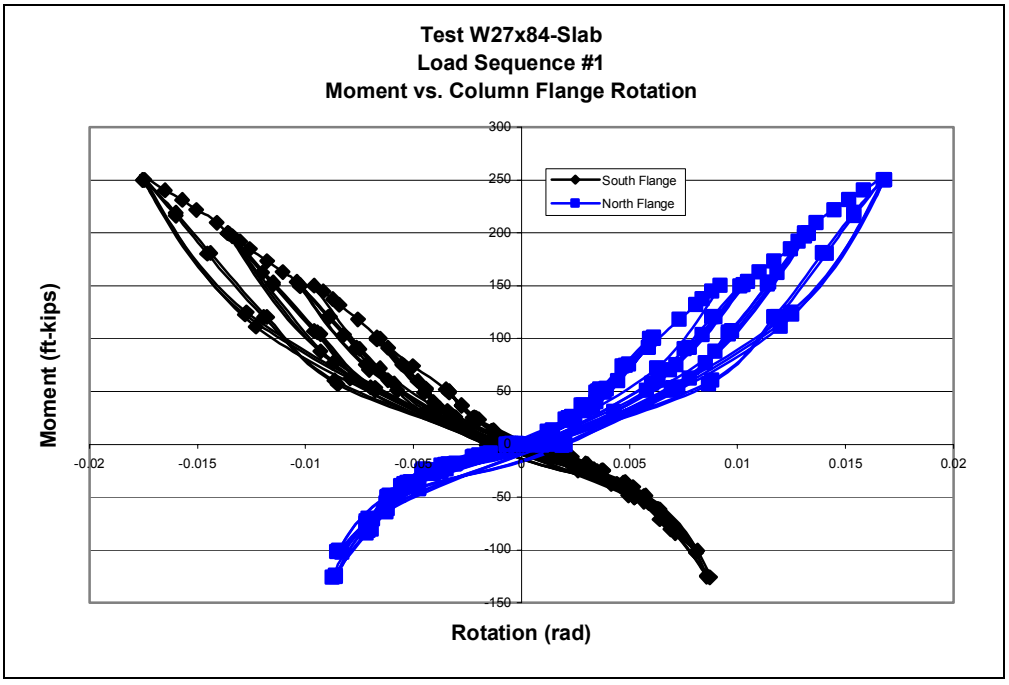

FIGURE 3.8: MOMENT VS. COLUMN FLANGE ROTATION, TEST W27x84-SLAB, LOAD SEQUENCE #1

3.4.2 Load Sequence #5

During Load Sequence #5, load was applied using the actuator attached to the top of the column. The connection was loaded in both the positive and negative directions. Each Load Step included three cycles in which the applied positive load was the same as the applied negative load. The loading sequence that was used, as well as the corresponding moment and measured column tip deflections for each load cycle, are shown in Table 3.3.

In the middle of both the positive and negative portions of Load Cycle 5.3, loud "crushing" sounds were heard. After each sound, the applied load immediately dropped approximately 10 kips. Once loading was resumed, the Load vs. Deflection plot returned to the point from which it dropped and continued with the same slope as it had before the sound. After the completion of the load cycle, crushing of the concrete was observed around the column flanges. The crushing sounds continued throughout all the remaining load cycles in Load Sequence #5. The crushing of the concrete around the east side of the column is shown in Figure 3.9.

Whitewash flaking was observed on the exterior sides and edges of the column flanges. The condition of the north and south column flanges after the load sequence is shown in Figures 3.10 and 3.11.

Figure 3.12 is a plot of the Moment vs. Column Web Rotation and Figure 3.13 is a plot of the Moment vs. Column Flange Rotation.

TABLE 3.3: LOAD SEQUENCE #5, TEST W27x84-SLAB

Load Applied to Top Column Tip (East - Positive)					
Step	Cycle	Moment (ft-kips)	Displacement (in.)	Moment (ft-kips)	Displacement (in.)
I	1	102.3	0.993	-103.5	-1.287
	2	100.3	0.986	-92.4	-1.214
	3	101.3	1.000	-100.5	-1.245
II	1	199.8	1.698	-201.8	-2.019
	2	199.7	1.708	-200.8	-2.003
	3	199.8	1.722	-201.0	-1.995
III	1	250.3	2.063	-249.5	-2.305
	2	249.5	2.073	-250.2	-2.317
	3	249.8	2.083	-249.3	-2.329
IV	1	301.0	2.577	-300.0	-3.082
	2	299.7	2.459	-299.8	-3.098
	3	299.7	2.486	-299.8	-3.117
V	1	336.9	3.004	-338.9	-3.681
	2	323.2	2.903	-322.8	-3.641
	3	328.4	3.007	-332.6	-3.676
VI	1	360.6	3.518	-363.4	-4.197
	2	353.7	3.505	-359.6	-4.207
	3	351.5	3.512	-355.0	-4.196
VII	1	376.8	4.016	-382.9	-4.702
	2	372.3	4.000	-374.3	-4.709
	3	368.0	4.009	-373.5	-4.705

FIGURE 3.9: CONCRETE CRUSHING ON EAST SIDE OF COLUMN

FIGURE 3.10: WHITEWASH FLAKING ON NORTH COLUMN FLANGE AFTER COMPLETION OF LOAD SEQUENCE #5

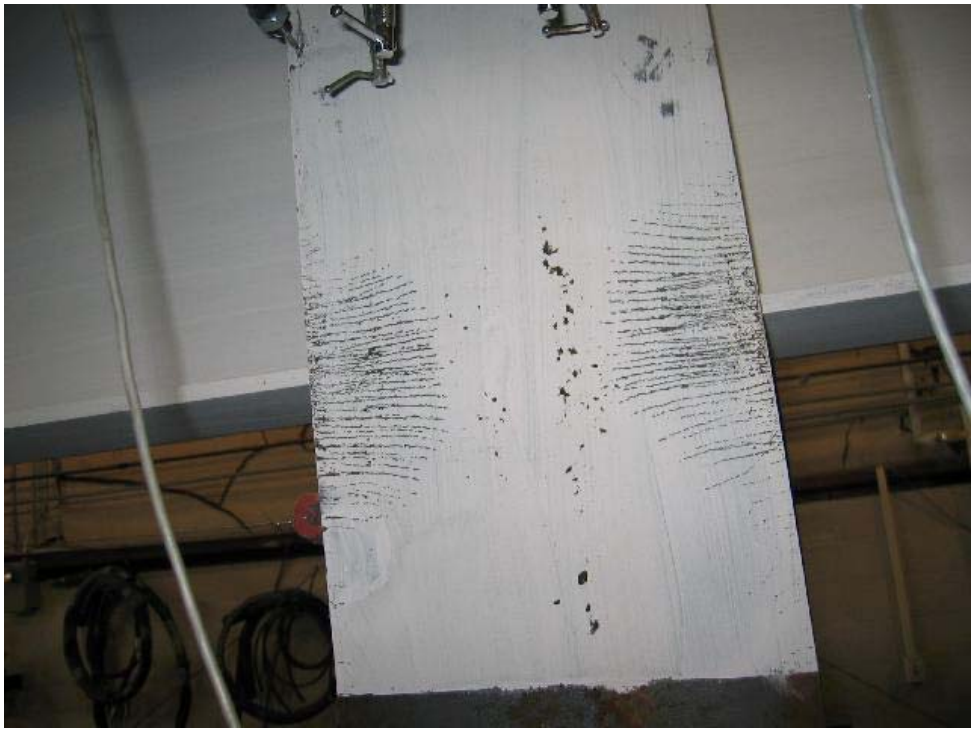

FIGURE 3.11: WHITEWASH FLAKING ON SOUTH COLUMN FLANGE AFTER COMPLETION OF LOAD SEQUENCE #5

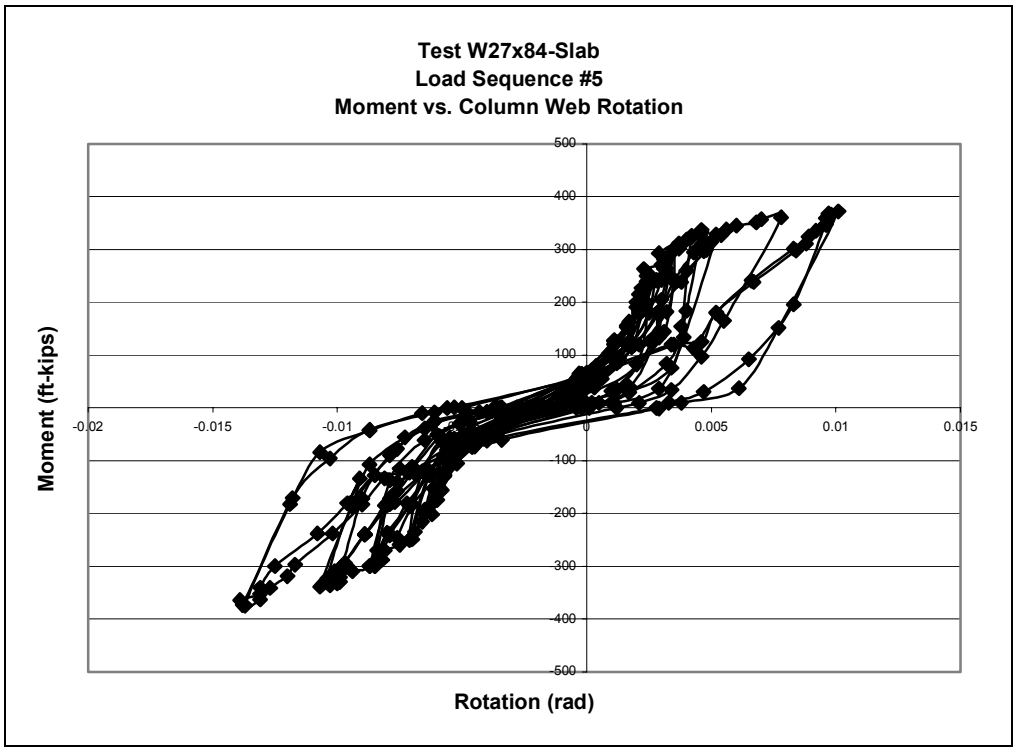

FIGURE 3.12: MOMENT VS. COLUMN WEB ROTATION, TEST W27x84-SLAB, LOAD SEQUENCE #5

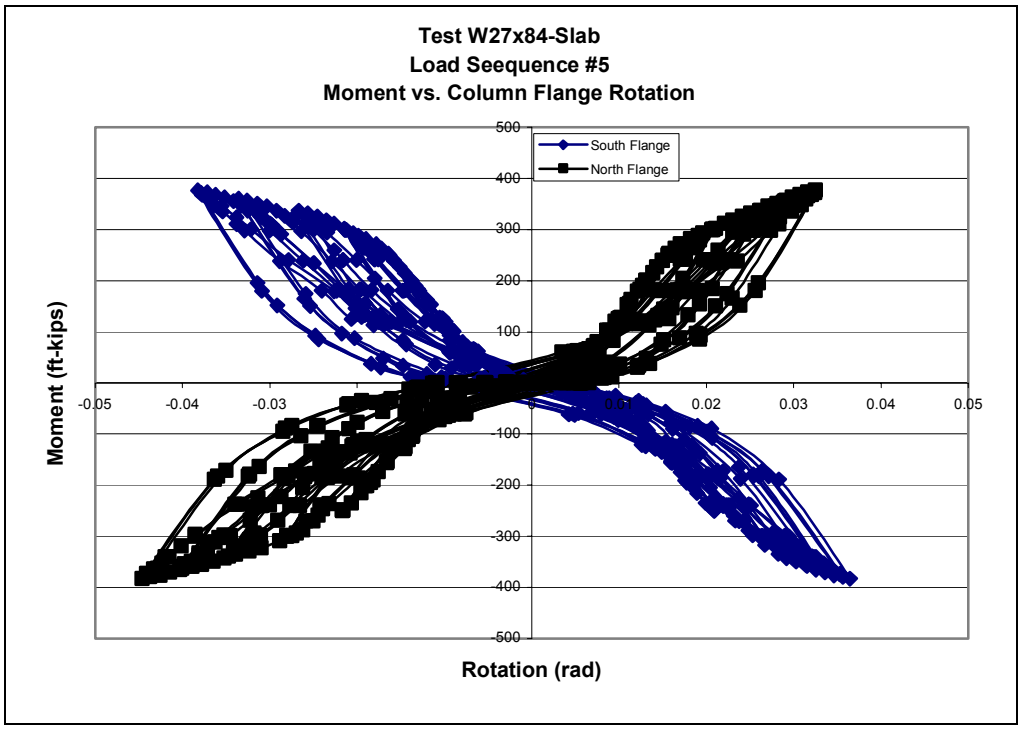

FIGURE 3.13: MOMENT VS. COLUMN FLANGE ROTATION, TEST W27x84-SLAB, LOAD SEQUENCE #5

3.4.3 Load Sequence #7

During Load Sequence #7, load was applied using only the east actuator. The east actuator was used to apply a positive (up) load to the tip of the east girder. The load was gradually increased until the connection failed.

At a moment of 754 ft-kips the two interior bolts in the bottom bolt configuration ruptured. Figure 3.14 is a photograph of the failed connection.

Figure 3.15 is a plot of the Moment vs. Column Web Rotation and Figure 3.16 is a plot of the Moment vs. Column Flange Rotation.

FIGURE 3.14: FAILED CONNECTION / INTERIOR BOLT RUPTURE, W27x84-SLAB

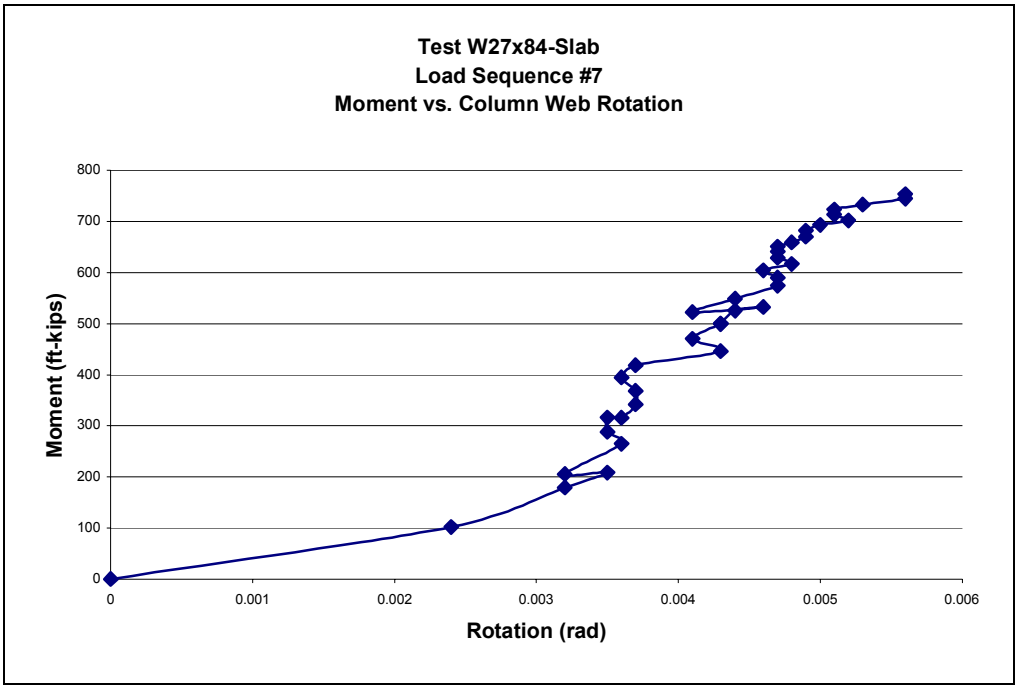

FIGURE 3.15: MOMENT VS. COLUMN WEB ROTATION, TEST W27x84-SLAB, LOAD SEQUENCE #7

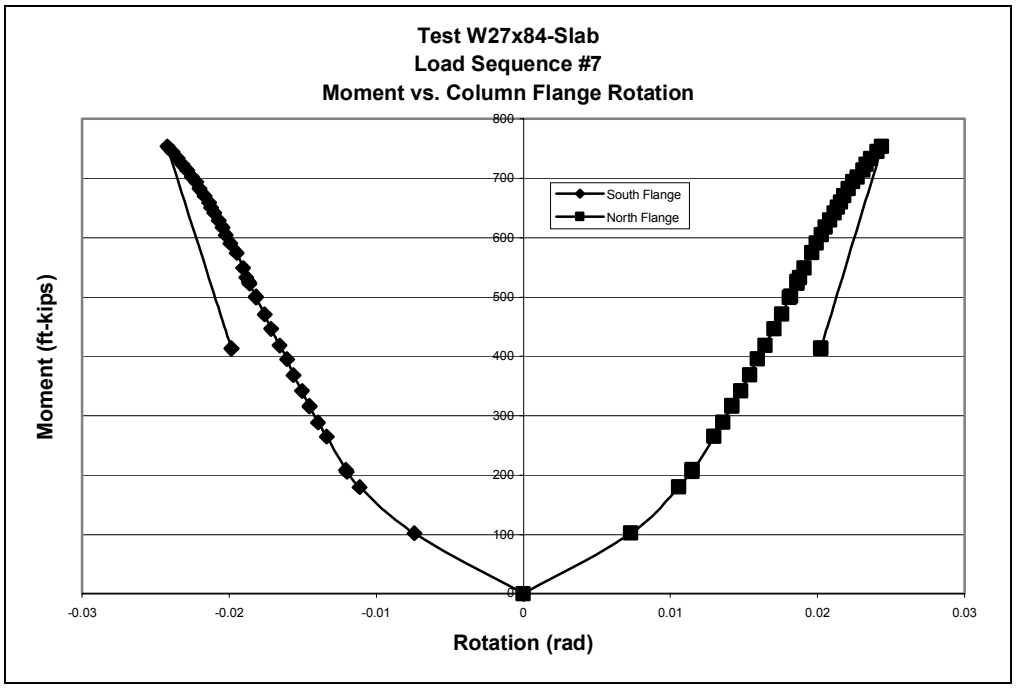

FIGURE 3.16: MOMENT VS. COLUMN FLANGE ROTATION, TEST W27x84-SLAB, LOAD SEQUENCE #7

3.5 Summary

In each experimental test a significant amount of column web deformation was observed and measured. In the bare steel tests, W24x55 and W27x84, the column web began to yield at approximately 50% of the connection failure moments. In test W27x84-Slab, the column web began to yield at approximately 25% of the connection failure moment. Column flange deformation was also observed in each test, however it was only measured in test W27x84-Slab.

All three tests failed due to bolt rupture on the tension side of the connection. Tests W27x84 and W27x84-Slab failed at nearly the same moment of 750 ft-kips.

CHAPTER 4

FINITE ELEMENT ANALYSIS

4.1 General

Linear elastic finite element models were created for each of the three experimental tests to investigate the elastic stiffness of the connections. The models were developed in the SAP2000, version 8.3.3, commercial software (SAP2000 Analysis Reference Manual, 2002). A simplified modeling procedure was developed to overcome the contact problems between the end-plates and the column web, and between the bolts and holes in the end-plates and web. The following sections describe the elements used, modeling procedures and techniques, individual model details, and results.

4.2 Element Selection

Four-node shell elements were used to create the models in SAP2000. Solid elements were also an option; however, they would have required an excessive amount of computer memory and analysis time. The shell element was chosen because it combines separate membrane and plate bending behavior. The membrane behavior includes translational in-plane stiffness components and a rotational stiffness component in the direction normal to the plane of the element. The plate-bending behavior includes two-way, out-of-plane, plate rotation stiffness components and a translational stiffness in the direction normal to the plane of the element (SAP2000 Analysis Reference Manual, 2002).

Two formulations exist for the shell element, thin-plate and thick-plate. The thin-plate formulation neglects transverse shearing deformation, while the thick-plate formulation includes the effects of transverse shearing deformation. The thick-plate formulation was used in these models.

The shell element also includes the option of modeling pure membrane behavior, pure plate behavior, or full shell behavior. Since the models are three-dimensional, the full shell behavior was chosen.

4.3 Mesh Selection

The column and girders in each test were modeled with a mesh that was one element thick. Each element was given a membrane and bending thickness that was the same as the corresponding thickness of the part of the specimen represented, except as noted in the simplified design procedure.

To maintain the geometry of the specimens, separate mesh sizes were used to model the girders, column, and end-plates. In general, a square mesh ranging between 1 in. by 1 in. to 1.3 in. by 1.3 in. was used. If allowed by the geometry of the specimens, the mesh was transitioned to a coarser mesh of 2 in. by 2 in. or 4 in. by 4 in. elements. The transition was made at a distance from the connection equal to twice the depth of the beam.

To maintain the geometry in the area of the connection, rectangular elements were used. When rectangular elements are used, the aspect ratio of the elements is a concern. The aspect ratio is defined as the ratio of the length to width of the element. Large aspect ratios can cause the program to generate an incorrect element stiffness.

An aspect ration between 1.0 and 1.5 is considered ideal for finite element modeling. The largest aspect ratio used in the models was 1.3, and therefore all elements were considered adequate.

4.4 Material Properties

All materials used in the models were considered to be linearly elastic. Since SAP2000 is incapable of representing the inelastic behavior of the connection, the models were only used to investigate its elastic stiffness.

The steel elements used in the model were assigned a modulus of elasticity of 29,000 ksi and a Poisson's ratio of 0.3. The lightweight concrete elements used in the W27x84-Slab model were assigned a modulus of elasticity of 3,600 ksi and a Poisson's ratio of 0.2.

4.5 Results Verification

A cantilever beam, representing the W27x84 girder section used in the models, was developed with shell elements to verify the deflection results from SAP2000. The beam was created with two separate mesh sizes, 1.1 in. by 1.1 in. and 0.55 in. by 0.55 in., to illustrate the convergence of the results

The beam was 80.3 in. long. The beam flanges were 8.8 in. wide and 0.64 in. thick, and the web was 26.4 in. high and 0.46 in. thick. A concentrated load of 10 kips was applied at the end of the section. The nodes on the other end of the beam were restrained for all translational and rotational degrees of freedom. The verification beam with the 1.1 in. by 1.1 in. mesh is shown in Figure 4.1.

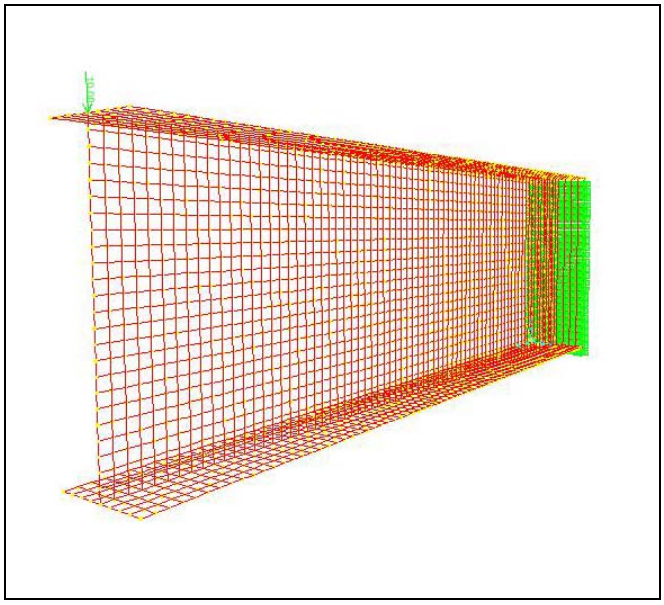

FIGURE 4.1: VERIFICATION BEAM WITH 1.1" x 1.1" MESH

A theoretical deflection was calculated for the beam using the formula

$$\Delta = \frac{PL^3}{3EI} + \frac{PL}{Gd_b t_w} \tag{4.1}$$

In Equation 4.1, Δ is the beam-tip deflection, P is the applied load, L is the length of the beam, E is the modulus of elasticity, I is the moment of inertia, G is the shear modulus of elasticity, d_b is the depth of the beam, and t_w is the width of the beam web. The theoretical deflection of the beam tip was 0.0282 in. The deflection values from SAP2000 were 0.0267 in. for both mesh sizes. This represents a 5.4% discrepancy between the theoretical and analytical deflections. Because both mesh sizes produced the same result, it was determined that the 1.1 in. by 1.1 in. mesh was adequate for predicting deflections.

4.6 Contact Problems

There are two contact problems associated with the connection models: the contact between the end-plates and column web, and the contact between the bolts and the holes in the end-plates and the column web. Neither of these problems is easily solved in SAP2000. Modeling the faying surfaces and the contact between the bolts and holes was beyond the scope of this research, so simplified modeling procedures were developed.

4.7 Simplified Modeling Procedures

The contact problems associated with the faying surfaces between the end-plates and the column web were eliminated by developing a simplified modeling procedure. Two simplified methods were investigated: modeling the end-plates and web with separate elements located in the same plane, and modeling the end-plates and web with a single mesh with an effective bending thickness. The second procedure proved to be more effective. This method also eliminated the need for modeling the bolts and the contact problem associated with them.

Instead of modeling an end-plate on the end of each girder and attempting to attach it to the column web, the elements in the section of the column web that would be in contact with the end-plates were given an effective bending thickness. All elements of the column web that were not in contact with the end-plates had a bending thickness equal to the thickness of the web. The bending thickness used for the elements in the end-plate/web section was calculated using

$$\frac{t_e^3}{12} = \frac{\Sigma t_i^3}{12} \tag{4.2}$$

where t_e is the effective bending thickness of the end-plate/web elements and t_i is the thickness of the individual end-plate and web components. The membrane thickness for the elements in the end-plate/web area was calculated using the equation

$$t_m = \Sigma t_i \tag{4.3}$$

In Equation 4.3, t_m is the membrane thickness of the end-plate/web elements and t_i is defined above. This process gave the connection the stiffness that was desired without the need to develop an intricate model that included the faying surfaces.

The other problem that was encountered was modeling the bolts in the connections and attaching the girders to the end-plate/column web at the appropriate locations. Because the end-plates and column web were not modeled separately, the bolts were not needed in the models; however, if the entire cross section of each girder is attached to the end-plate/web section, then the forces are not transferred at the right locations. On the tension side of the end-plate, it is desirable to transfer the load to the column web at the location of the bolts since the bolts are pulling on the web. On the compression side of the connection, it is desirable to transfer the load to the web through the girder flange because the flange is pushing on the web. Because the girders were not modeled with the end-plates attached to the ends, it was not possible to transfer the load at the location of the bolts. To overcome this problem, each girder end was offset from the column web by 0.11 in. and a very stiff plate was attached to the girder end. These plates did not contribute to the stiffness of the connection. They were only used to allow load transfer at the location of the bolts. Pipe sections with the same material properties and moment of inertia as the bolts were used to attach the stiff plate to the end-plate/web section at the locations of the

bolts on the tension side of the connection. Rigid links were used to attach each node along the girder compression flange to the end-plate/web section. The attachment of the girders to the end-plate/web section is illustrated in Figure 4.2.

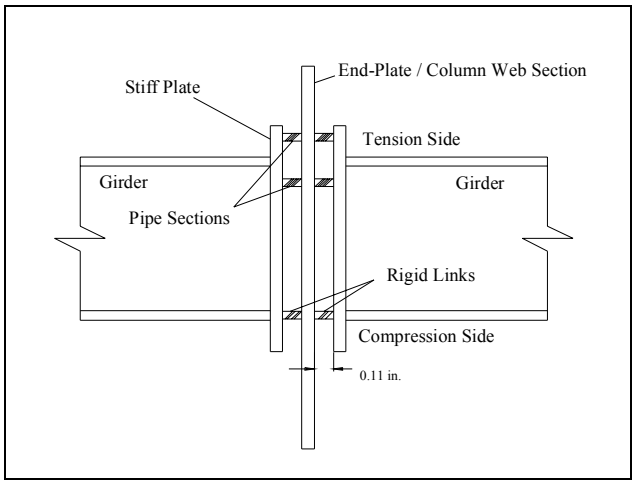

FIGURE 4.2: ATTACHMENT OF GIRDERS TO END-PLATE/WEB SECTION

4.8 Loading

The moments applied to the connections were chosen based on the experimental results of each test. The moments that were chosen had produced elastic column web rotations in the experimental tests and could be matched to a specific web rotation value from each test.

4.9 Model Descriptions

4.9.1 Bare Steel Model W24x55

Test W24x55 was modeled with a W14x99 column that was 265.2 in. long and two W24x55 girder sections that were 144.1 in. long (East) and 130.9 in. long (West).

The shell elements that were used to create the flanges and web of each section were given a bending and membrane thickness equal to the actual thickness of the experimental section's flange or web. The end-plate/web elements were given a calculated bending thickness and membrane thickness of 0.986 in. and 1.985 in., respectively. The model for test W24x55 is shown in Figure 4.3.

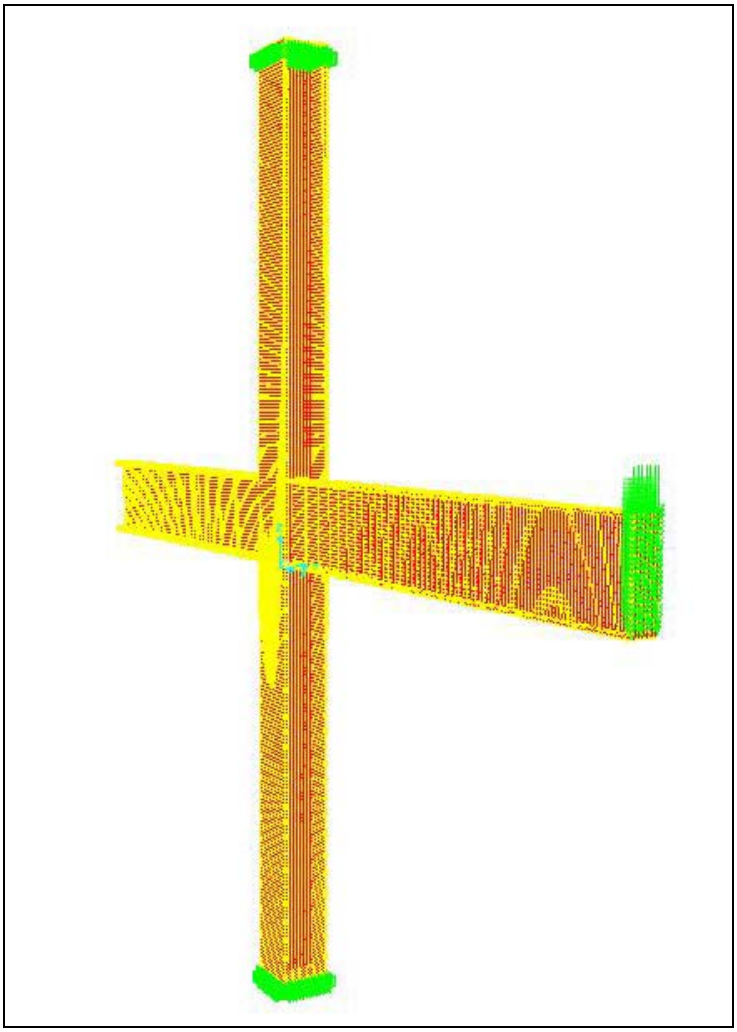

FIGURE 4.3: MODEL OF TEST W24x55

Each girder was attached to the end-plate/web section of the column using the simplified modeling procedure described in Section 4.7. On the tension side of the connection, the girder was attached to the end-plate/web section with Standard Weight ½ in. diameter steel pipe sections at the locations of the bolts, and on the compression side of the connection the girder was attached with rigid links at every node along the girder flange.

All nodes on both ends of the column were restrained for all six degrees of freedom, representing a fixed support. A stiff end-plate was modeled on the East girder end, opposite of the connection. This plate represented the clevis that was used for load application during the experimental test. The moment was applied to the connection by applying a uniformly distributed load to the nodes of this plate. The East girder was used to apply a moment of 161 ft-kips to the connection. The end of the West girder, opposite the connection, was allowed to move freely.

4.9.2 Bare Steel Model W27x84

Test W27x84 was modeled with a W14x99 column that was 265.2 in. long and two W27x84 girder sections that were 144.1 in. (East) and 130.9 in. long (West). The shell elements that were used to create the flanges and web of each section were given a bending and membrane thickness equal to the actual thickness of the experimental section's flange or web. The end-plate/web elements were given a calculated bending thickness and membrane thickness of 1.283 in. and 2.485 in., respectively. The model for test W27x84 is sown in Figure 4.4.

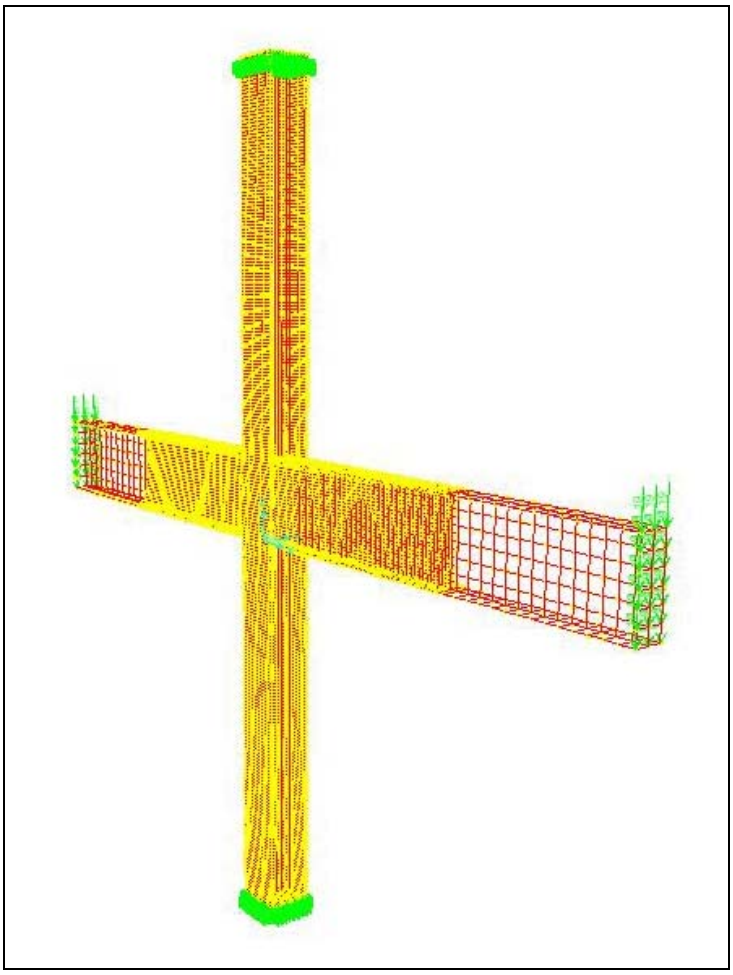

FIGURE 4.4: MODEL OF TEST W27x84

Each girder was attached to the end-plate/web section of the column using the simplified modeling procedure described in Section 4.7. On the tension side of the connection, the girder was attached to the end-plate/web section with Standard Weight ¾ in. diameter steel pipe sections at the locations of the bolts, and on the compression side of the connection the girder was attached with rigid links at every node along the girder flange.

All nodes on both ends of the column were restrained for all six degrees of freedom, representing a fixed support. A stiff end-plate was modeled on the East and

West girder ends, opposite of the connection. Each plate represented the clevis that was used for load application during the experimental test. The moment was applied to the connection by applying a uniformly distributed load to the nodes of each plate. The west girder was used to apply a moment of 130 ft-kips, and the east girder was used to apply a moment of 300 ft-kips.

4.9.3 W27x84-Slab

Test W27x84-Slab was modeled with a W14x99 column that was 152.8 in. long and two W27x84 girder sections that were 126.5 in. long. The shell elements that were used to create the flanges and web of each section were given a bending and membrane thickness equal to the actual thickness of the experimental section's flange or web. The end-plate/web elements were given a calculated bending thickness and membrane thickness of 1.283 in. and 2.485 in., respectively.

This model also included a lightweight concrete slab supported by the girders. The slab was 252 in. long and 72 in. wide. It was modeled with shell elements with a bending thickness and membrane thickness of 4.4 in. and 5.25 in., respectively. The bending thickness was developed using equation 4.2 with a concrete thickness of 4.25 in. and a deck thickness of 2.0 in. A fine mesh of 1.1 in. by 1.1 in. was used to match the slab to the mesh of the column. The slab elements that were in contact with the column shared similar nodes with the column elements. This was done to model the slab confining the column and top of the connection. At a distance equal to the depth of the column, the mesh was transitioned to a 4.4 in by 4.4 in. mesh for the remaining area of the slab. The slab was attached to the center of the girder flanges with rigid

links at the locations of the filler beams. It was assumed that the shear studs in the filler beams would transfer forces to the center of the girder flange. The model for test W27x84-Slab is shown in Figure 4.5.

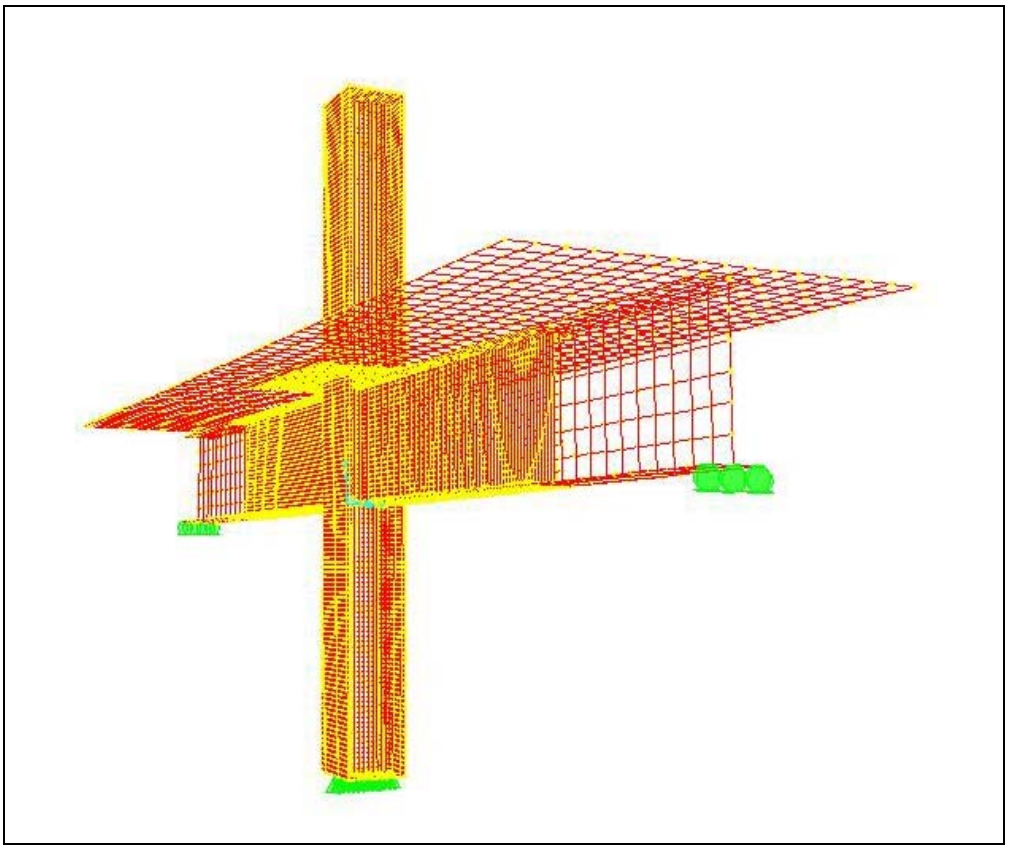

FIGURE 4.5: MODEL OF TEST W27x84-SLAB

Each girder was attached to the end-plate/web section of the column using the simplified modeling procedure described in Section 4.7. The test setup and loading method used in this test put the bolts on both ends of the connection in tension. Therefore, the girders were attached to the end-plate/web section with Standard Weight ¾ in. diameter steel pipe sections at the locations of the bolts on both ends of the end-plate.

A 1-inch thick plate was modeled on each end of the column to reduce the flange rotations and represent the plates on the experimental column. The nodes along the column web at the base of the column were restrained in the three translational degrees of freedom to represent a pinned support. The nodes along the bottom flange of each girder end, opposite the connection, were restrained in two translational degrees of freedom to represent a roller support. The girders were allowed to move in the direction of the applied load. A ½ in. stiffener was modeled on the side of the column opposite the side where the clevis was attached for the experimental test. This prevented unwanted web deformation in the area of the load application. A moment was applied to the connection by placing forces where each of the four bolts attached the clevis to the column web. These forces applied a moment of 100 ft-kips to the connection.

4.10 Results

Web deflections were taken from each model at locations just above and below the end-plate/web section. Web rotations were calculated by taking the difference between the top and bottom deflections and dividing by the distance between the two points where the deflections were measured. The column web rotations from the three finite element models and the applied moments are shown in Table 4.1.

TABLE 4.1: COLUMN WEB ROTATIONS – SAP2000

Test	Applied Moment (ft-kips)	Column Web Rotation (radians)
W24x55-2	161.1	0.0059
W27x84-2	300 (East) / 130 (West)	0.0017
W27x84-Slab	100	0.0012

CHAPTER 5

YIELD LINE ANALYSES

5.1 General

Yield line analysis is often used for designing plates. It was originally developed for analysis of reinforced concrete slabs but it has been successfully applied to plates, steel grids, box columns, and the webs of rolled members.

When the load on a plate reaches the plastic moment capacity at certain locations on the plate, yielding will occur. As yielding occurs, the curvature of the plate at the yielding section increases sharply, and the deflection increases disproportionately. Because the elastic deformation is very small compared to the plastic deformation, it is assumed that the plate sections between yield lines remain rigid and all deformation takes place at the yield lines.

A yield line is a continuous formation of plastic hinges along a straight or curved path. Along a yield line, the bending moment is assumed constant and equal to the plastic moment capacity of the plate. A failure mechanism is assumed to exist when the yield lines form a kinematically valid collapse mechanism.

The following guidelines are typically used for establishing yield lines:

- Yield lines are generally straight.
- Lines of support are generally axes of rotation.
- Yield lines pass through the intersection of the axes of rotation of adjacent plate segments.

Two methods exist for analyzing yield line mechanisms: the equilibrium method and the kinematic method. Typically the kinematic method is used because it utilizes the theory of virtual work. The yield line mechanisms discussed in the following sections were analyzed using the kinematic method.

The kinematic method gives an upper bound solution, therefore the least upper bound must be found. The least upper bound is the mechanism giving the least failure load for a given plastic moment, or the mechanism giving the greatest plastic moment for a given load.

The kinematic method of analysis involves calculating the external work of the applied loads due to an imposed virtual displacent and setting it equal to the internal work of the plate due to rotation at the yield lines. The internal work is the summation of the internal work for each individual yield line in the mechanism. The internal work for the mechanism is calculated using the formula

$$W_i = \sum_{n=1}^{N} \int_{L_n} m_p \theta_n ds = \sum_{n=1}^{N} m_p \theta_n L_n \tag{5.1}$$

where m_p is the plastic moment capacity of the plate, θ_n is the normal rotation of the n^{th} yield line, ds is the elemental length of the n^{th} yield line, L_n is the length of the n^{th} yield line, and N is the total number of yield lines. The plastic moment capacity of the plate is calculated using the formula

$$m_p = \frac{F_y t_w^2}{4} \tag{5.2}$$

where F_y is the yield strength of the plate and t_w is the thickness of the plate.

It has been noted by several researchers that the ultimate capacity of a plate is far in excess of the yield strength. Some have suggested that the ultimate strength, F_u, be

used instead of the yield strength, F_y (Ellifritt and Sputo, 1999). Packer and Bruno (1986) have suggested the following "effective" yield stress:

$$F^* = F_y + \frac{2}{3}(F_u - F_y) \tag{5.3}$$

The yield line patterns investigated will be analyzed for both yield strength and the "effective" strength, F*.

The external work has the same form for each mechanism. It is calculated using the formula

$$W_e = P_u \Delta \tag{5.4}$$

where P_u is the ultimate design load for the mechanism and Δ is the virtual displacement imposed on the column web.

The moment at the connection can be viewed as a couple with the concentrated forces acting at the bolt group, on the tension side, and the beam flange, on the compression side. On the tension side of the connection, the bolts transfer the force into the web, and on the compression side of the connection, the beam flange transfers the load to the web. The failure mechanisms on the tension and compression sides of each connection can be analyzed individually. For each mechanism, an ultimate design load, P_u, can be calculated. The ultimate design moment for the connection is then the smaller of the P_u values from the tension and compression sides times the beam depth.

The following sections discuss the mechanisms investigated for the tension and compression sides of each test, and the results from the yield line analysis.

5.2 Yield Line Mechanisms - Tension Side

On the tension side of the connection, the force is transferred to the column web through the bolt configuration. Two yield line mechanisms were investigated for this side of the connection. A virtual displacement of one unit was imposed at the location of each bolt. With a virtual displacement of one unit, setting the external work equal to the internal work of the system results in an ultimate design load for the configuration, P_u, equal to the internal work of the system. The two yield line mechanisms investigated are shown in Figure 5.1.

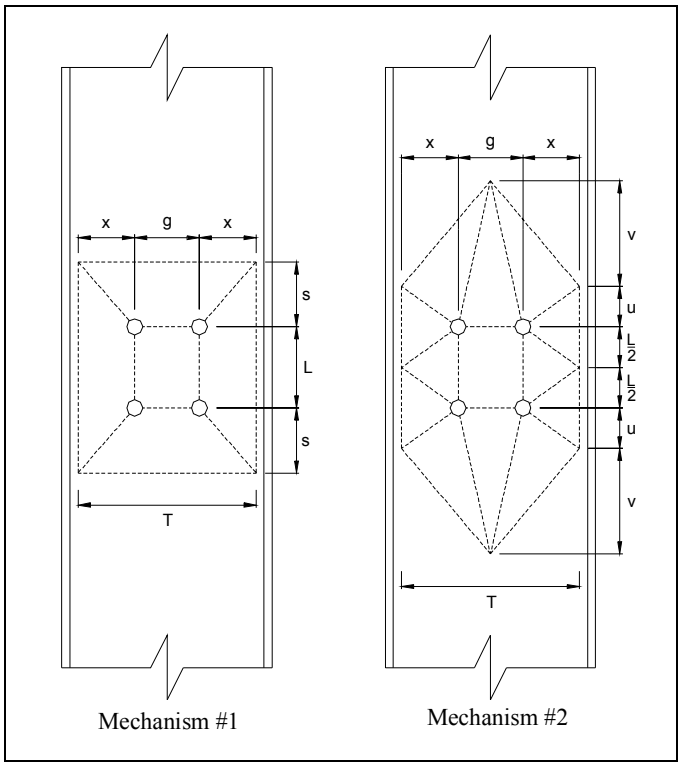

FIGURE 5.1: YIELD LINE MECHANISMS FOR TENSION SIDE

Each yield line mechanism was evaluated with the dimension *T* equal to the tabulated T-distance of the column section (AISC, 2001), and *T* equal to the distance

($d-2t_f$). Because tests W27x84 and W27x84-Slab consisted of the same column and end-plate configuration, each yield line mechanism had to be evaluated for only one of the tests.

5.2.1 Mechanism #1

Yield line mechanism #1 is the same configuration used by Kapp (1974) to analyze a bolted connection in direct tension. Mechanism #1 is shown in detail in Figure 5.2.

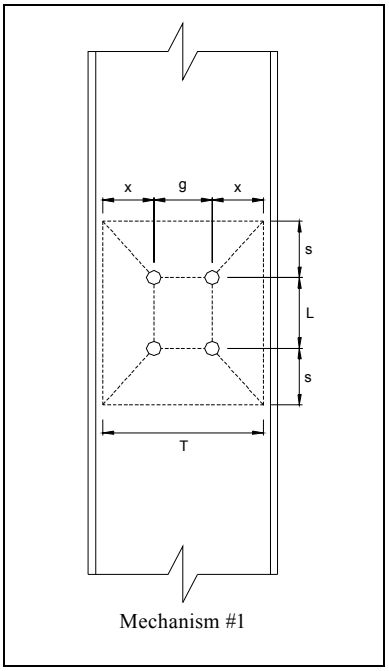

FIGURE 5.2: MECHANISM #1

In Figure 5.2, *g* is the bolt gage, *L* is the vertical bolt spacing, and *x* is the horizontal distance between the center of the hole and the location of the yield line along the column flange. The dimension *x* varies for different values of *T*. The dimension *s* is an unknown dimension that is found by differentiating Equation 5.1

with respect to *s* and setting the resultant expression equal to zero. The resulting value of *s* produces the least upper bound solution for the yield line configuration.

5.2.2 Mechanism #2

Yield line mechanism #2 is a modification of the configuration used by Ellifritt and Sputo (1999) to analyze a weak-axis stiffened seat connection. This configuration was chosen for analysis because the geometry of the yield lines was similar to the areas of high Von Mises Stress concentration predicted by the finite element models. Von Mises Stress concentration plots are located in Appendix C. The Von Mises Stress provides a measure of the shear, or distortional, stress in the column web. Mechanism #2 is shown in detail in Figure 5.3.

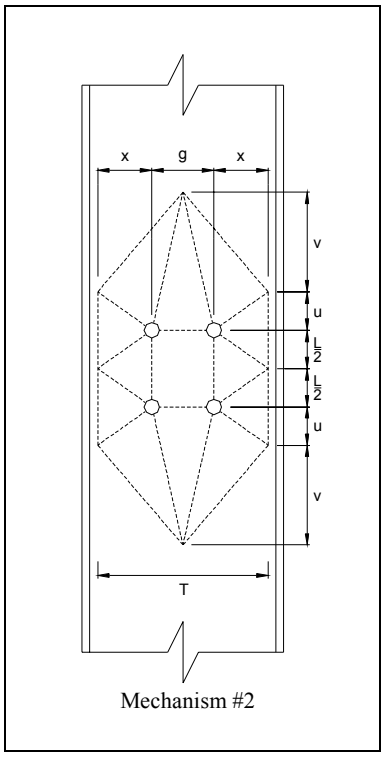

FIGURE 5.3: MECHANISM #2

In Figure 5.3, the dimensions g, L, and x are the same as defined for mechanism #1. For mechanism #2, u and v are functions of the bolt gage and the dimension T. Ellifritt and Sputo (1999) define u and v as

$$u = \frac{T+g}{2}\sqrt{\frac{T-g}{3T+g}} \tag{5.5}$$

$$v = \frac{T}{2}\sqrt{\frac{T-g}{3T+g}} \tag{5.6}$$

The dimensions x, u, and v all vary for different values of T.

5.3 Yield Line Mechanisms - Compression Side

On the compression side of the connection, the force is transferred to the column web through the beam flange. Two yield line mechanisms were investigated for this side of the connection. A virtual displacement of one unit was imposed along the width of the beam flange. With a virtual displacement of one unit, setting the external work equal to the internal work of the system results in an ultimate design load for the configuration, P_u, equal to the internal work of the system. The yield line mechanisms investigated are shown in Figure 5.4.

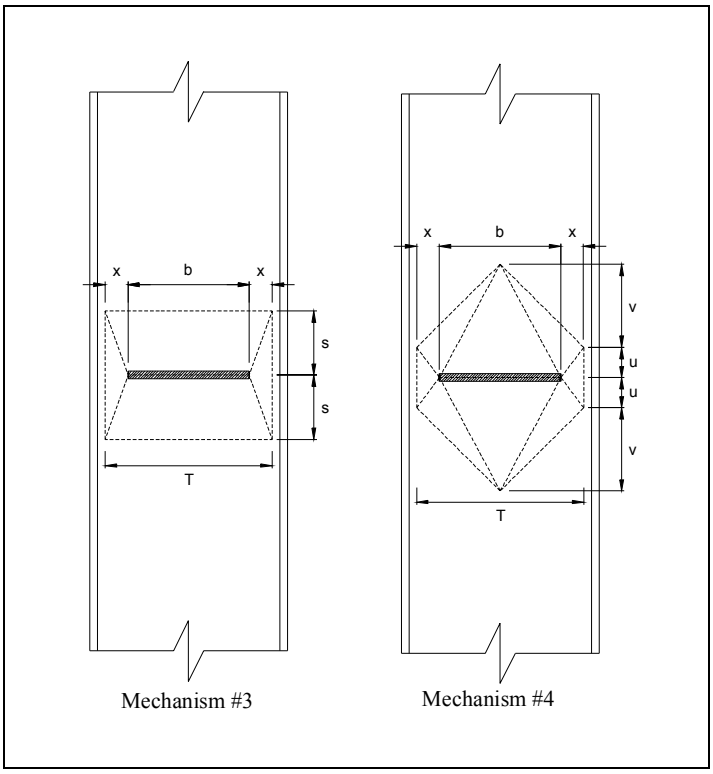

FIGURE 5.4: YIELD LINE MECHANISMS FOR COMPRESSION SIDE

Each yield line mechanism was evaluated with the dimension *T* equal to the distance (d-2k), and *T* equal to the distance (d-2t_f). The tabulated T dimension was not used because it is equal to the dimension *b* for the W27x84 tests. For both mechanisms, the beam flange is assumed to have a thickness of zero. Since tests W27x84 and W27x84-Slab consisted of the same column and end-plate configuration, each yield line mechanism only had to be evaluated for one of the tests.

5.3.1 Mechanism #3

Yield line mechanism #3 is the same configuration used by Blodgett (1966) to analyze a beam flange welded to a built-up box column. Mechanism #3 is shown in detail in Figure 5.5.

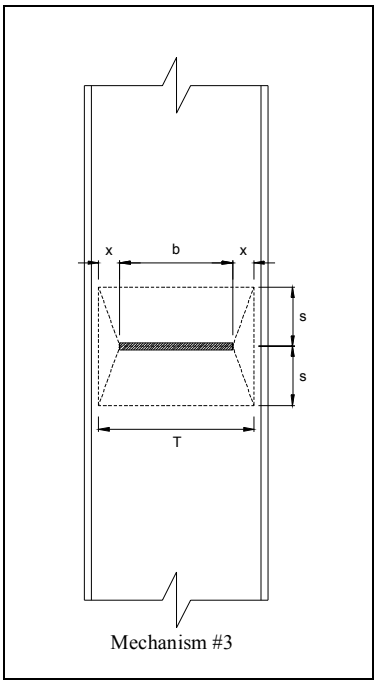

FIGURE 5.5: MECHANISM #3

In Figure 5.5, *b* is the flange width and *x* is the horizontal distance between the edge of the beam flange and the location of the yield line along the column flange. The dimension *x* varies for different values of *T*. The dimension *s* is an unknown dimension that is found by differentiating Equation 5.1 with respect to *s* and setting the resultant expression equal to zero. The resulting value of *s* produces the least upper bound solution for the yield line configuration.

5.3.2 Mechanism #4

Yield line mechanism #4 is a modification of the configuratioin used by Ellifritt and Sputo (1999) to analyze a weak-axis stiffened seat connection. This configuration was chosen for analysis because the geometry of the yield lines was similar to the areas of high Von Mises Stress concentration predicted by the finite

element models. Von Mises Stress concentration plots are located in Appendix C. The Von Mises Stress provides a measure of the shear, or distortional, stress in the column web. Mechanism #4 is shown in detail in Figure 5.6.

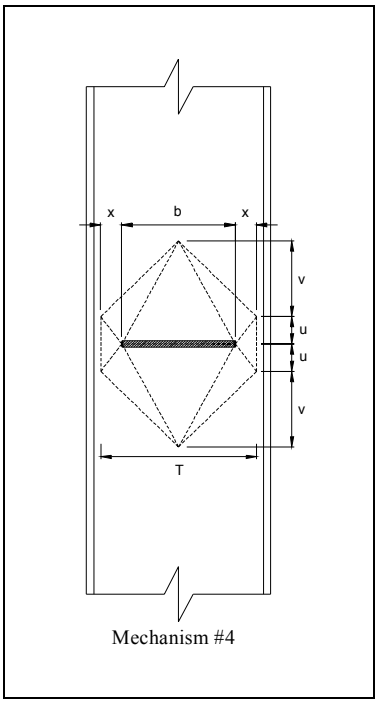

FIGURE 5.6: MECHANISM #4

In Figure 5.3, the dimensions b and x are the same as defined for mechanism #3. For mechanism #4, u and v are functions of the beam flange width and the dimension T. Ellifritt and Sputo (1999) define u and v as

$$u = \frac{T+b}{2}\sqrt{\frac{T-b}{3T+b}} \tag{5.7}$$

$$v = \frac{T}{2}\sqrt{\frac{T-b}{3T+b}} \tag{5.8}$$

The dimensions x, u, and v all vary for different values of T.

5.4 Results

The results from the yield line analysis are presented in Table 5.1. Each connection was analyzed for the four mechanisms. Ultimate design loads and moments are presented for two separate values of the dimension *T*. They are also presented for the yield strength, F_y, and the "effective" yield strength, F*, suggested by Packer and Bruno (1986). Results were calculated with the yield line equations shown in Appendix B.

TABLE 5.1: YIELD LINE ANALYSIS RESULTS

Tension Side			W24x55		W27x84		W27x84-Slab	
			F_y=58.0 ksi, F_u=72.0 ksi		F_y=58.0 ksi, F_u=72.0 ksi		F_y=54.7 ksi, F_u=67.1 ksi	
Mechanism	T (in.)	F	P_u (kips)	M_u (ft-kips)	P_u (kips)	M_u (ft-kips)	P_u (kips)	M_u (ft-kips)
1	12.64 [1]	F_y	79.4	156.2	81.0	180.2	76.4	170.0
		F*	92.2	181.3	94.0	209.2	90.0	200.3
	10.00 [2]	F_y	89.8	176.6	92.0	204.7	88.0	195.8
		F*	104.2	204.9	106.8	237.6	100.0	222.5
2	12.64 [1]	F_y	159.0	312.7	158.4	352.4	149.4	332.4
		F*	184.5	362.9	183.9	409.2	172.1	382.9
	10.00 [2]	F_y	153.2	301.3	154.6	344.0	145.8	324.4
		F*	177.8	349.7	179.4	399.2	167.9	373.6

Compression Side			W24x55		W27x84		W27x84-Slab	
			F_y=58.0 ksi, F_u=72.0 ksi		F_y=58.0 ksi, F_u=72.0 ksi		F_y=54.7 ksi, F_u=67.1 ksi	
Mechanism	T (in.)	F	P_u (kips)	M_u (ft-kips)	P_u (kips)	M_u (ft-kips)	P_u (kips)	M_u (ft-kips)
3	12.64 [1]	F_y	81.8	160.9	118.5	263.7	111.8	248.8
		F*	94.9	186.6	137.5	305.9	128.7	286.4
	11.44 [3]	F_y	87.7	172.5	151.7	337.5	143.1	318.4
		F*	101.8	200.2	176.1	391.8	164.8	366.7
4	12.64 [1]	F_y	105.4	207.3	135.7	301.9	128.0	284.8
		F*	122.3	240.5	157.5	350.4	147.4	328.0
	11.44 [3]	F_y	108.9	214.2	169.3	376.7	159.7	355.3
		F*	126.3	248.4	196.5	437.2	183.9	409.2

[1] T = d-2t_f

[2] T = tabulated value

[3] T = d-2k_{design}

Mechanisms #1 and #3 predict the smallest plastic moment capacity for the tension and compression sides of the connection, respectively. As expected, the "effective" yield stress predicted a higher plastic moment than the yield stress predicted for each of the connections. The two values used for the dimension *T* produced varying results for the different mechanisms.

CHAPTER 6

ANALYSES OF RESULTS

6.1 General

In this chapter, the results from the three experimental tests are compared to analytical results. The experimental strengths of the connections are compared to predicted values using the procedure from AISC Design Guide 16 (Murray and Shoemaker, 2002) and the results from the yield line analysis presented in Chapter 5. The experimental stiffness of each connection is compared to the results from the finite element analysis presented in Chapter 4.

A stiffness analysis is also presented for test W27x84-Slab to investigate how the concrete slab affects the stiffness of the connection. This includes an investigation of the connection stiffness after five load sequences had been applied and a comparison of test W27x84-Slab to the bare steel test W27x84.

6.2 Failure Strength of Connections

Table 6.1 summarizes the predicted strengths of the girder side of each connection. The strengths were determined using measured dimensions and measured material properties. The procedures from Table 4.2 in Chapter 4 of the AISC/MBMA Design Guide 16 "Flush and Extended Multiple-Row Moment End-Plate Connections" (Murray and Shoemaker, 2002) were used to determine the bolt rupture and end-plate yielding strengths. The procedures in Chapter 5 of the AISC Manual of Steel Construction "Load and Resistance Factor Design", Third Edition,

were used to calculate the girder strengths. The weld rupture strengths were determined assuming F_u = 70 ksi, measured fillet weld sizes (see Appendix A), and net flange weld lengths (flange width for outside welds, and flange width minus girder web thickness for inside welds). Appropriate moment arms were used to determine the corresponding weld rupture moments. Resistance factors, ϕ, were excluded in all calculations. The predicted controlling moment is shaded.

TABLE 6.1: PREDICTED CONNECTION LIMIT STATES

Test	Bolt Rupture M_{bolt} (ft-kips)	Plate Yielding M_{pl} (ft-kips)	Girder Strength M_p (ft-kips)	Weld Rupture M_{weld} (ft-kips)
W24x55	319*	341	684	545
W27x84	792	888	1145	1003
W27x84-Slab	760	839	1149	880

* Includes Prying Action

Test W24x55 was predicted to exhibit bolt-prying action, which was taken into account in the calculations. The calculated bolt prying forces were 5.0 kips and 10.0 kips for the inside and outside tension bolts, respectively.

For the calculation of the predicted moments corresponding to the bolt rupture and plate yielding limit states, a moment arm was used equal to the distance to the connection faying surface from the point of application of the load. For the calculation of applied moment corresponding to the girder strength limit state, a moment arm was used equal to the distance to the connection faying surface from the point of application of the load minus one-half the girder depth, corresponding to the predicted location of a plastic hinge, should one develop.

The test results are summarized in Table 6.2. For all three tests, the predicted controlling limit state, bolt rupture, occurred. It is noted that for Test W24x55, the predicted strengths for the limit states of bolt rupture and plate yielding are nearly the same. The ratios of experimental to predicted strength range from 0.95 to 1.10.

TABLE 6.2: SUMMARY OF CONNECTION FAILURE RESULTS

Test	Predicted Failure Moment and Limit State		Experimental Failure Moment and Limit State		Ratio of Experimental to Predicted Strengths
	Moment (ft-kips)	Limit State	Moment (ft-kips)	Limit State	
W24x55	319/341	Bolt Rupture/Plate Yielding	350	Bolt Rupture	1.10 / 1.03
W27x84	792	Bolt Rupture	751	Bolt Rupture	0.95
W27x84-Slab	760	Bolt Rupture	754	Bolt Rupture	0.99

For test W24x55, the predicted failure moment was 319 ft-kips. The maximum applied moment was 350 ft-kips, or 109.7% of the predicted strength. As predicted from the limit state strengths, the connection failed due to bolt rupture. Nearly all of the inelastic deformation observed is attributed to end-plate and column web rotation, as shown in the plot of Moment vs. Column Web Rotation in Figure 3.3. The rotation was due to a combination of bolt strain, plate yielding, and column web yielding. Plots of Bolt Tension vs. Moment for Test W24x55 are located in Appendix E.

For test W27x84, the predicted failure moment was 792 ft-kips. The maximum applied moment was 751 ft-kips, or 94.8% of the predicted strength. This represents a 5.2% decrease in the capacity of the connection. As predicted from the limit state strengths, the connection failed due to bolt rupture. Nearly all of the inelastic deformation observed is attributed to end-plate and column web rotation, as shown in

the plot of Moment vs. Column Web Rotation in Chapter 3 (Figure 3.6). The cause of the rotation is a combination of bolt strain, plate yielding, and column web yielding. Plots of Bolt Tension vs. Moment for Test W27x84 are located in Appendix F.

For test W27x84-Slab, the predicted failure moment was 760 ft-kips. The maximum applied moment was 754 ft-kips, or 99.2% of the predicted strength. This represents a 0.8% decrease in the capacity of the connection. As predicted from the limit state strengths, the connection failed due to bolt rupture. Nearly all of the inelastic deformation observed is attributed to end-plate and column web rotation, as shown in the plot of Moment vs. Column Web Rotation in Figure 3.15. The cause of the rotation is a combination of bolt strain, plate yielding, and column web yielding. Plots of Bolt Tension vs. Moment for Test W27x84-Slab are located in Appendix G.

6.3 Plastic Strength of Column Web

The experimental plastic moment strength of the column web was derived from the moment vs. column web rotation plots for each test. The plastic moment strength was predicted as the moment at the intersection between a line tangent to the elastic section of the curve and a line tangent to the curve just before failure occurred, as shown in Figure 6.1. The plots used to determine the experimental plastic moments are located in Appendix D; the resulting moments are tabulated in Table 6.3.

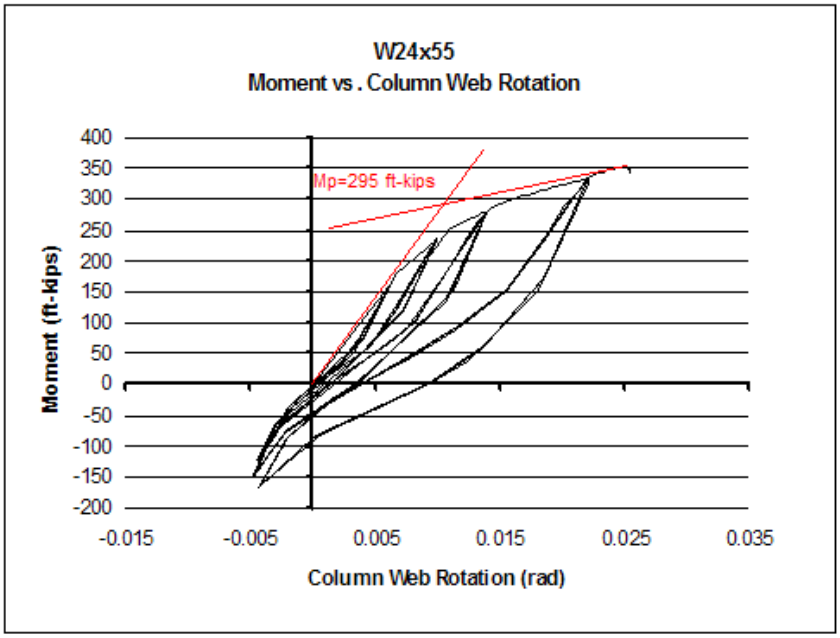

FIGURE 6.1: PREDICTED PLASTIC MOMENT STRENGTH OF COLUMN WEB

TABLE 6.3: SUMMARY OF PLASTIC STRENGTH RESULTS

Test	Predicted Plastic Moment Capacity and Controlling Yield Line Mechanism		Experimental Plastic Moment Capacity	Ratio of Experimental to Predicted Strength
	Moment (ft-kips)	Mechanism	Moment (ft-kips)	
W24x55	248.4	Mechanism #4, T=11.44 in, F*=67.3 ksi	295	1.19
W27x84	409.2	Mechanism #2, T=12.64 in, F*=67.3 ksi	650	1.59
W27x84-Slab	382.9	Mechanism #2, T=12.64 in, F=63.0 ksi	650	1.70

All of the predicted moments from the yield line analyses, Table 5.1, are less than the experimental moments, possibly because of catenary action in the column web. The results from mechanisms #1 and #3 were more conservative than those from mechanisms #2 and #4.

The predicted and experimental results are summarized in Table 6.3. The plastic moment capacity shown for each connection is the minimum of the maximum moments predicted for each side of the connection using mechanisms #2 and #4 with the effective yield stress, F*. These moments were chosen to compensate for some of the catenary behavior exhibited in the experimental tests. The ratios of experimental to predicted strength range from 1.19 to 1.70.

For test W24x55, the predicted plastic moment was 248.4 ft-kips. The experimental plastic moment was 295 ft-kips, or 119% of the predicted strength. This represents a 19% increase in the plastic strength of the column web.

For tests W27x84, the predicted plastic moment was 409.2 ft-kips. The experimental plastic moment was 650 ft-kips, or 159% of the predicted strength. This represents a 59% increase in the plastic strength of the column web.

For tests W27x84-Slab, the predicted plastic moment was 382.9 ft-kips. The experimental plastic moment was 650 ft-kips, or 170% of the predicted strength. This represents a 70% increase in the plastic strength of the column web.

The predicted plastic moment capacity from the yield line analyses was very conservative for all three tests. It is noted that the results for mechanisms #1 and #3 are more conservative than those predicted by the more complex mechanisms #2 and #4.

6.4 Elastic Connection Stiffness

The experimental elastic stiffness of each connection is compared to the results from the finite element models in Table 6.4. The experimental elastic rotations used for comparison were chosen from the plots of moment vs. column web rotation for each connection. The rotation chosen to represent the elastic stiffness of Test W27x84-Slab was taken from Load Sequence #1, as the first load sequence is the best representation of the elastic stiffness because no cracks existed in the slab and the specimen had only been subjected to a small test load prior to the load sequence. The moments applied to the connections in the finite element models were the same as the moments corresponding to the chosen experimental elastic rotations. The ratios of experimental to predicted rotation range from 1.00 to 1.24.

TABLE 6.4: SUMMARY OF ELASTIC STIFFNESS RESULTS

Test	Applied Moment (ft-kips)	Finite Element Model Colmn Web Rotation (rad.)	Experimental Column Web Rotation (rad.)	Ratio of Experimental to Predicted Rotation
W24x55	161.1	0.0059	0.0061	1.03
W27x84	300 (East) / 130 (West)	0.0017	0.0021	1.24
W27x84-Slab	100	0.0012	0.0012	1.00

The finite element model for test W27x84-Slab predicted the elastic stiffness of the connection. For the bare steel tests, the finite element models predicted rotations that were slightly to very conservative. The models for tests W24x55 and W27x84 predicted 96.7% and 81.0% of the experimental connection stiffness, respectively.

6.5 Stiffness Analysis of Test W27x84-Slab

6.5.1 Stiffness After Five Load Sequences and Concrete Crushing

Figure 6.2 is a plot of Moment vs. Column Tip Deflection from Test W27x84-Slab, Load Sequence #5. The dashed line in the figure is the corresponding predicted elastic deflection. The predicted elastic line has been adjusted horizontally to the left and right by 1 in. so it is not located within the area where the previous load sequences and concrete crushing caused the connection to lose stiffness. Many of the plotted load steps run nearly parallel to the adjusted predicted elastic lines. This illustrates that the connection recovers much of its stiffness after loading has been increased beyond that of previous cycles and after the concrete around the column has crushed.

.

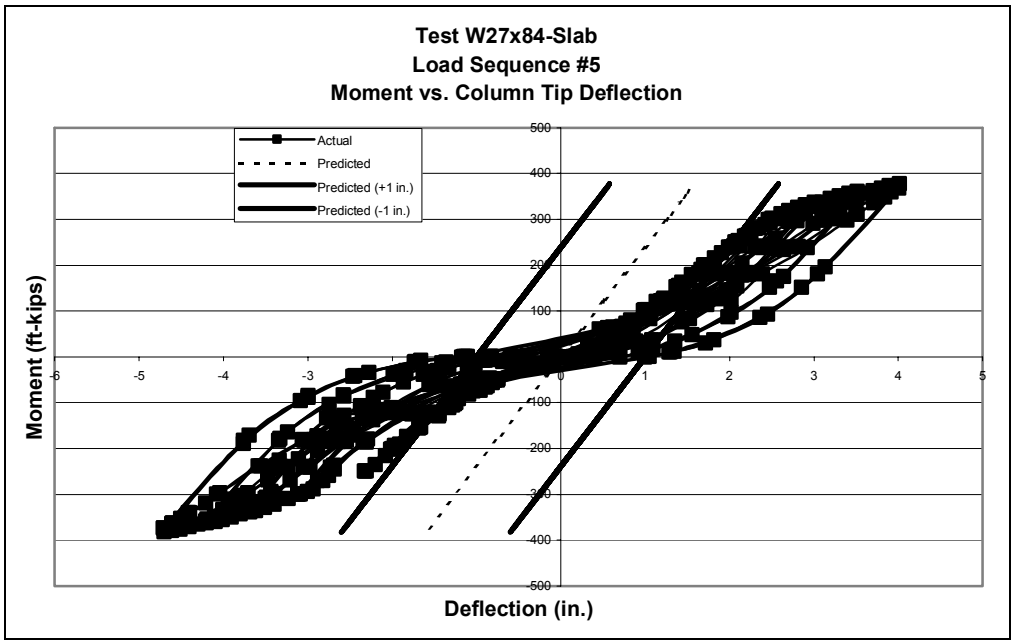

FIGURE 6.2: MOMENT VS. COLUMN TIP DEFLECTION, LOAD SEQUENCE #5

6.5.2 Comparison to Test W27x84

Figure 6.3 is a plot of Moment vs. Column Web Rotation. The plot includes the web rotations from test W27x84, Load Cycle 5.1 from Load Sequences #1 (W27x84-Slab), and Load Cycle 6.1 from Load Sequence #5 (W27x84-Slab). The plot for Load Cycle 5.1 of Load Sequence #1 has been adjusted to remove the added deflection caused by the loosening of the column web instrumentation brackets discussed in Sections 2.3.3 and 3.4.1. The plot for test W27x84 has been adjusted to remove the 130 ft-kip moment that was applied by the west girder.

Prior to the concrete crushing around the column (Load Sequence #1), the connection of test W27x84-Slab exhibited less web rotation than test W27x84 at the same applied moment. In the elastic range, prior to concrete cracking and crushing, test W27x84-Slab had up to twice the stiffness of test W27x84. After concrete crushing had occurred test W27x84-Slab began to lose stiffness. Load Sequences #5 represents the loss of stiffness in the W27x84-Slab connection after four load sequences had been applied and the concrete had cracked and crushed around the column.

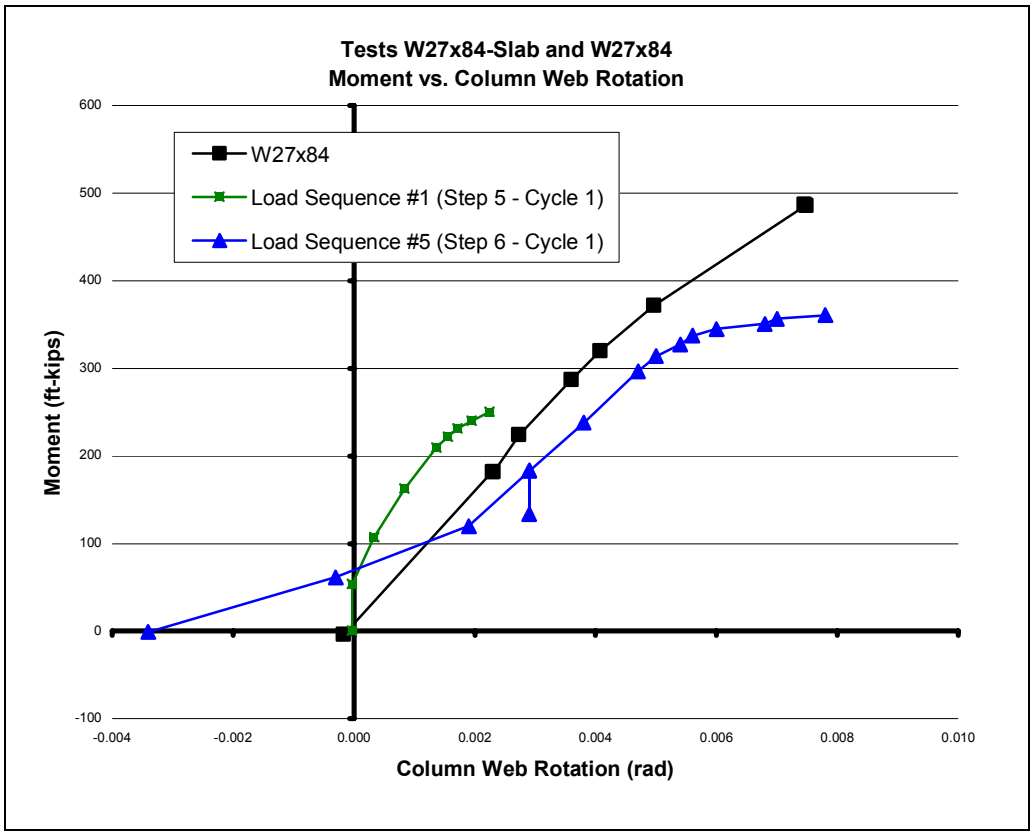

FIGURE 6.3: MOMENT VS. COLUMN WEB ROTATION, TESTS W27x84-SLAB AND W27x84

CHAPTER 7

CONCLUSIONS

7.1 Summary

The research objective of this study was to investigate the strength and stiffness of four-bolt extended, weak-axis, moment end-plate connections. Three full-scale experimental tests were conducted and the results were compared to predicted values for the strength and stiffness of each connection. Two of the tests were conducted with bare steel specimens and the third with a concrete slab in place.

The procedures in Chapter 4 of the AISC/MBMA Design Guide 16 "Flush and Extended Multiple-Row Moment End-Plate Connections" (Murray and Shoemaker, 2002) and Chapter 5 of the AISC Manual of Steel Construction "Load and Resistance Factor Design", Third Edition, were used to predict the strengths of the end-plates, bolts, and girders.

Yield line theory was used to predict the plastic strength of the column web. Yield line mechanisms were developed for the column web by modifying the configurations used in the past for other types of weak-axis connections.

The commercial software SAP2000 was used to develop finite element models to predict the elastic stiffness of each connection. A simplified modeling procedure was developed to overcome the contact problems between the end-plates and the column web, and between the bolts and holes in the end-plates and web.

The experimental stiffness of the test with the concrete slab confining the top extension of the end-plate was compared to the stiffness of a similar test without a slab.

7.2 Conclusions

7.2.1 Connection Strength

The experimental results indicate that the AISC/MBMA Design Guide 16 procedure accurately predicted the failure mode and the nominal strength of each connection. Design Guide 16 does not take into account the column-side limit states of the connection, specifically the strength of the column web for a weak-axis connection. Because the three experimental tests were all conducted with a W14x99 column, it can not be concluded that the strength of the column web will not be the controlling limit state for a different column and connection.

7.2.2 Column Web Strength

All yield line mechanisms investigated for the column web predicted ultimate failure moments much less than those obtained in the experimental tests. It is believed that the column webs developed catenary behavior in the area of the column web, resulting in larger deflections and a higher plastic moment capacity than predicted by the yield line analysis.

Two sets of yield line mechanisms were investigated for each connection. Each set included a separate mechanism for the tension and compression sides of the connection. Mechanisms #2 and #4 (Figures 5.3 and 5.6) predicted the closest results

for the plastic moment capacity of the column web when compared to the experimental results. Both sets of yield line mechanisms were examined using the yield strength, F_y, and the "effective" yield strength, F*, suggested by Packer and Bruno (1986). The "effective" yield strength, F*, produced the highest plastic moment capacities for the column webs; however, they were still very conservative.

7.2.3 Connection Stiffness

The finite element models that were developed with the simplified modeling procedure accurately predicted the initial elastic stiffness of the three connections within 19.0% of the experimental elastic stiffness. The elastic stiffness of two of the connections was predicted within 3.3%. All experimental tests were performed on a W14x99 column with end-plates having a bolt gage of 4 in. It is concluded that the simplified modeling procedure will accurately predict the web rotations for tests having the same column and end-plate geometries as those tested.

7.2.4 Connection Stiffness with Concrete Slab

The concrete slab of Test W27x84-Slab significantly increased the elastic stiffness of the connection. However, once the slab had cracked and crushed around the column, the stiffness decreased rapidly. Test W27x84-Slab had been exposed to numerous loading sequences that greatly reduced the stiffness of the connection. Therefore, it is difficult to predict how much of the stiffness reduction should be attributed to the slab cracking and how much should be attributed to the load sequences.

In conclusion, a concrete slab that is cast tightly around the column and top extension of a weak-axis moment end-plate connection will increase the elastic stiffness of the connection beyond the elastic stiffness of a bare steel connection. However, in the event that the concrete cracks, the stiffness will be reduced.

7.3 Suggestions on Future Research

Additional experimental testing is required to verify the conclusions of this study. The testing should include several weak-axis moment end-plate connections with varying columns, girders, and end-plate configurations. By varying the column web thickness, bolt gage, and girder flange width, a data set could be established and the recommended yield line mechanisms could be modified to make a more accurate prediction of the plastic moment strength. Further research is also required to investigate the catenary behavior believed to develop in the column web.

Varying column sizes and end-plate configurations, specifically bolt gage and girder flange width, would assist in verifying the simplified finite element modeling procedure. Since the models only predict the elastic stiffness of the column web, the modeling procedure should be expanded to investigate inelastic behavior.

Further research is also required to investigate the effects that concrete slabs have on the strength and stiffness of weak-axis moment end-plate connections.

REFERENCES

Abolitz, A. L. and Warner, M. E. (1965). "Bending Under Seated Connections," *Engineering Journal*, American Institute of Steel Construction, Vol. 2, No. 1, 1-5.

AISC (2001). *Manual of Steel Construction, Load and Resistance Factor Design,* American Institute of Steel Construction, 3rd Ed.

AISC (1995). *Manual of Steel Construction, Load and Resistance Factor Design,* American Institute of Steel Construction, Vol. 2, 2nd Ed.

AISC (1997). *Seismic Provisions for Structural Steel Buildings,* American Institute of Steel Construction, Chicago.

Blodgett, O. W. (1966). *Design of Welded Structures*, James F. Lincoln Arc Welding Foundation, Cleveland, Ohio.

Dominisse, K. R. and Murray, T. M. (2003). *Strength Evaluation of Six Extended Moment End-Plate Connections,* Research Report No. CE/VPI-ST 03/10, Virginia Polytechnic Institute and State University, Blacksburg, Virginia.

Dominisse, K. R. and Murray, T. M. (2004). *Strength Evaluation of Weak-Axis Extended Moment End-Plate Connection with Lightweight Concrete Slab,* Research Report No. CE/VPI-ST 04/03, Virginia Polytechnic Institute and State University, Blacksburg, Virginia.

Ellifritt, D. S. and Sputo, T. (1999). "Design Criteria for Stiffened Seated Connections to Column Webs," *Engineering Journal*, American Institute of Steel Construction, Vol. 36, No. 1, 160-168.

Hopper, B. E., Batson, G. B., and Ainso H. (1985). "Bracket Loaded Webs with Low Slenderness Ratios," *Engineering Journal*, American Institute of Steel Construction, Vol. 22, No. 1, 11-18.

Hoptay, J. M. and Ainso, H. (1981). "An Experimental Look at Bracket-Loaded Webs," *Engineering Journal*, American Institute of Steel Construction, Vol. 18, No. 1, 1-7.

Kapp, R. H. (1974). "Yield Line Analysis of a Web Connection in Direct Tension," Engineering Journal, American Institute of Steel Construction, Vol. 11, No. 1, 38-41.

Murray, T. M. and Shoemaker, W. L. (2002). *Steel Design Guide 16: Flush and Extended Multiple-Row Moment End-Plate Connections*, American Institute of Steel Construction, Chicago.

Packer, J. A. and Bruno, T. (1986). "Behavior of Bolted Flange-Plate Connections in Rectangular Hollow Tension Members," *Proceedings of the 10th Australian Conference on Mechanics of Structures and Materials.*

SAP2000 (2002). *Analysis Reference Manual,* Version 8.0, Computers and Structures, Inc., Berkeley, CA.

Stockwell, F. W., Jr. (1974). "Yield Line Analysis of Column Webs with Welded Beam Connections," *Engineering Journal*, American Institute of Steel Construction, Vol. 11, No. 1, 12-17.

APPENDIX A

AS-MEASURED CONNECTION DRAWINGS

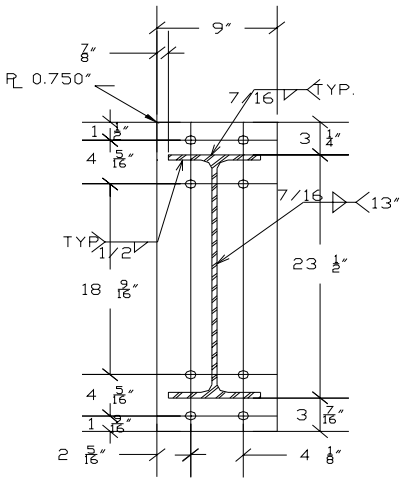

Nominal hole diameter 13/16 ".

W24x55 - East

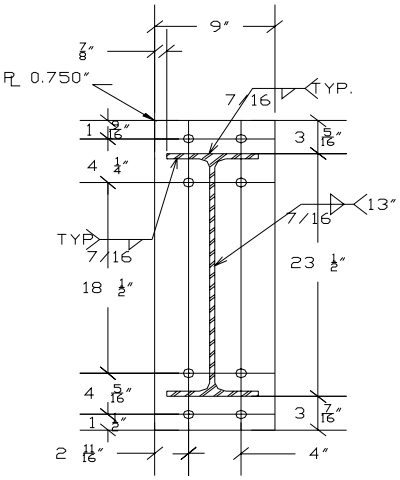

Nominal hole diameter 13/16 ".

W24x55 - West

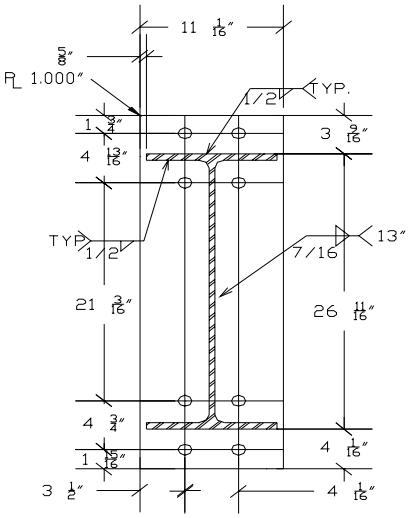

Nominal hole diameter 1 1/16 ".

W27x84 - East

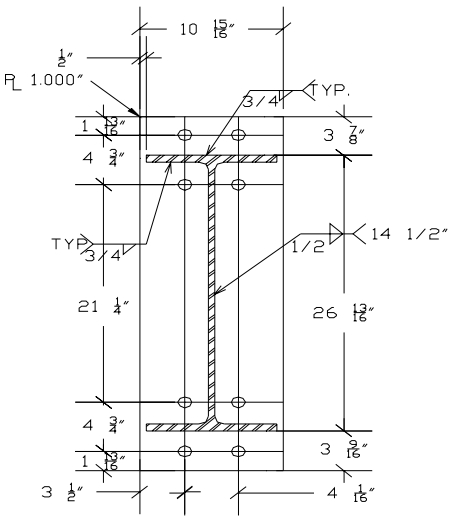

Nominal hole diameter 1 1/16 ".

W27x84 - West

Notes:
1. All plate material, A36.
2. All rolled beams, A572, grade 50.

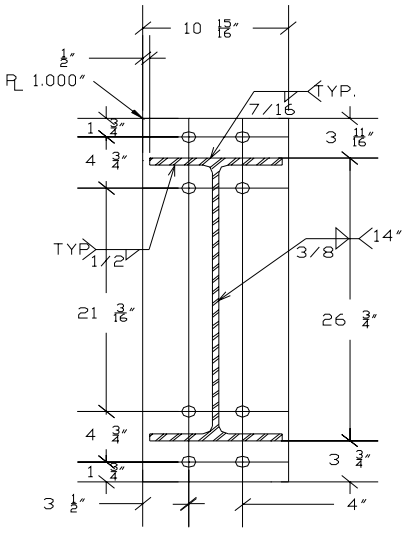

Nominal hole diameter 1 1/16 ".

W27x84-SLAB - EAST

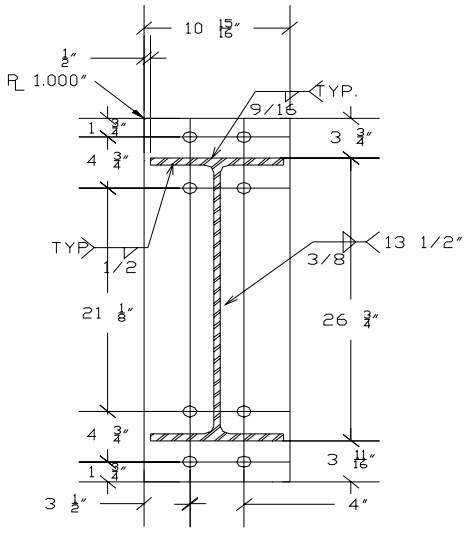

Nominal hole diameter 1 1/16 ".

W27x84-SLAB - WEST

Notes:
1. All plate material, A36.
2. All rolled beams, A572, grade 50.

APPENDIX B

YIELD LINE EQUATIONS

MECHANISM #1

$$M_n = \frac{F_w t_w^2 Y d_b}{2}$$

where: F_w = *Column Web Strength (F_y, F_u, or F*)*
t_w = *Thickness of Column Web*
d_b = *Depth of Beam*

$$Y = \frac{2s^2 + Ls + x(2x + g)}{sx}$$

where: $$s = \frac{\sqrt{2x}\sqrt{2x + g}}{2}$$

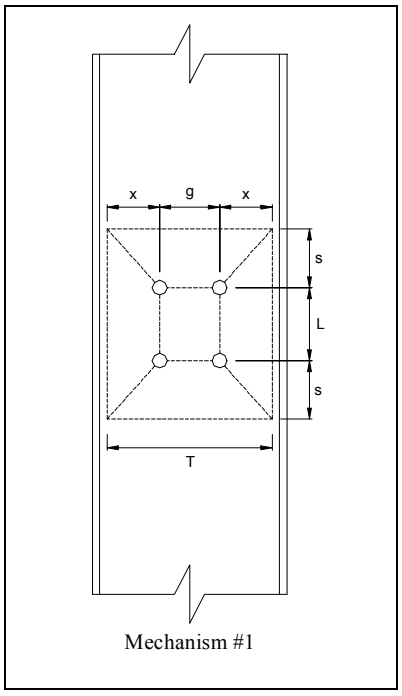

Mechanism #1

TABLE B.1: MECHANISM #1
YIELD LINE SOLUTION PARAMETER VALUES

Mechanism #1						
Parameter	**Test W24x55**		**Test W27x84**		**Test W27x84-Slab**	
F_y (ksi)	58.0		58.0		54.7	
F_u (ksi)	72.0		72.0		67.1	
F*(ksi)	67.3		67.3		63.0	
t_w (in.)	0.485		0.485		0.485	
d_b (in.)	23.6		26.7		26.7	
g (in.)	4.0		4.0		4.0	
L (in.)	4.25		4.75		4.75	
T (in.)	12.64	10.00	12.64	10.00	12.64	10.00
x (in.)	4.32	3.00	4.32	3.00	4.32	3.00
s (in.)	5.23	3.87	5.23	3.87	5.23	3.87
Y	5.82	6.58	5.94	6.75	5.94	6.75
M_n (ft-kips) (F_w=F_y)	156.2	176.6	180.2	204.7	170.0	193.1
M_n (ft-kips) (F_w=F*)	181.3	204.9	209.2	237.6	195.8	222.5

MECHANISM #2

$$M_n = \frac{F_w t_w^2 Y d_b}{2}$$

where: F_w = *Column Web Strength (F_y, F_u, or F*)*
t_w = *Thickness of Column Web*
d_b = *Depth of Beam*

$$Y = \frac{g}{u+v} + \frac{2u(x+g)}{gx} + \frac{x}{u} + \frac{gLx\sqrt{4v^2+(2x+g)^2} + d\left[4Lvx + g(4x^2+3L^2)\right]}{2dgLx}$$

where:

$$d = \sin\left[\cos^{-1}\left[\frac{\left(\frac{g}{2}\right)^2 + (v+u)^2 + \left(x+\frac{g}{2}\right)^2 + v^2 - x^2 - u^2}{2\sqrt{\left(\frac{g}{2}\right)^2 + (v+u)^2}\sqrt{\left(x+\frac{g}{2}\right)^2 + v^2}}\right]\right]\sqrt{\left(x+\frac{g}{2}\right)^2 + v^2}$$

$$u = \frac{T+g}{2}\sqrt{\frac{T-g}{3T+g}} \qquad v = \frac{T}{2}\sqrt{\frac{T-g}{3T+g}}$$

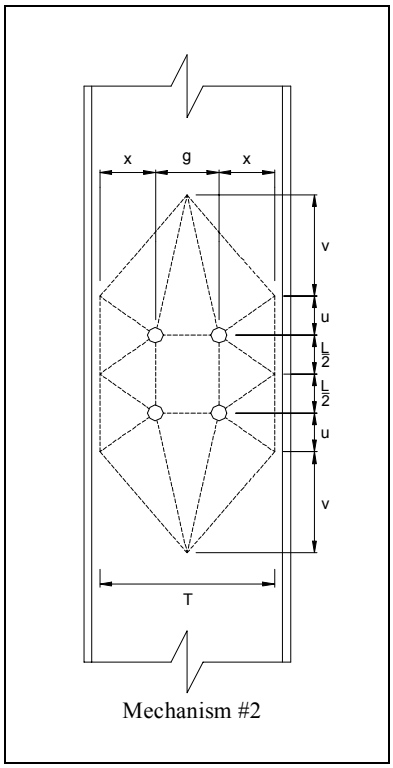

Mechanism #2

TABLE B.2: MECHANISM #2
YIELD LINE SOLUTION PARAMETER VALUES

Mechanism #2						
Parameter	**Test W24x55**		**Test W27x84**		**Test W27x84-Slab**	
F_y (ksi)	58.0		58.0		54.7	
F_u (ksi)	72.0		72.0		67.1	
F*(ksi)	67.3		67.3		63.0	
t_w (in.)	0.485		0.485		0.485	
d_b (in.)	23.6		26.7		26.7	
g (in.)	4.0		4.0		4.0	
L (in.)	4.25		4.75		4.75	
T (in.)	12.64	10.00	12.64	10.00	12.64	10.00
x (in.)	4.32	3.00	4.32	3.00	4.32	3.00
u (in.)	3.78	2.94	3.78	2.94	3.78	2.94
v (in.)	2.87	2.10	2.87	2.10	2.87	2.10
d (in.)	5.23	3.87	5.23	3.87	5.23	3.87
Y	11.65	11.23	11.61	11.33	11.61	11.33
M_n (ft-kips) (F_w=F_y)	312.7	301.3	352.4	344.0	332.4	324.4
M_n (ft-kips) (F_w=F*)	362.9	349.7	409.2	399.2	382.9	373.6

MECHANISM #3

$$M_n = \frac{F_w t_w^2 Y d_b}{2}$$

where: F_w = *Column Web Strength (F_y, F_u, or F*)*
t_w = *Thickness of Column Web*
d_b = *Depth of Beam*

$$Y = \frac{2s^2 + x(2x+b)}{sx}$$

where: $$s = \frac{\sqrt{2x}\sqrt{2x+b}}{2}$$

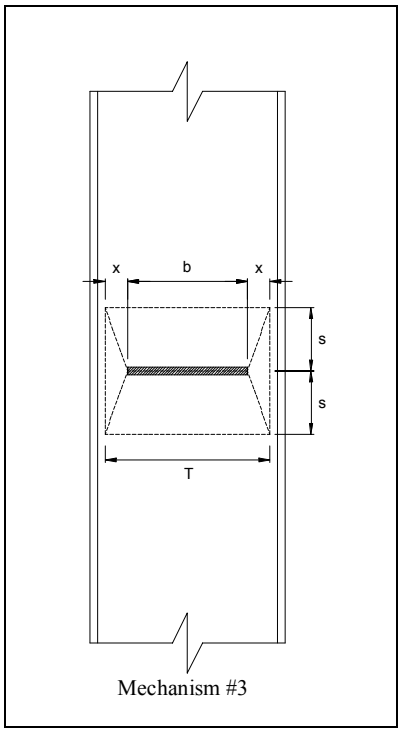

Mechanism #3

TABLE B.3: MECHANISM #3
YIELD LINE SOLUTION PARAMETER VALUES

Mechanism #3						
Parameter	**Test W24x55**		**Test W27x84**		**Test W27x84-Slab**	
F_y (ksi)	58.0		58.0		54.7	
F_u (ksi)	72.0		72.0		67.1	
F*(ksi)	67.3		67.3		63.0	
t_w (in.)	0.485		0.485		0.485	
d_b (in.)	23.6		26.7		26.7	
b (in.)	7.01		9.96		9.96	
T (in.)	12.64	11.44	12.64	11.44	12.64	11.44
x (in.)	2.82	2.22	1.34	0.74	1.34	0.74
s (in.)	4.22	3.56	2.91	2.06	2.91	2.06
Y	5.99	6.43	8.69	11.12	8.69	11.12
M_n (ft-kips) (F_w=F_y)	160.9	172.5	263.7	337.5	248.7	318.4
M_n (ft-kips) (F_w=F*)	186.6	200.2	305.9	391.8	286.4	366.7

MECHANISM #4

$$M_n = \frac{F_w t_w^2 Y d_b}{2}$$

where: F_w = *Column Web Strength (F_y, F_u, or F*)*
t_w = *Thickness of Column Web*
d_b = *Depth of Beam*

$$Y = \frac{b}{u+v} + \frac{2u(x+b)}{bx} + \frac{x}{u} + \frac{b\sqrt{4v^2 + (2x+b)^2} + 4dv}{2bd}$$

where:

$$d = \sin\left[\cos^{-1}\left[\frac{\left(\frac{b}{2}\right)^2 + (v+u)^2 + \left(x+\frac{b}{2}\right)^2 + v^2 - x^2 - u^2}{2\sqrt{\left(\frac{b}{2}\right)^2 + (v+u)^2}\sqrt{\left(x+\frac{b}{2}\right)^2 + v^2}}\right]\right]\sqrt{\left(x+\frac{b}{2}\right)^2 + v^2}$$

$$u = \frac{T+b}{2}\sqrt{\frac{T-b}{3T+b}} \qquad v = \frac{T}{2}\sqrt{\frac{T-b}{3T+b}}$$

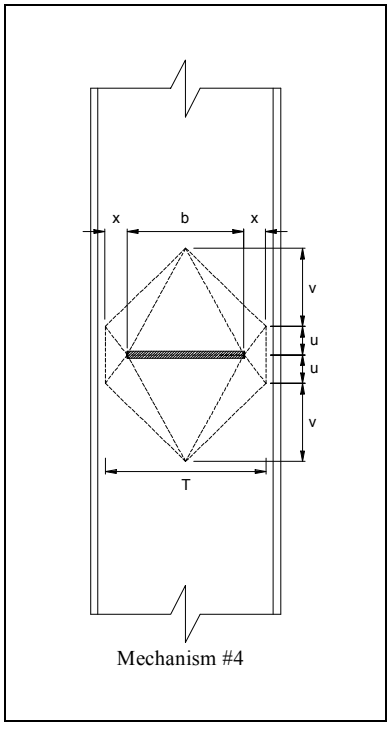

Mechanism #4

TABLE B.4: MECHANISM #4

Mechanism #4						
Parameter	**Test W24x55**		**Test W27x84**		**Test W27x84-Slab**	
F_y (ksi)	58.0		58.0		54.7	
F_u (ksi)	72.0		72.0		67.1	
F*(ksi)	67.3		67.3		63.0	
t_w (in.)	0.485		0.485		0.485	
d_b (in.)	23.6		26.7		26.7	
b (in.)	7.01		9.96		9.96	
T (in.)	12.64	11.44	12.64	11.44	12.64	11.44
x (in.)	2.82	2.22	1.34	0.74	1.34	0.74
u (in.)	3.48	3.02	2.67	1.96	2.67	1.96
v (in.)	2.24	1.87	1.50	1.05	1.50	1.05
d (in.)	4.22	3.56	2.91	2.06	2.91	2.06
Y	7.73	7.98	9.95	12.41	9.95	12.41
M_n (ft-kips) (F_w=F_y)	207.3	214.2	301.9	376.7	284.8	355.3
M_n (ft-kips) (F_w=F*)	240.5	248.4	350.4	437.2	328.0	409.2

YIELD LINE SOLUTION PARAMETER VALUES

APPENDIX C

STRESS CONCENTRATION PLOTS

TEST W24x55 - VON MISES STRESS CONCENTRATION PLOT

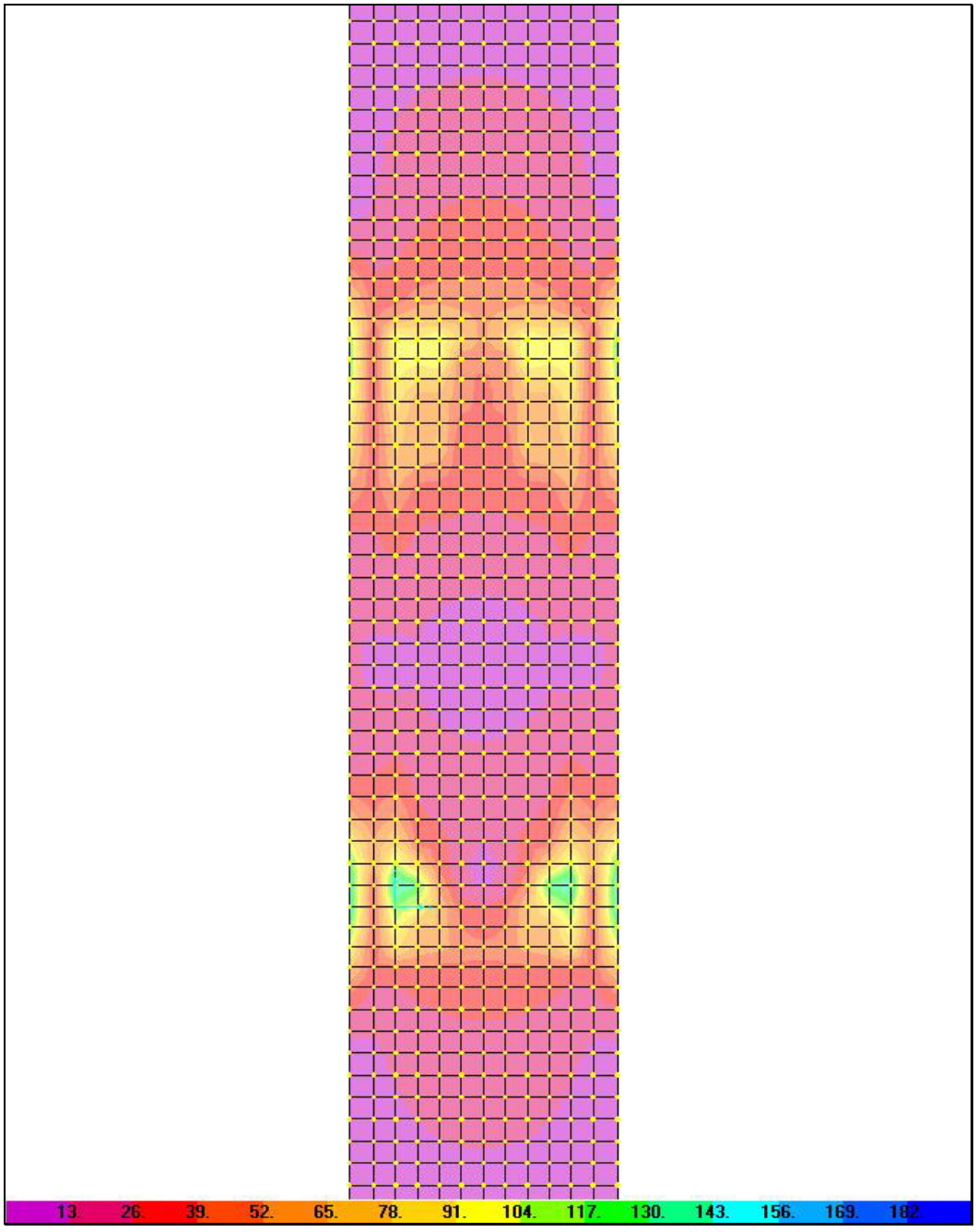

TEST W27x84 - VON MISES STRESS CONCENTRATION PLOT

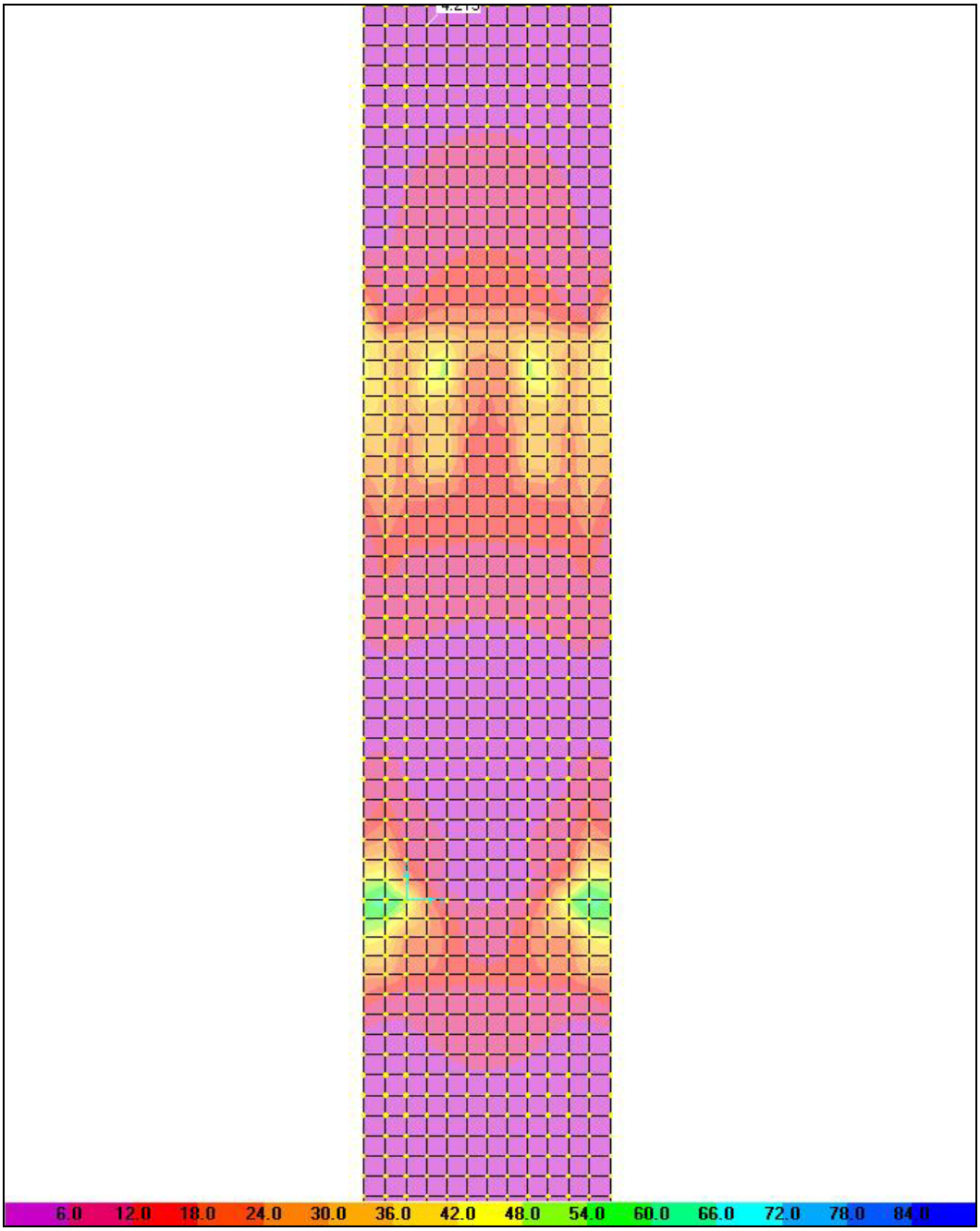

TEST W27x84-SLAB - VON MISES STRESS CONCENTRATION PLOT

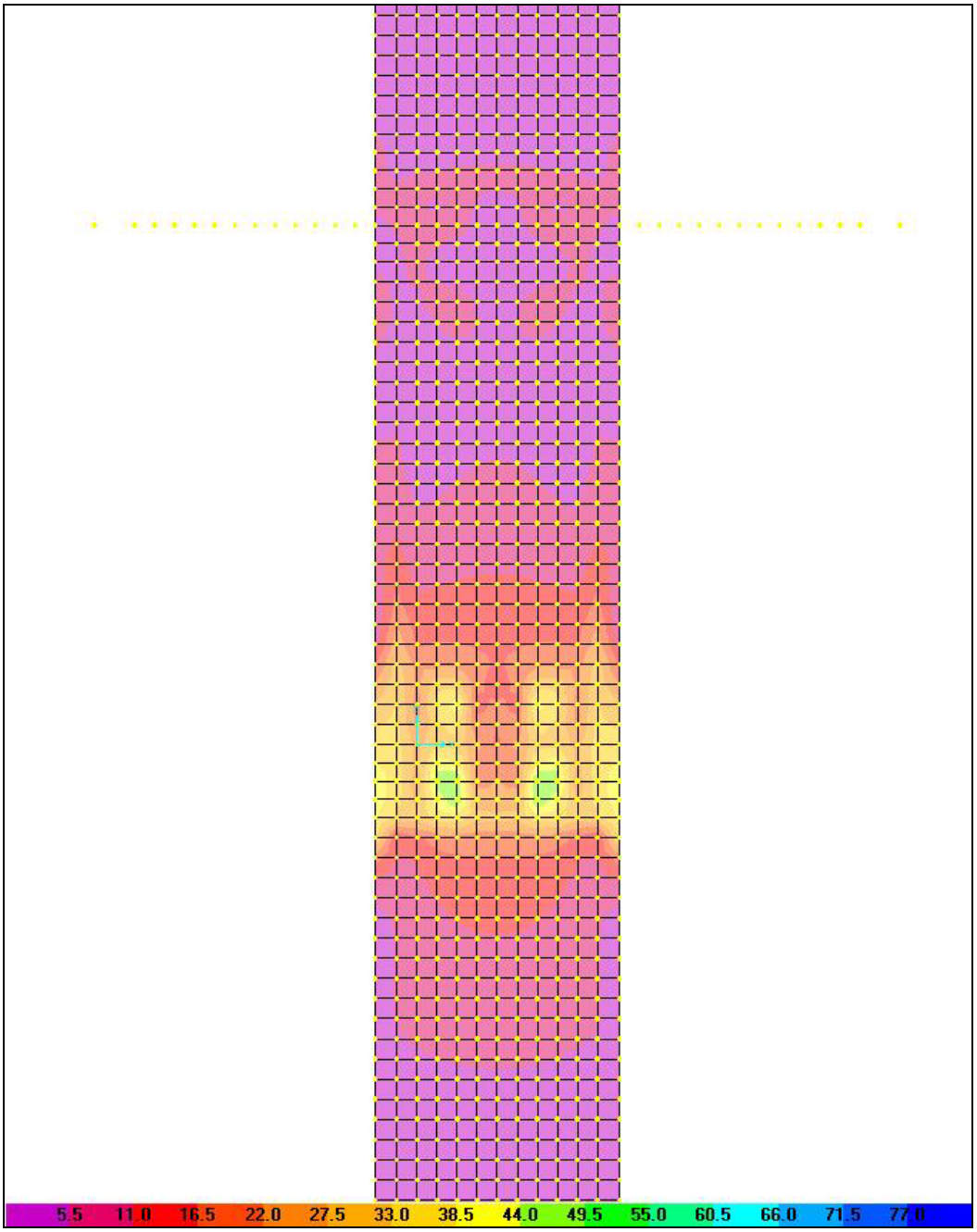

APPENDIX D

EXPERIMENTAL PLASTIC STRENGTHS OF COLUMN WEB

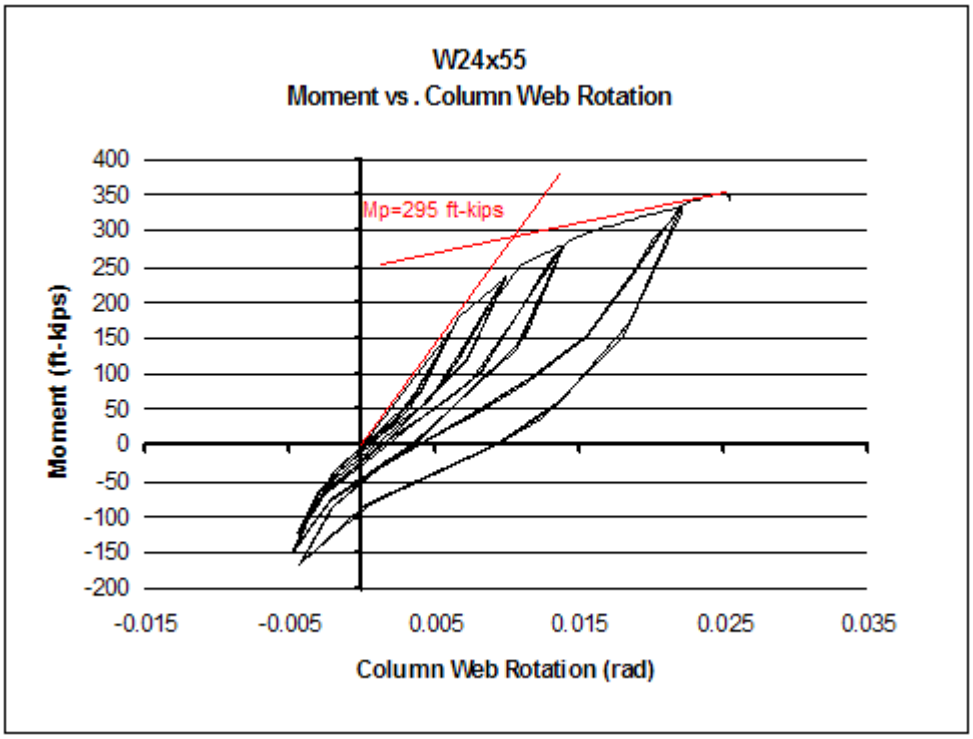
W24x55
Moment vs . Column Web Rotation
Mp=295 ft-kips
Moment (ft-kips)
400
350
300
250
200
150
100
50
0
-50
-100
-150
-200
-0.015
-0.005
0.005
0.015
0.025
0.035
Column Web Rotation (rad)

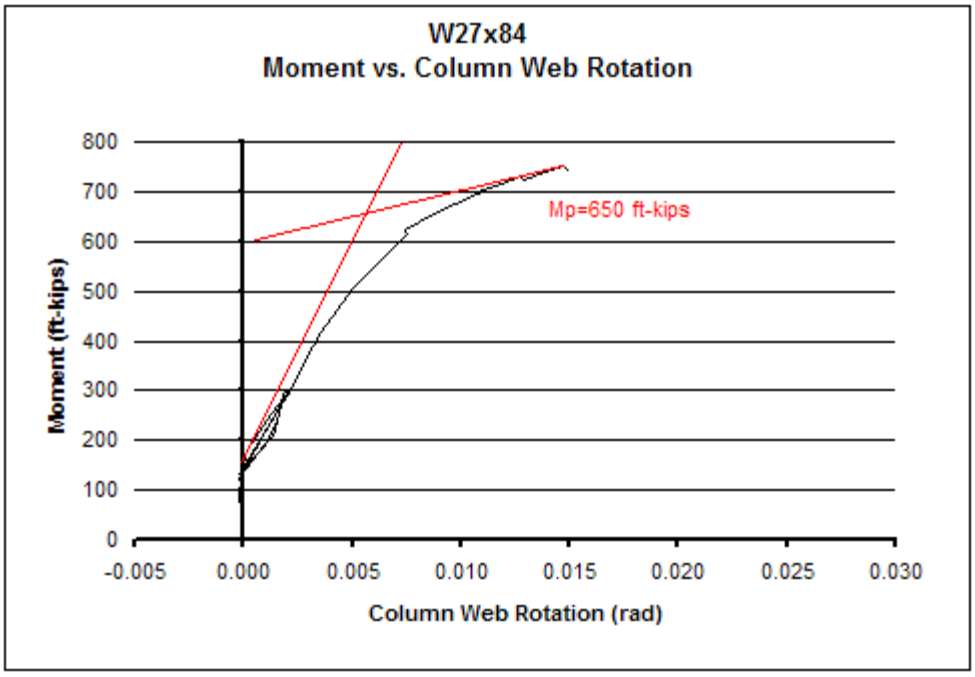
W27x84
Moment vs. Column Web Rotation
Mp=650 ft-kips
Moment (ft-kips)
800
700
600
500
400
300
200
100
0
-0.005
0.000
0.005
0.010
0.015
0.020
0.025
0.030
Column Web Rotation (rad)

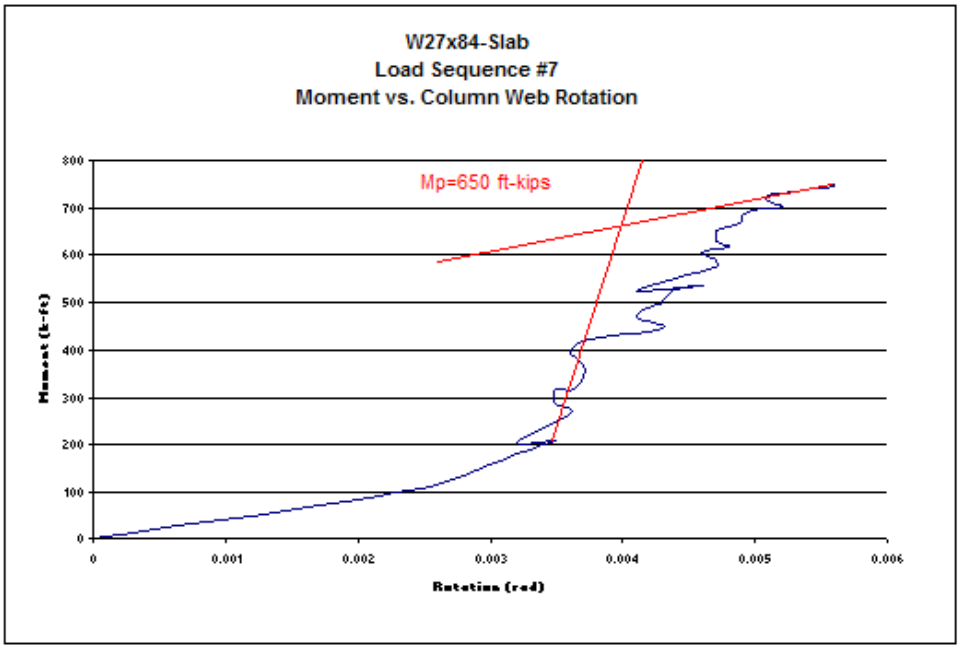
W27x84-Slab
Load Sequence #7
Moment vs. Column Web Rotation
Mp=650 ft-kips
Moment (k-ft)
Rotation (rad)
800
700
600
500
400
300
200
100
0
0
0.001
0.002
0.003
0.004
0.005
0.006

APPENDIX E

W24x55 EXPERIMENTAL TEST PLOTS

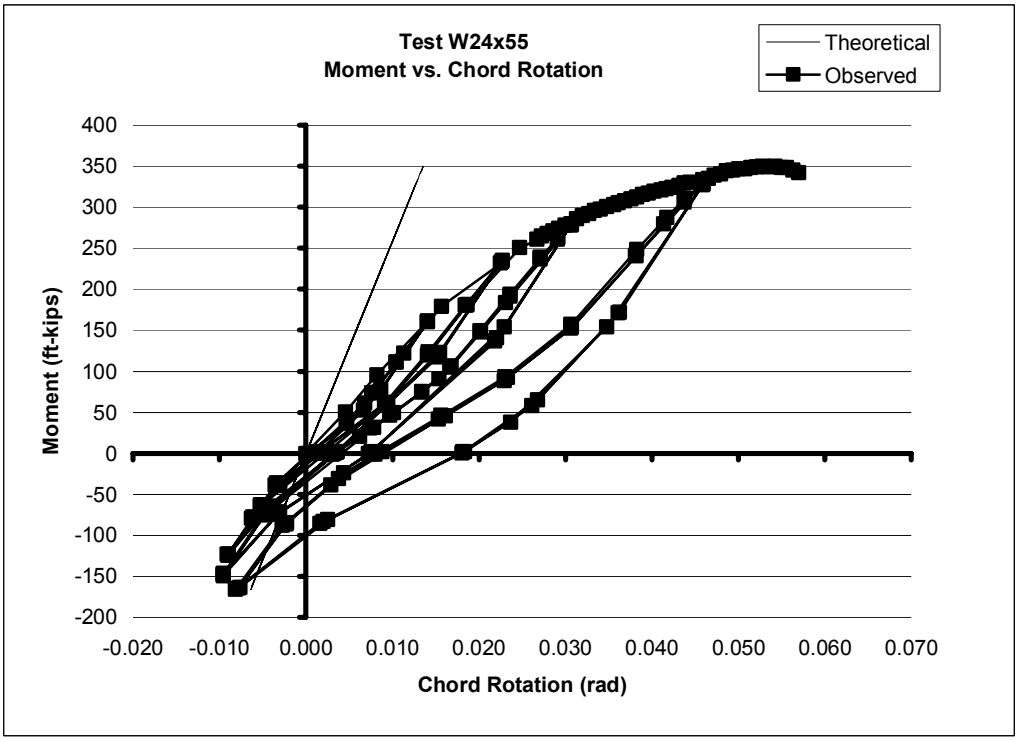
Test W24x55
Moment vs. Chord Rotation
Theoretical
Observed
Moment (ft-kips)
400
350
300
250
200
150
100
50
0
-50
-100
-150
-200
-0.020
-0.010
0.000
0.010
0.020
0.030
0.040
0.050
0.060
0.070
Chord Rotation (rad)

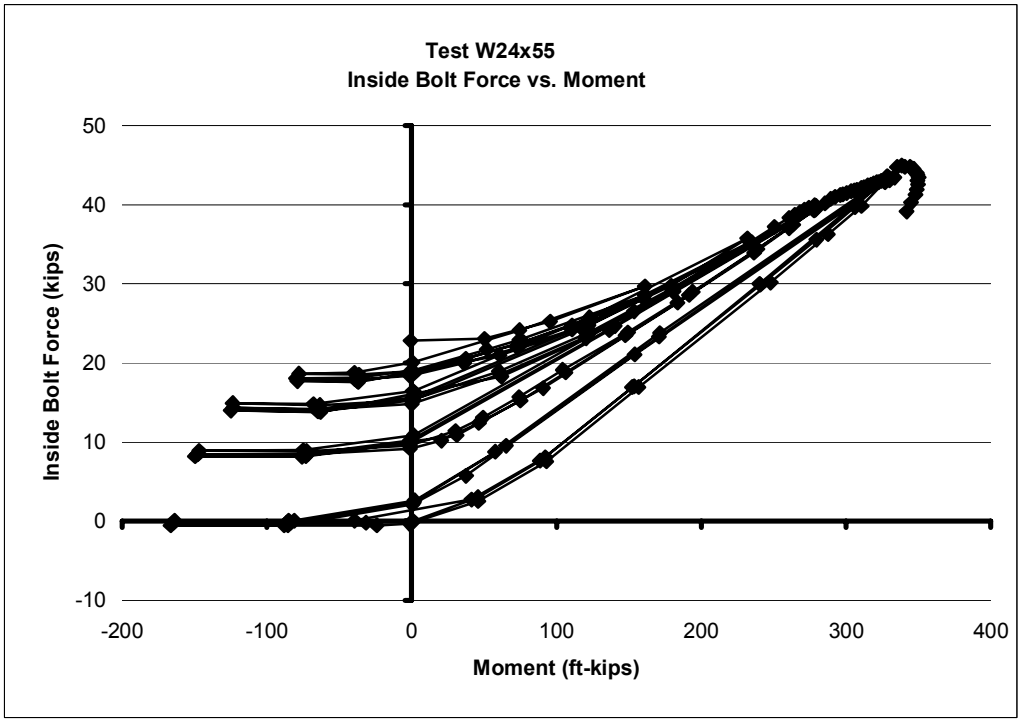
Test W24x55
Inside Bolt Force vs. Moment
Inside Bolt Force (kips)
50
40
30
20
10
0
-10
-200
-100
0
100
200
300
400
Moment (ft-kips)

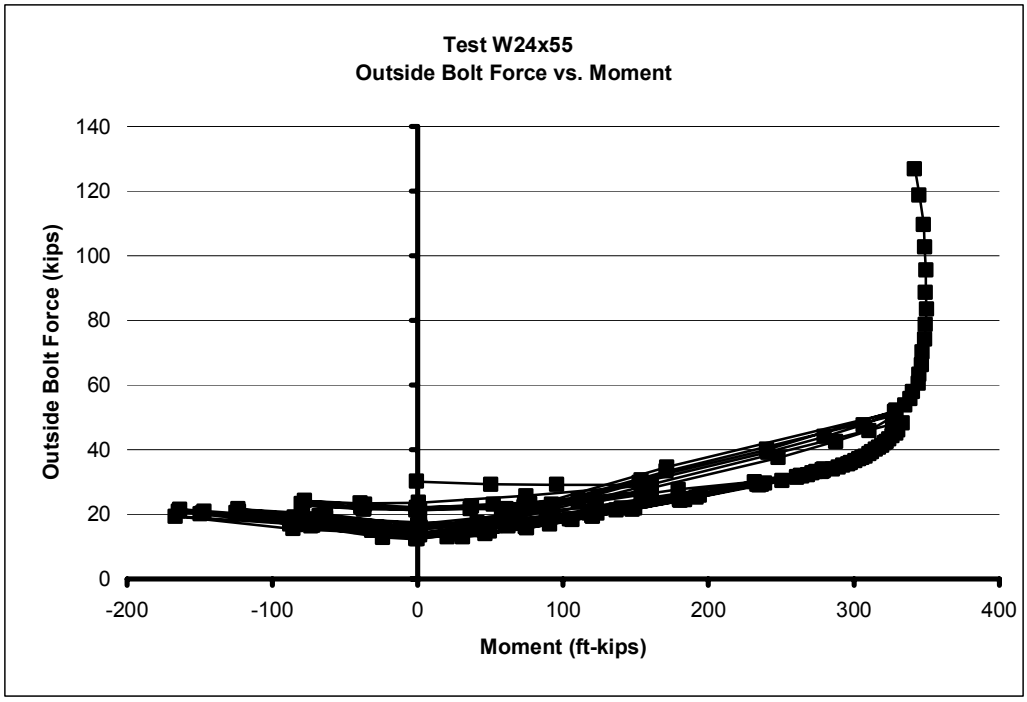
Test W24x55
Outside Bolt Force vs. Moment
Outside Bolt Force (kips)
140
120
100
80
60
40
20
0
-200
-100
0
100
200
300
400
Moment (ft-kips)

APPENDIX F

W27x84 EXPERIMENTAL TEST PLOTS

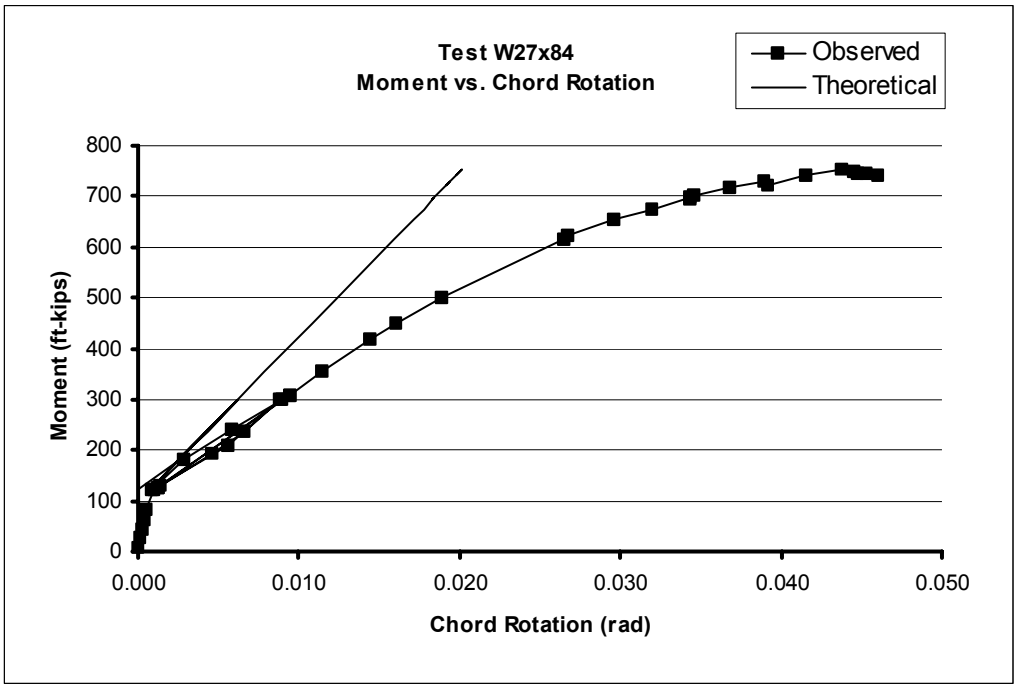
Test W27x84
Moment vs. Chord Rotation
Observed
Theoretical
Moment (ft-kips)
800
700
600
500
400
300
200
100
0
0.000
0.010
0.020
0.030
0.040
0.050
Chord Rotation (rad)

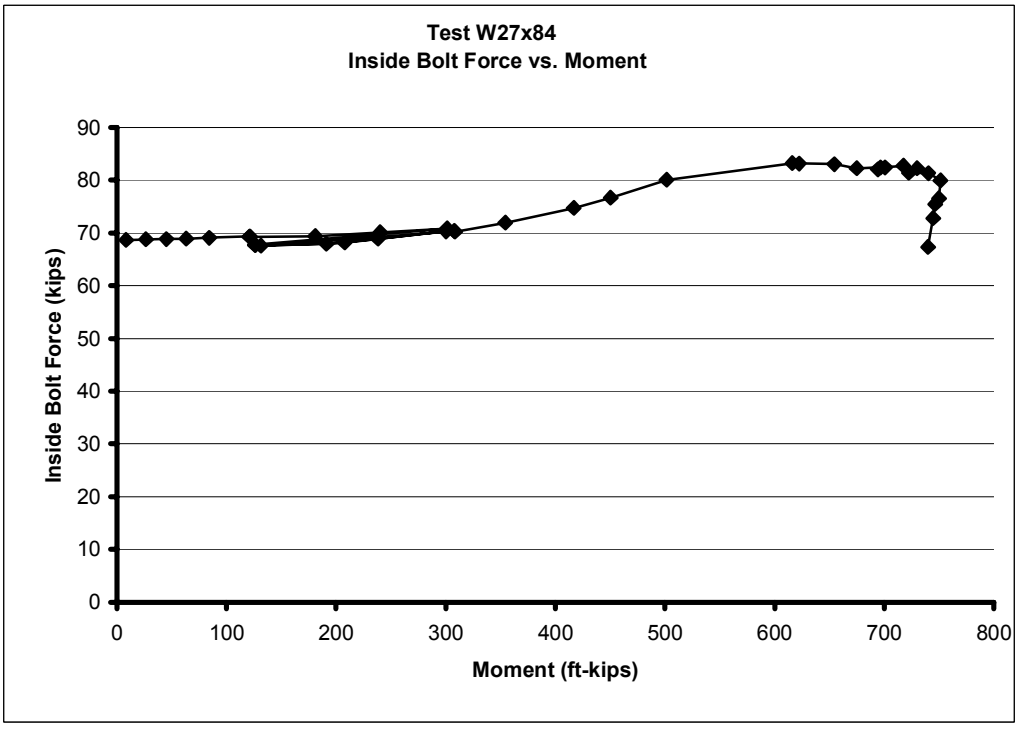
Test W27x84
Inside Bolt Force vs. Moment
Inside Bolt Force (kips)
90
80
70
60
50
40
30
20
10
0
0
100
200
300
400
500
600
700
800
Moment (ft-kips)

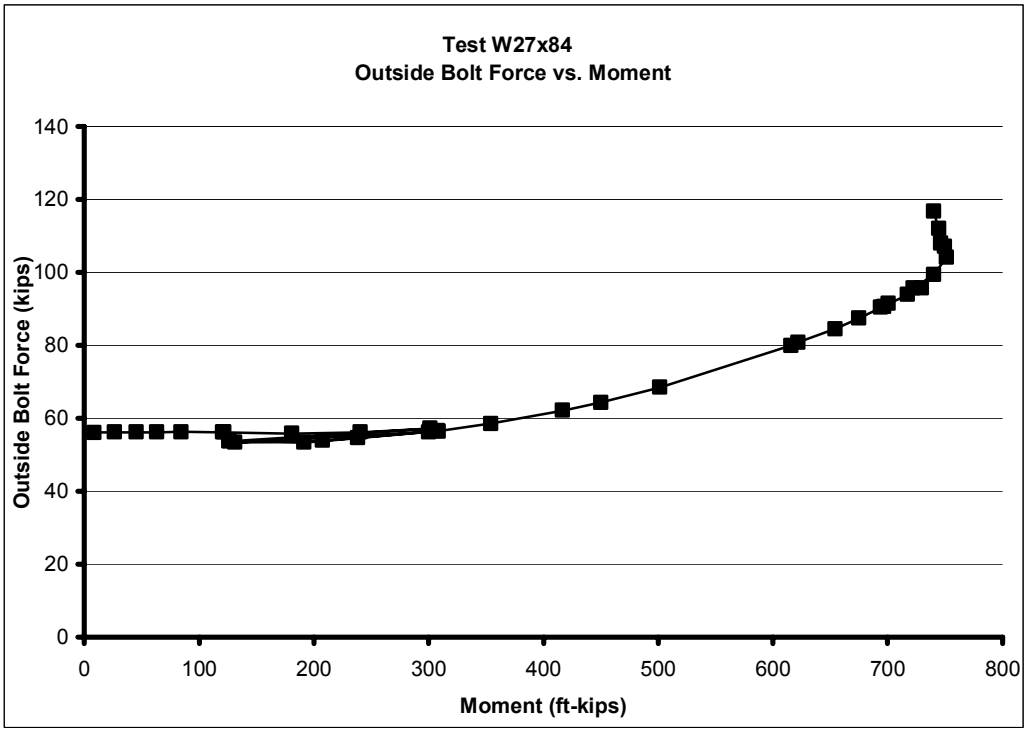
Test W27x84
Outside Bolt Force vs. Moment
Outside Bolt Force (kips)
140
120
100
80
60
40
20
0
0
100
200
300
400
500
600
700
800
Moment (ft-kips)

APPENDIX G

W27x84-SLAB EXPERIMENTAL TEST PLOTS

G.1 LOAD SEQUENCE #1 PLOTS

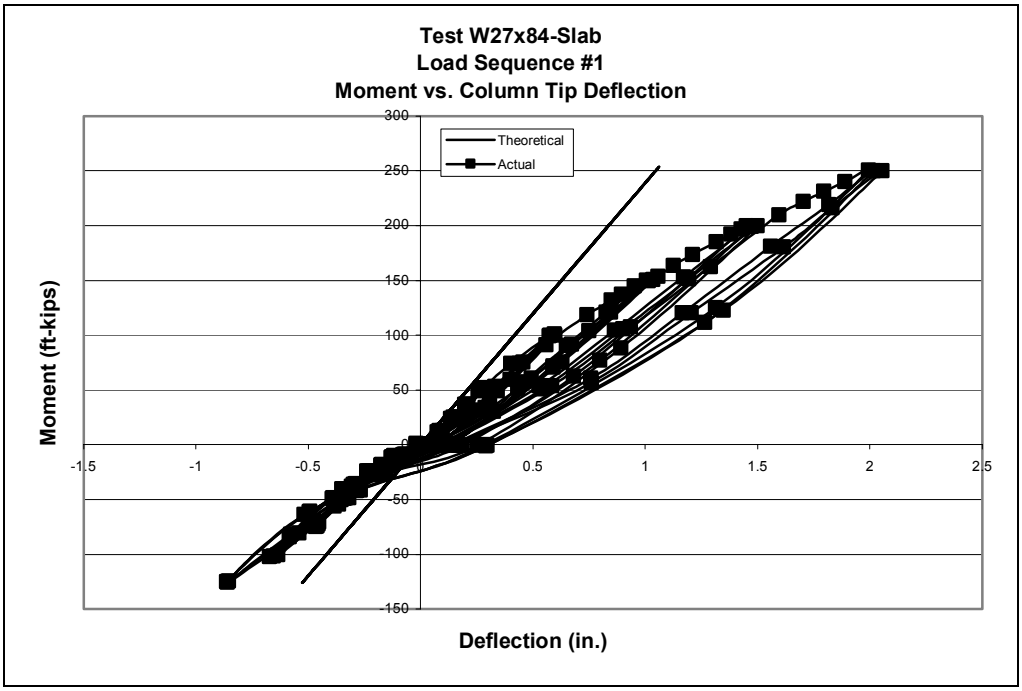

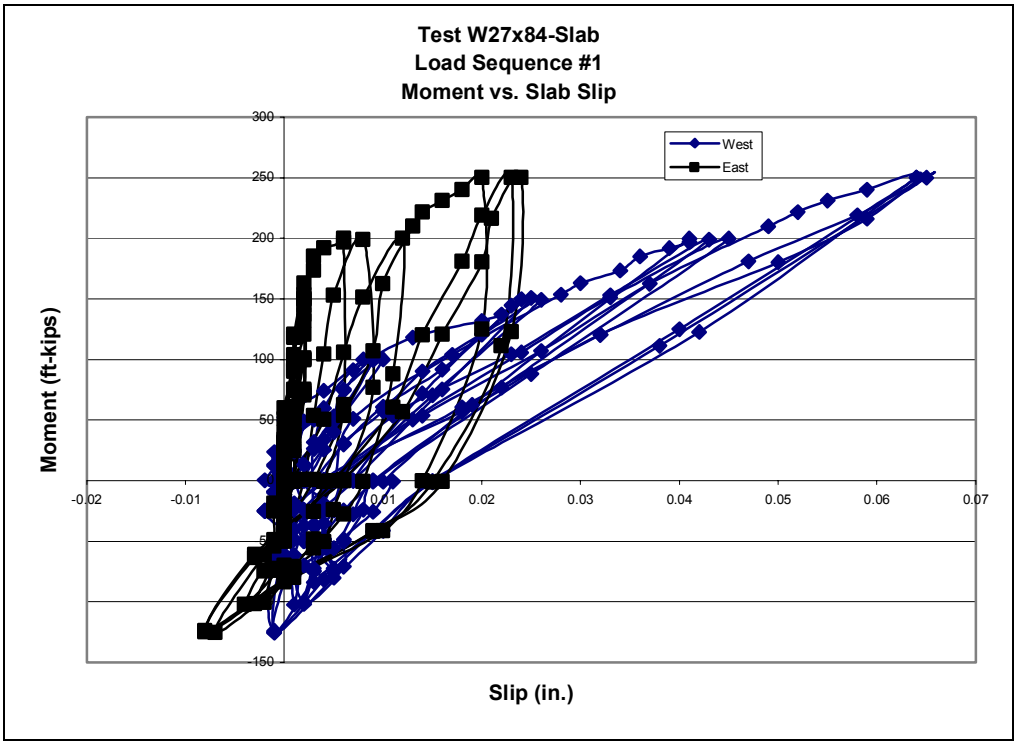

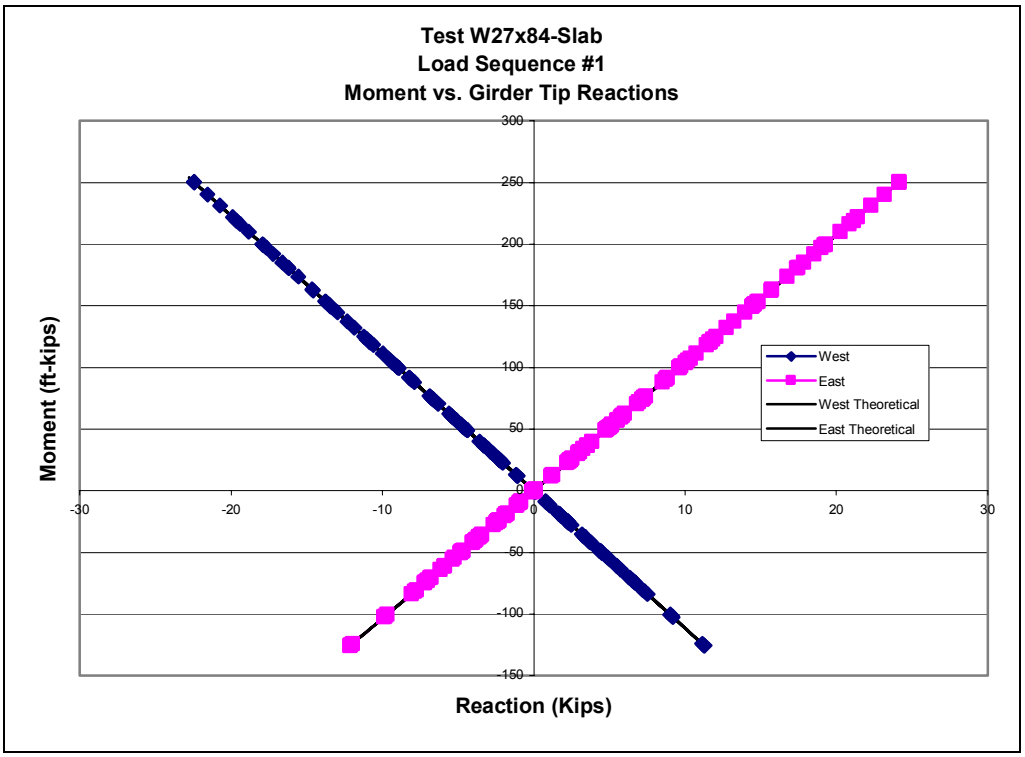
Test W27x84-Slab
Load Sequence #1
Moment vs. Girder Tip Reactions
Moment (ft-kips)
Reaction (Kips)
West
East
West Theoretical
East Theoretical
300
250
200
150
100
50
0
-50
-100
-150
-30
-20
-10
0
10
20
30

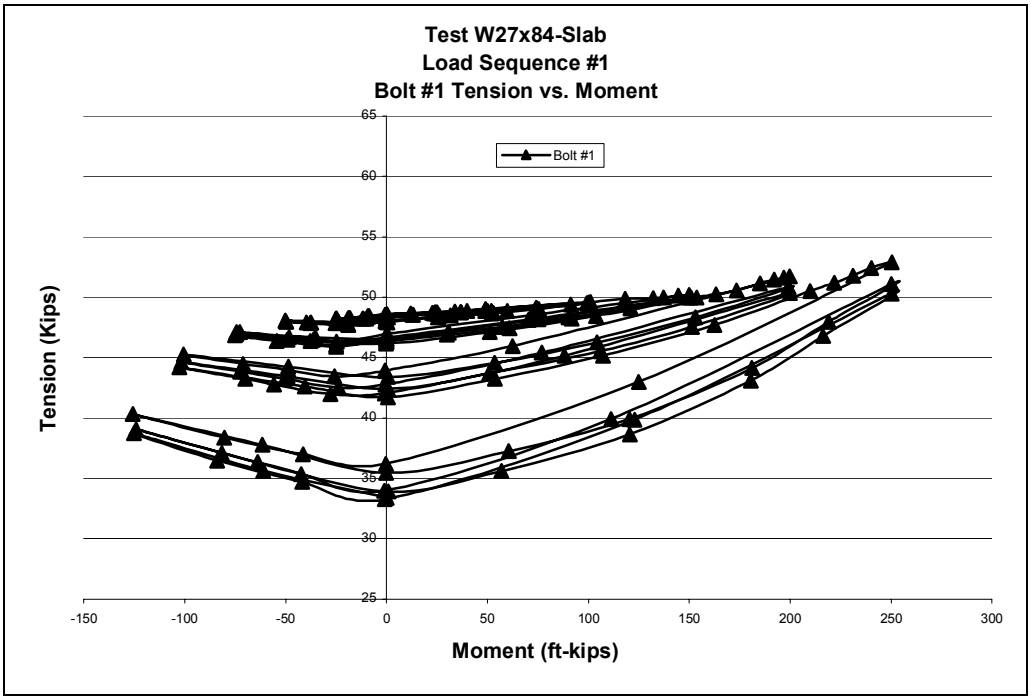
Test W27x84-Slab
Load Sequence #1
Bolt #1 Tension vs. Moment
Tension (Kips)
Moment (ft-kips)
Bolt #1
65
60
55
50
45
40
35
30
25
-150
-100
-50
0
50
100
150
200
250
300

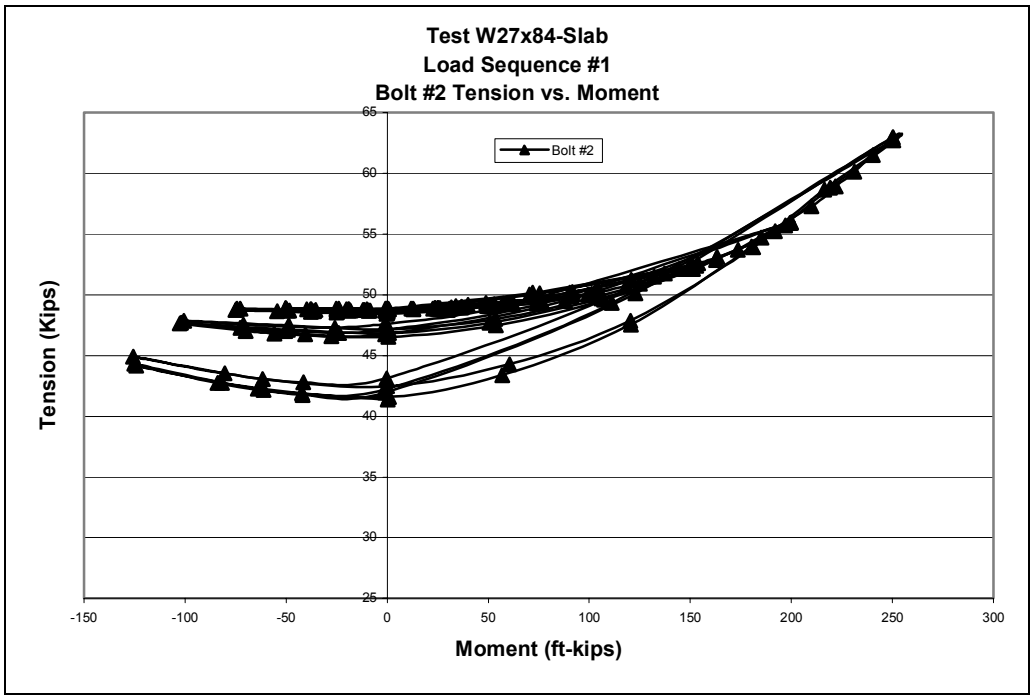
Test W27x84-Slab
Load Sequence #1
Bolt #2 Tension vs. Moment
Bolt #2
Tension (Kips)
65
60
55
50
45
40
35
30
25
-150
-100
-50
0
50
100
150
200
250
300
Moment (ft-kips)

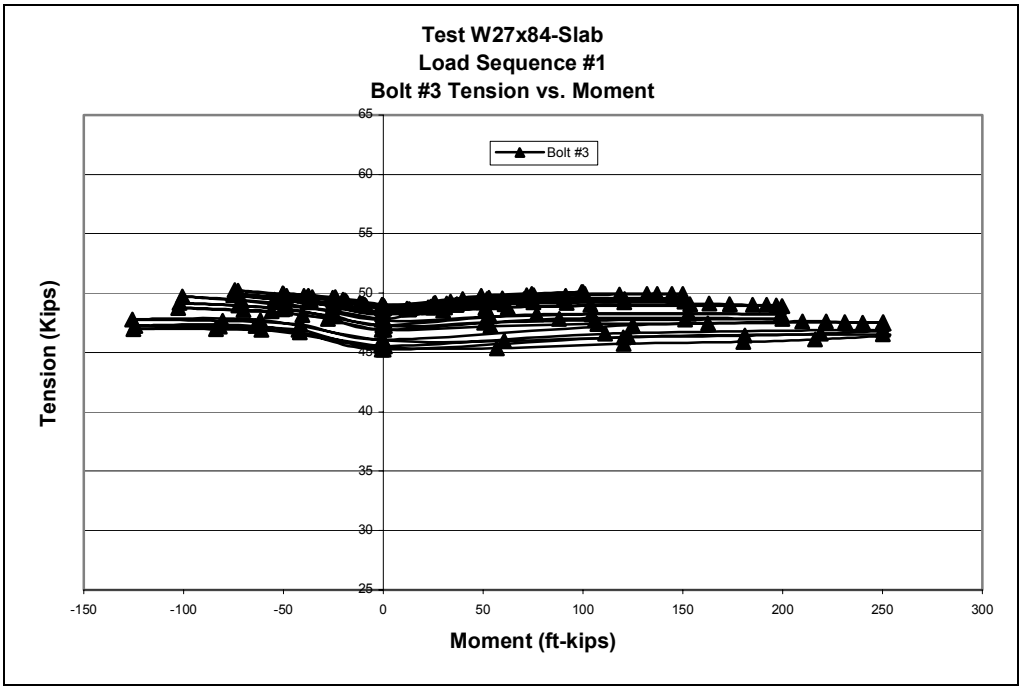
Test W27x84-Slab
Load Sequence #1
Bolt #3 Tension vs. Moment
Bolt #3
Tension (Kips)
65
60
55
50
40
35
30
25
-150
-100
-50
0
50
100
150
200
250
300
Moment (ft-kips)

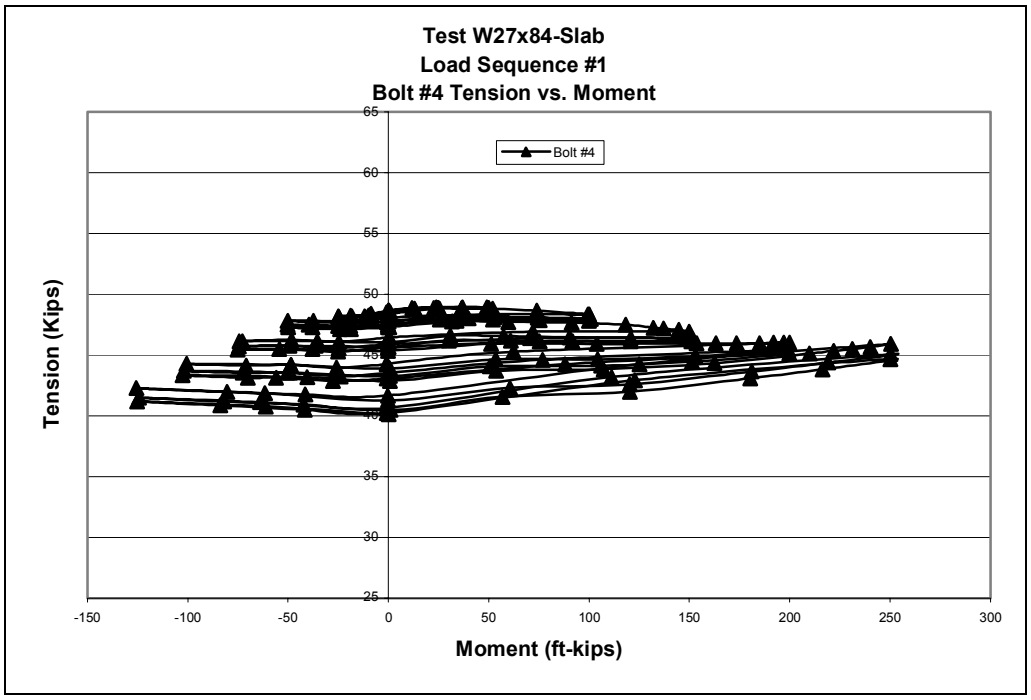
Test W27x84-Slab
Load Sequence #1
Bolt #4 Tension vs. Moment
Bolt #4
Tension (Kips)
65
60
55
50
35
30
25
-150
-100
-50
0
50
100
150
200
250
300
Moment (ft-kips)

G.2 LOAD SEQUENCE #5 PLOTS

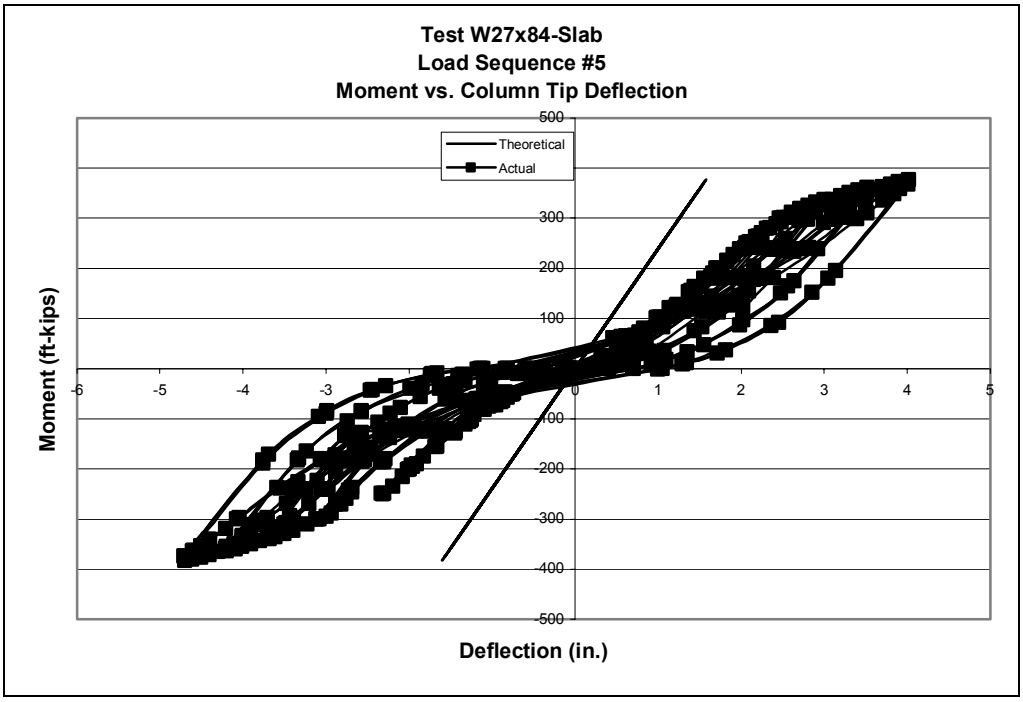

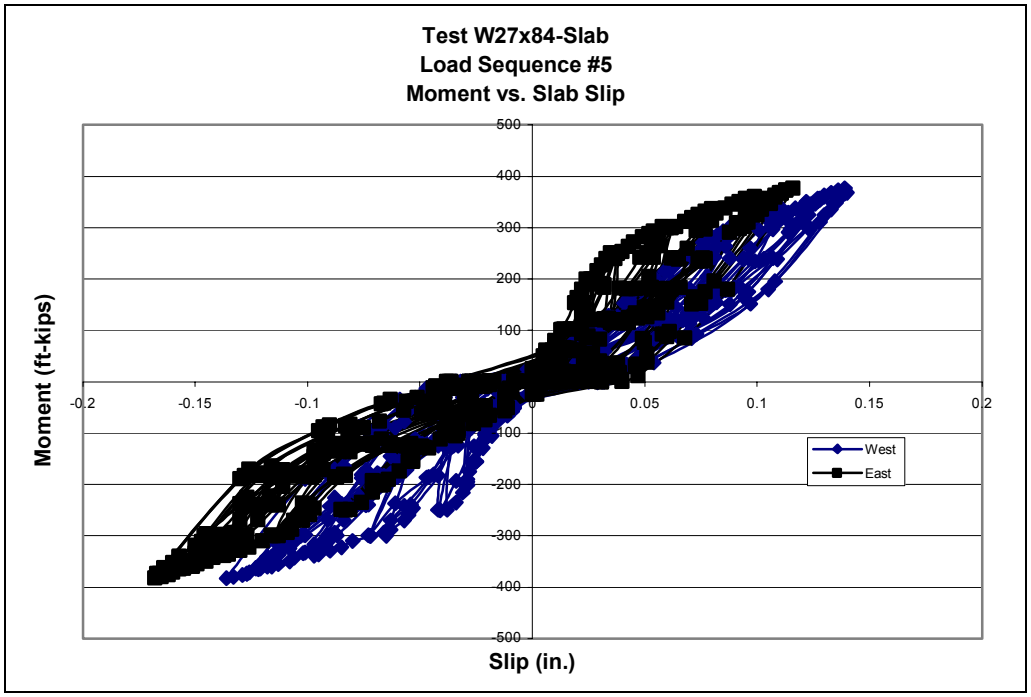

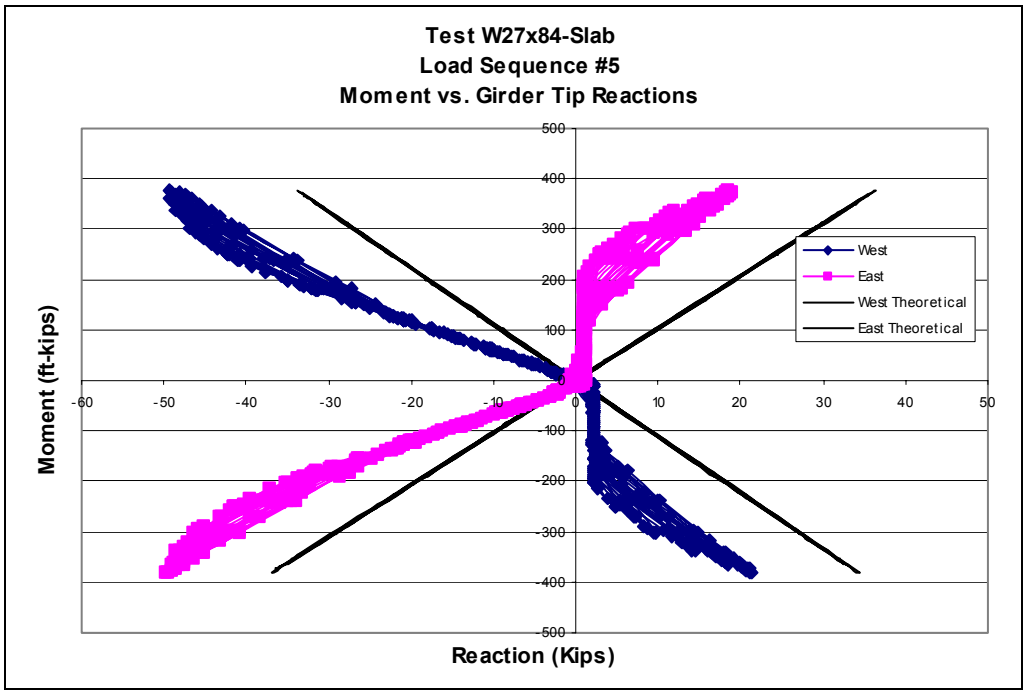
Test W27x84-Slab
Load Sequence #5
Moment vs. Girder Tip Reactions
Moment (ft-kips)
Reaction (Kips)
West
East
West Theoretical
East Theoretical
500
400
300
200
100
0
-100
-200
-300
-400
-500
-60
-50
-40
-30
-20
-10
0
10
20
30
40
50

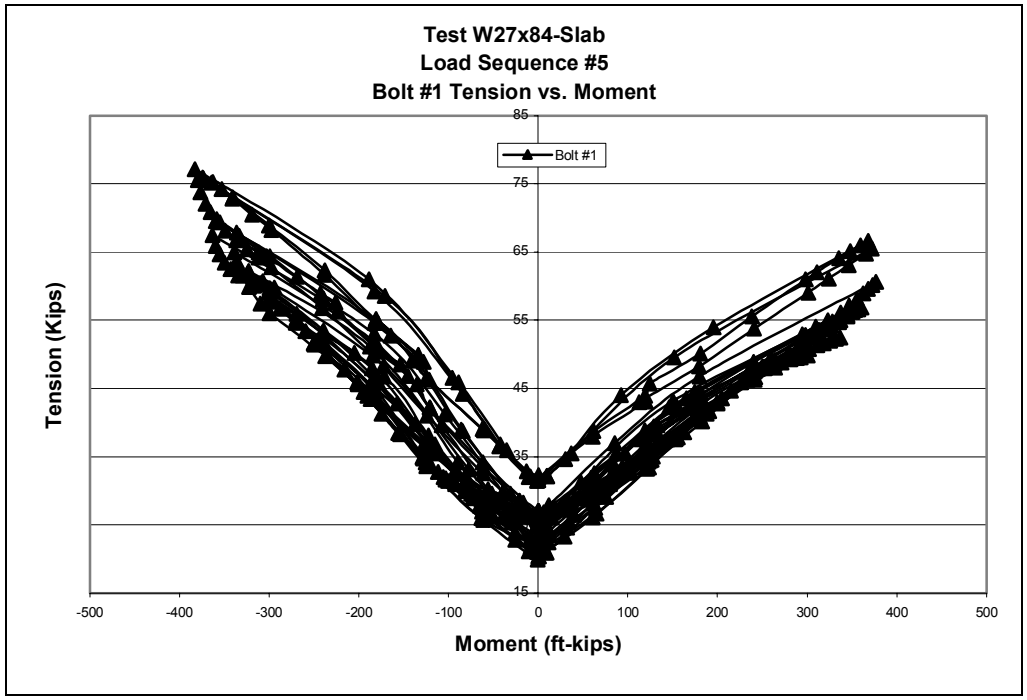
Test W27x84-Slab
Load Sequence #5
Bolt #1 Tension vs. Moment
Tension (Kips)
Moment (ft-kips)
Bolt #1
85
75
65
55
45
35
15
-500
-400
-300
-200
-100
0
100
200
300
400
500

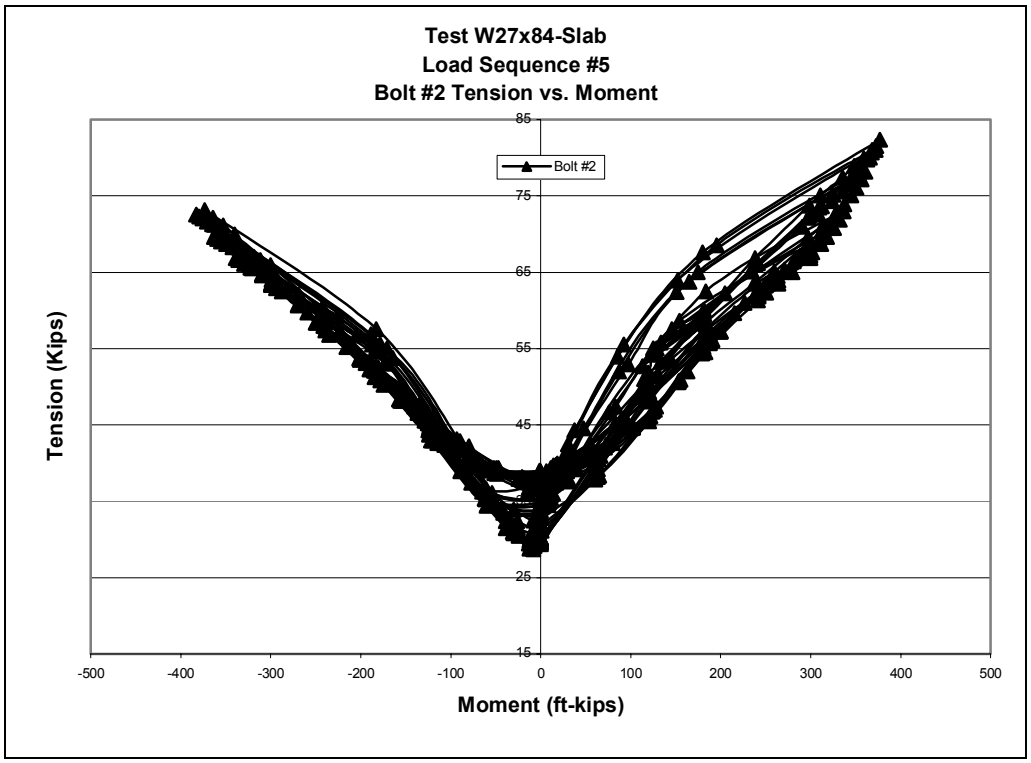
Test W27x84-Slab
Load Sequence #5
Bolt #2 Tension vs. Moment
Bolt #2
Tension (Kips)
85
75
65
55
45
25
15
-500
-400
-300
-200
-100
0
100
200
300
400
500
Moment (ft-kips)

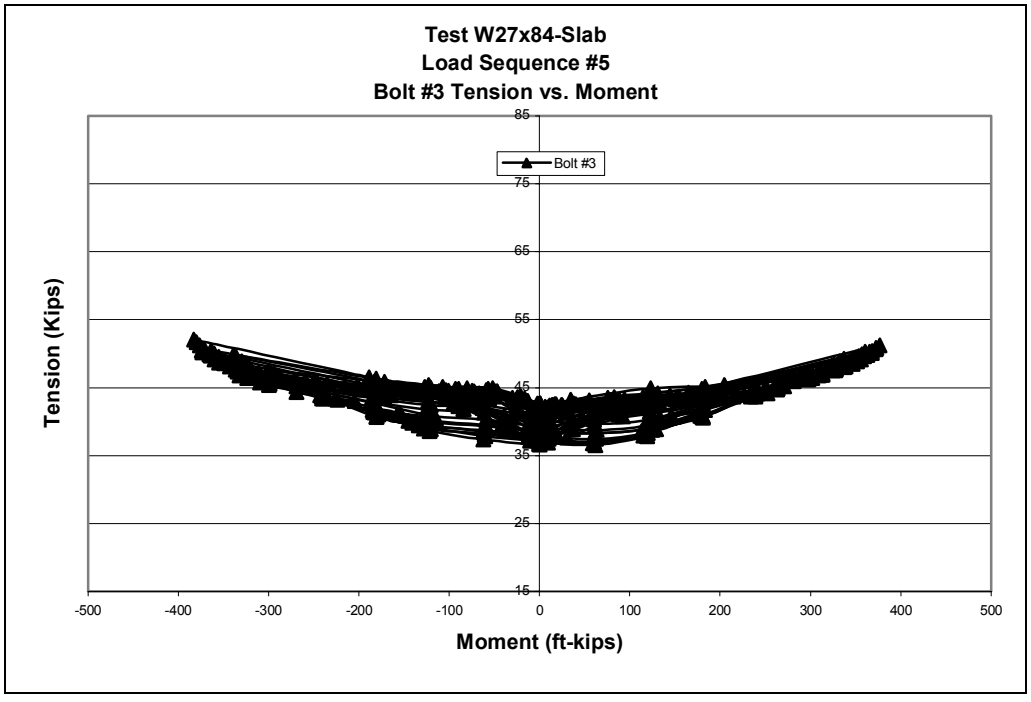
Test W27x84-Slab
Load Sequence #5
Bolt #3 Tension vs. Moment
Bolt #3
Tension (Kips)
85
75
65
55
45
35
25
15
-500
-400
-300
-200
-100
0
100
200
300
400
500
Moment (ft-kips)

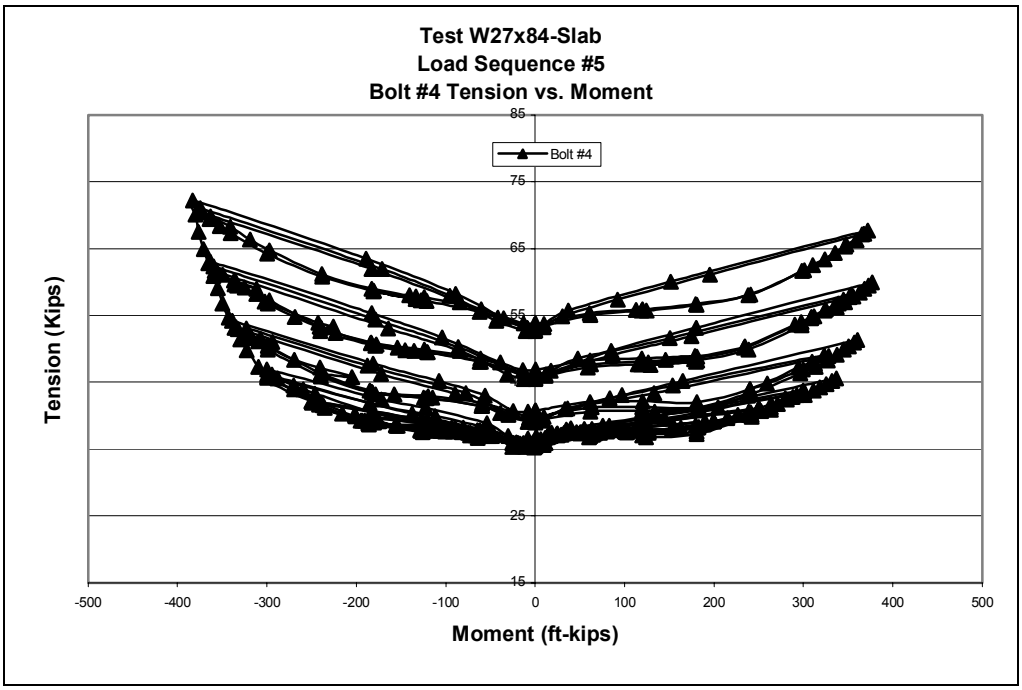
Test W27x84-Slab
Load Sequence #5
Bolt #4 Tension vs. Moment
Bolt #4
Tension (Kips)
85
75
65
55
25
15
-500
-400
-300
-200
-100
0
100
200
300
400
500
Moment (ft-kips)

G.3 LOAD SEQUENCE #7 PLOTS

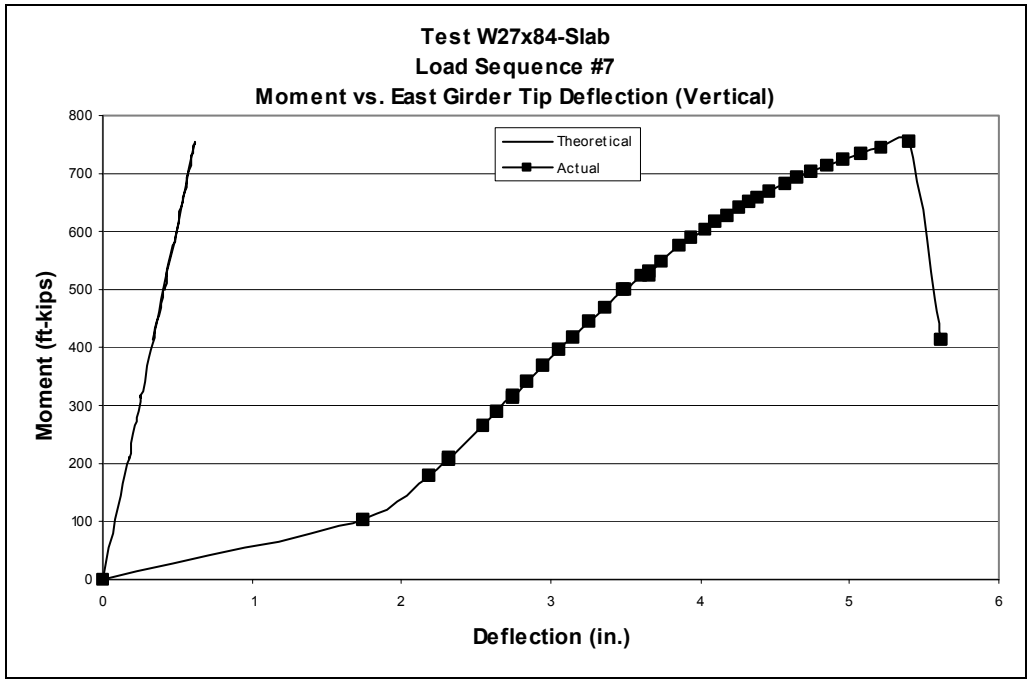

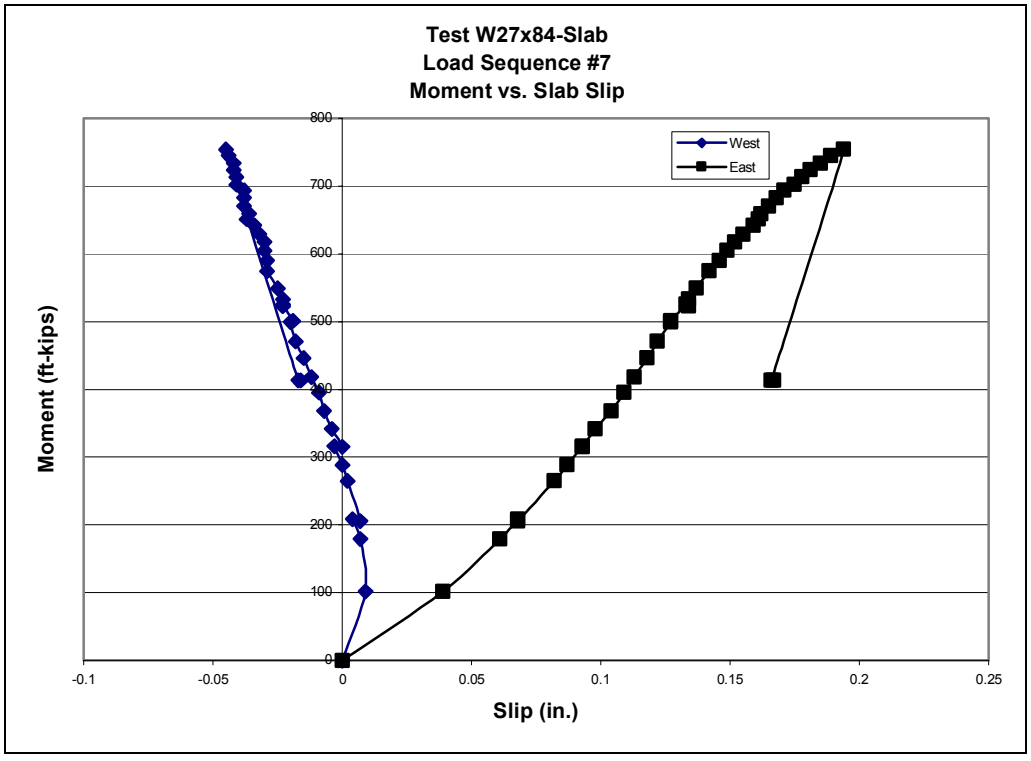

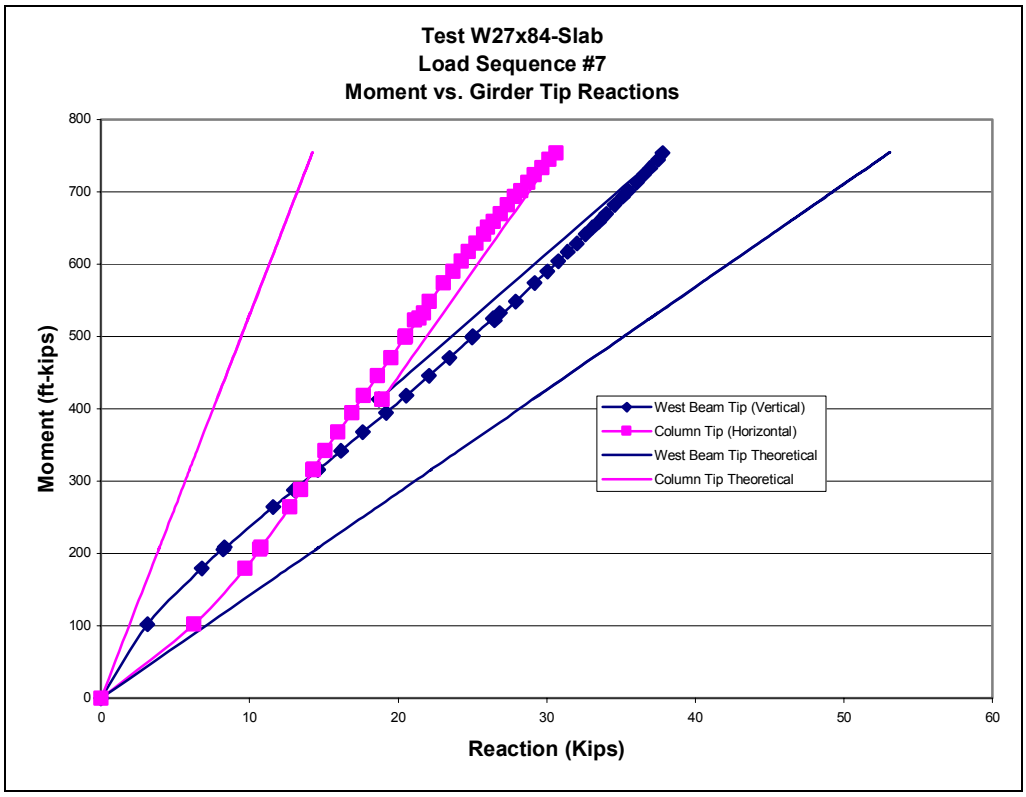
Test W27x84-Slab
Load Sequence #7
Moment vs. Girder Tip Reactions
Moment (ft-kips)
800
700
600
500
400
300
200
100
0
0
10
20
30
40
50
60
Reaction (Kips)
West Beam Tip (Vertical)
Column Tip (Horizontal)
West Beam Tip Theoretical
Column Tip Theoretical

VITA

Kyle Richard Dominisse was born on June 2, 1980, in Osmond, NE, to Richard and Karen Dominisse. He is the oldest child of the family with one younger sister. After completing high school in May, 1999, in Randolph, NE, he enrolled at the University of Nebraska – Omaha and obtained a Bachelor of Science degree in Civil Engineering in May, 2003. Following that, he enrolled in the graduate program in Civil and Environmental Engineering - Structures and Materials Program at Virginia Polytechnic Institute and State University in August, 2003, in pursuit of a Master of Science degree.